Radial-Hydride-Induced Embrittlement of High-Burnup ZIRLO Cladding Exposed to Simulated Drying Conditions

T.A. Burtseva, Y. Yan, and M.C. Billone
Argonne National Laboratory
June 30, 2010

Summary

Two experiments were conducted with ZIRLO cladding sectioned and defueled from a high-burnup (70 GWd/MTU) fuel rod irradiated in the North Anna reactors. Sealed, pressurized rodlets were fabricated from cladding segments with corrosion layers of 33 µm and 52 µm and corresponding average hydrogen contents of 425 wppm and 650 wppm. Room-temperature (RT) pressures of 6.4 MPa and 8.0 MPa were used to induce 110-MPa and 140-MPa cladding hoop stresses at 400°C. The rodlets were subjected to one heating-cooling cycle: heat sample holder to 400°C in 45 minutes, stabilize rodlet temperature at 400°C for 15 minutes, hold at 400°C for one hour, and cool at 5°C/h under conditions of decreasing pressure and hoop stress. The primary purposes of these experiments were to determine if radial hydrides formed under these cooling conditions and if they were long enough to induce cladding embrittlement.

The pressurized rodlets subjected to one-cycle, radial-hydride treatment (RHT) were characterized in terms of corrosion-layer and metal-wall thicknesses, hydrogen content, hydride distribution across the cladding wall, and extent of radial hydride formation. The radial hydride continuity factor, which is defined as the percentage of the cladding wall for which radial hydrides form a continuous, interconnected pathway within an arc width of 150 µm, was used to assess the extent of radial hydride formation. Ring compression testing was used to determine cladding ductility and extent of through-wall cracking. Tests were conducted at 5 mm/s displacement rate to 2-mm total displacement. If rings exhibited ductility at 150°C, then sibling rings were tested at RT. For cracks >50% of the wall thickness, it was assumed that through-wall cracks and fission gas release would occur due to gas pressure inside a high-burnup fuel rod.

In the as-irradiated condition, most of the hydrogen in the cladding is located in the dense hydride rim at the corrosion-layer/metal interface. This rim consists of densely packed hydride platelets. During one-cycle RHT, only a very small fraction of hydrogen redistributed across the cladding wall. Based on visible hydrides, about 50% of the cladding had ≤100 wppm hydrogen after one-cycle RHT. This cladding region is vulnerable to the formation of long radial hydrides.

The first rodlet tested contained an average of 650 wppm hydrogen. Following RHT with cooling from 400°C at 140-MPa hoop stress, the radial hydride continuity factor was 65±15%. The two rings tested at 150°C were brittle with no plastic strain prior to crack initiation. One sample developed 2 cracks that were essentially through-wall. The second ring had 3 cracks and was in two pieces. The second rodlet tested (425-wppm hydrogen) was cooled from 400°C at 110-MPa hoop stress. Lowering the hoop stress to 110 MPa resulted in a smaller radial hydride continuity factor (27±10%) and higher ductility (10-15% at 150°C). One of three rings survived the 2-mm displacement with no cracking. The other two rings developed partial-wall cracks after 1.7±0.1 mm total displacement. The 4th ring, tested at RT, was brittle.

1. Background

During 2000-2005, a number of tests were conducted with defueled Zry-4 cladding sectioned from high-burnup (67 GWd/MTU) fuel rods irradiated in the H. B. Robinson Unit 2 Reactor: annealing studies to determine redistribution of hydrogen across the wall of the cladding and time at temperature to anneal out irradiation damage; thermal creep studies; and radial-hydride embrittlement studies for samples cooled at constant stress. Data and observations from the annealing studies are reviewed in the following.

Cladding rings sectioned from near the mid-plane of an H. B. Robinson (HBR) fuel rod were subjected to stress-free annealing with temperatures ranging from 420°C to 500°C and times ranging from 2 hours to 72 hours. The Zry-4 hydrogen content near the fuel mid-plane was measured to be 580±70 wppm based on four quarter-ring readings. Figure 1 shows the hydride distribution for this cladding in the as-irradiated condition. The inner-half of the cladding wall has little-to-no visible hydrides. The hydride density in the outer-half of the cladding increases somewhat from mid-wall to the hydride rim and then increases significantly within the hydride rim near the corrosion layer. For the circumferential location shown in Fig. 1, the hydrogen content is estimated to be <500 wppm.

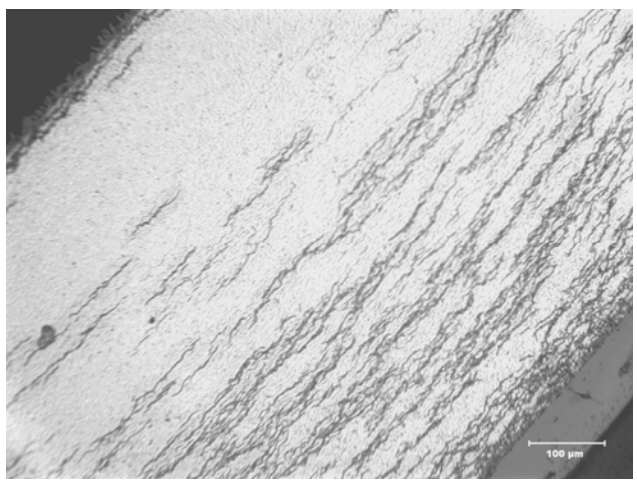

Fig. 1. Distribution of circumferential hydrides across the wall of Zry-4 cladding sectioned from near the mid-plane of an HBR fuel rod (A02) irradiated to 67 GWd/MTU.

Cladding samples were subjected to one-cycle heating-cooling with a heating time of about 45 minutes to reach target temperature and with a fast cooling rate of 1°C/minute to 200°C. Redistribution of hydrogen across the radius was complete (i.e., uniform hydride distribution) after 72 hours at 420°C, 48 hours at 450°C, and 2 hours at 500°C. More relevant to the current study are the hydride distributions at the lowest test temperatures and annealing times: 20 hours at 420°C and 2 hours at 450°C. Figures 2 and 3, respectively, indicate some redistribution after 20 hours at 420°C (mild) and after 2 hours at 450°C (extensive). Thus, for the current study, we can expect relatively little hydrogen redistribution after only one hour at 400°C, although with the much slower cooling rate (5°C/h) the time the sample is above 390°C is greater than 3 hours.

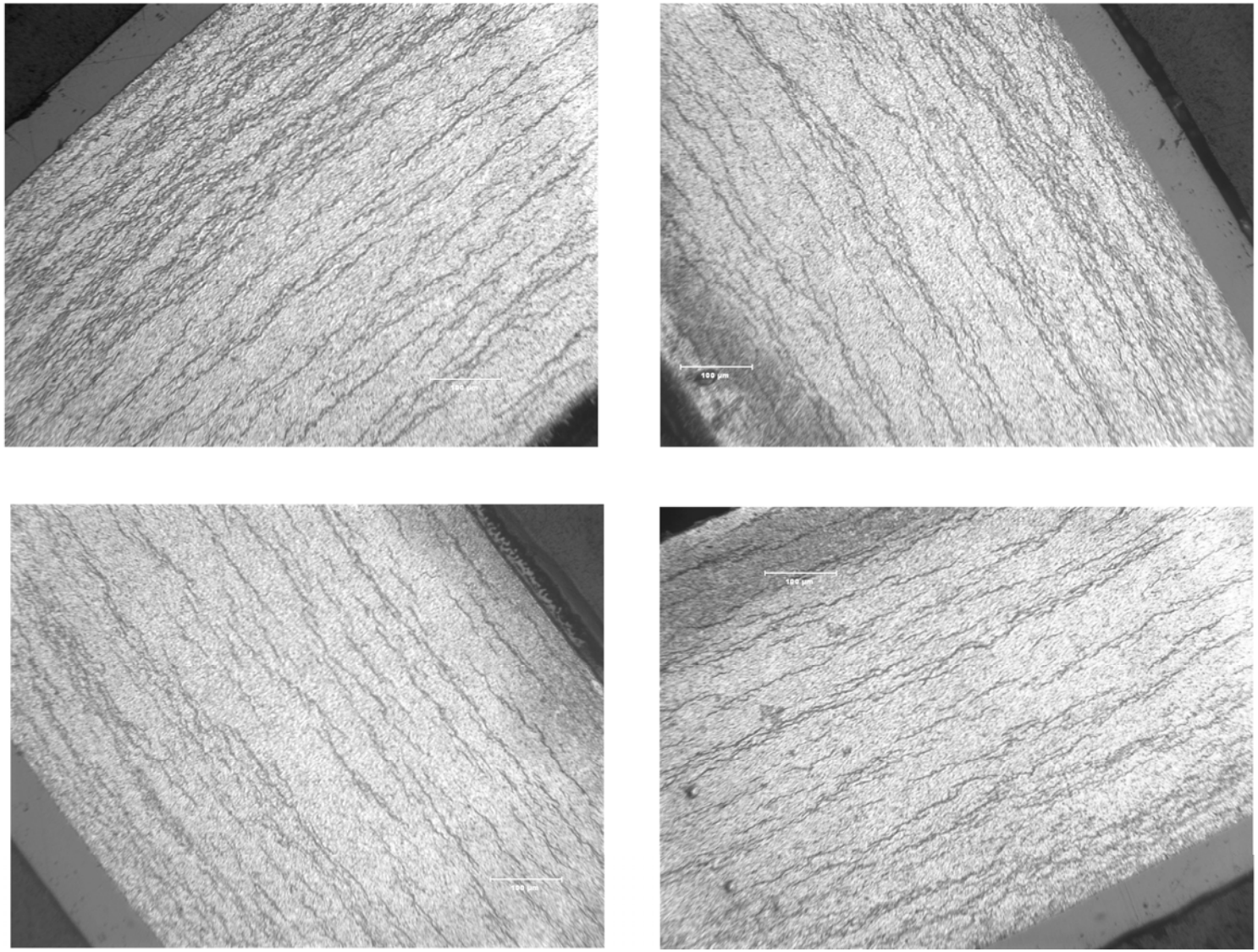

Fig. 2. Partial redistribution of circumferential hydrides for HBR cladding following stress-free annealing at 420°C for 20 hours.

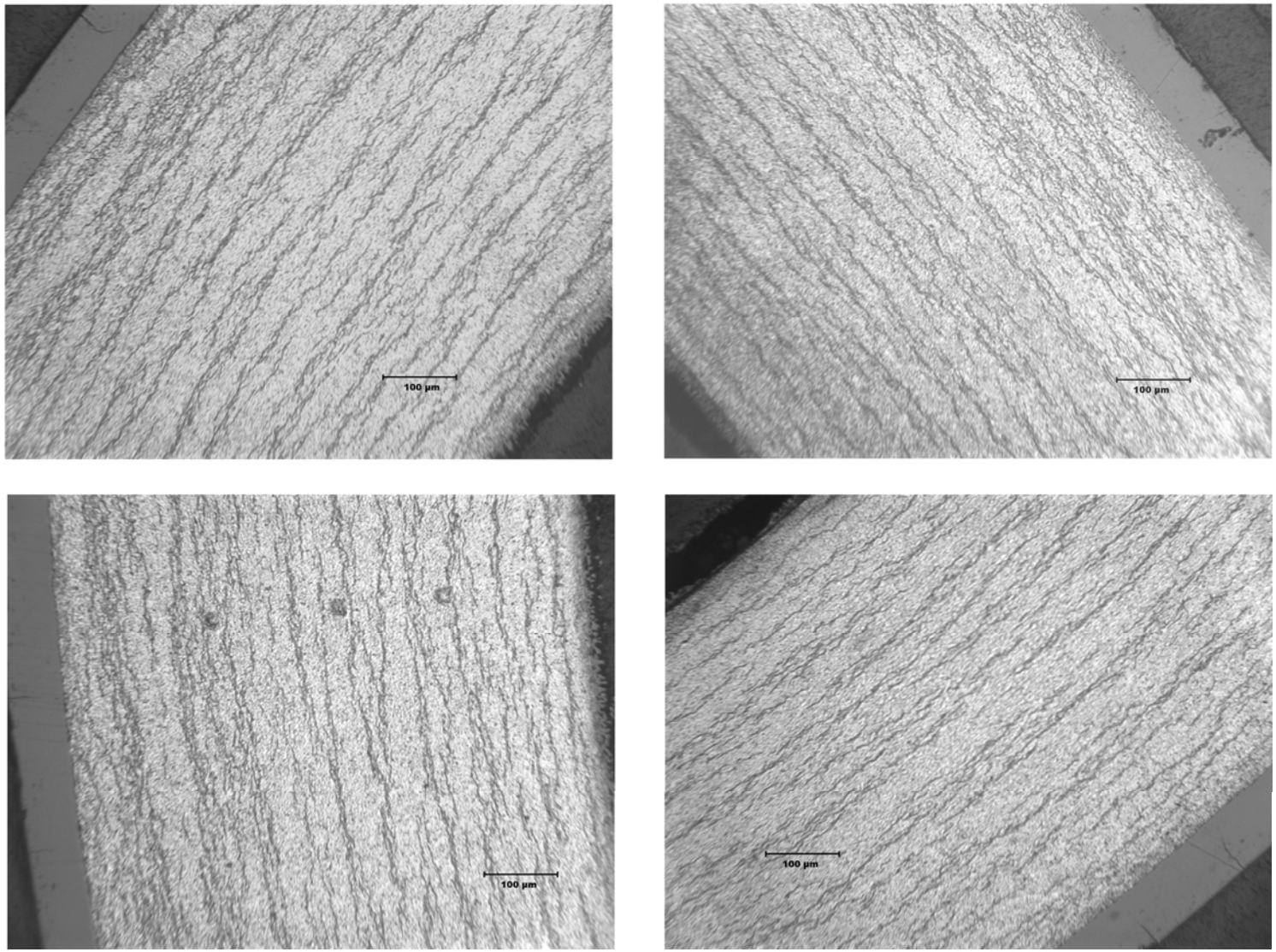

Fig. 3. Partial redistribution of circumferential hydrides for HBR cladding following stress-free annealing at 450°C for 2 hours. Notice that redistribution is more extensive than what is shown in Fig. 2 for 20-hour annealing at 420°C.

2 Introduction

2.1 Test results for pre-hydrided unirradiated cladding alloys

Prior to conducting radial-hydride treatment (RHT) and embrittlement studies with high-burnup cladding rodlets, a large number of tests were conducted with pre-hydrided Zry-4 and ZIRLO cladding. Variables in the test matrix included hydrogen concentration, hoop-stress level at 400°C, and number of heating-cooling cycles. Pressurized and sealed rodlets were heated to 400°C, held at 400°C for one hour, cooled from 400°C to 200°C at 5°C/h, and cooled at a faster rate from 200°C to RT (see Fig. 4 for 1-cycle cooling). The purpose of these tests was to narrow the test matrix for comparable tests using high-burnup ZIRLO and Zry-4 samples and to determine a radial-hydride metric that correlated with embrittlement. Following cooling under stress, rings were sectioned from the pressurized rodlets for hydrogen analysis, metallography, and ring-compression testing. Ring compression tests were conducted at 150°C and RT and at a displacement rate of 5 mm/s to a maximum displacement of 2 mm based on Instron 5566 settings. The 2-mm Instron-recorded displacement corresponded to a ring displacement of about 1.7 mm. Rings were assessed as "brittle" if a crack penetrated >50% of the wall thickness. This is based on the ability of the cladding to withstand internal pressure during crush-type loading simulated by the ring-compression test. Samples which exhibited no cracks or cracks penetrating ≤50% of the wall were assessed as "ductile." Both load-displacement curves and visual inspections under low magnification were used to determine if cracking had occurred. If the load-displacement curve indicated cracking that could not be detected at low magnification, then high magnification metallography was used to assess the crack location and depth.

The results indicated that radial-hydride-induced embrittlement increased with increasing hoop stress and decreasing hydrogen content. The effects of temperature cycling were secondary compared to the effects of high hoop stress and low hydrogen content. It was also observed that the radial-hydride continuity factor (RHCF) across the cladding wall was the best metric for correlating hydride morphology with embrittlement. The RHCF is the fraction of cladding wall within a 150-µm arc length for which radial hydrides form a continuous path (see Appendix A).

For samples cooled from 400°C and 150-MPa hoop stress, the ductile-to-brittle transition hydrogen content was 275±25 wppm. For samples cooled from 400°C and 135-MPa hoop stress, the ductile-to-brittle transition hydrogen content was 200±20 wppm. Below these transition hydrogen contents, the RHT ZIRLO behaved in a brittle manner at 150°C. However, for ZIRLO cooled from 400°C at 120-MPa hoop stress, the material remained ductile at 150°C for hydrogen contents as low as about 110 wppm. The results obtained from ring-compression testing of Zry-4 and ZIRLO at 150°C and 5 mm/s are shown in Fig. 5. These results were used to determine that the internal pressure for high-burnup cladding should be limited such that the wall-averaged hoop stress would be <135 MPa at 400°C.

The pass-fail criterion described above is overly conservative in that it does not give credit for rings that may have exhibited plastic flow prior to crack initiation. In Figure 6, the offset strain prior to crack initiation is plotted vs. hydrogen content for hoop stresses of 150, 135, and 120 MPa at 400°C. The results can be used to assess high-burnup cladding performance following RHT. For ZIRLO cladding, offset strains ≥10% indicate high ductility.

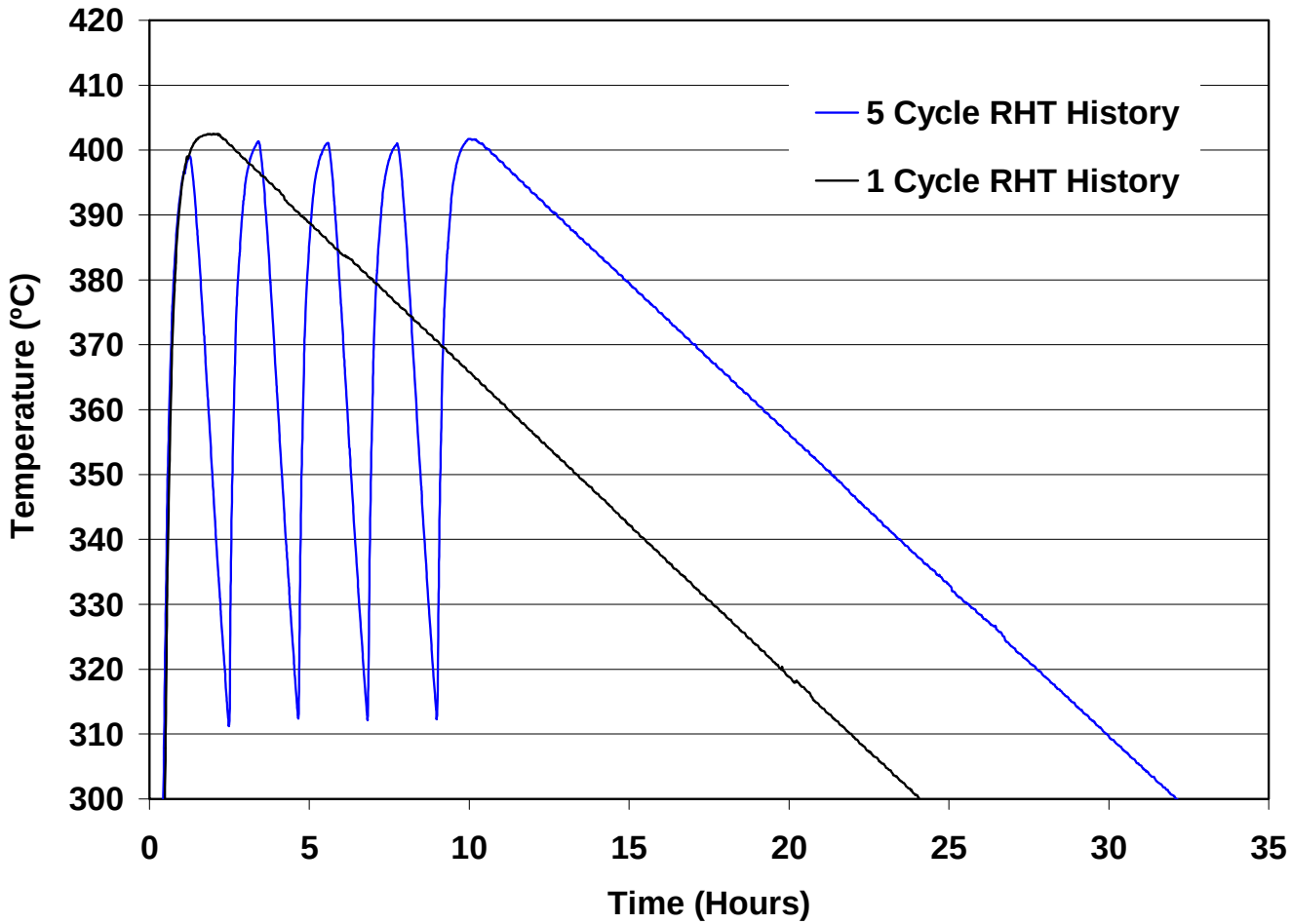

Fig. 4. Temperature histories for the reference one heating-cooling cycle for pressurized rodlets and for five heating-cooling cycles.

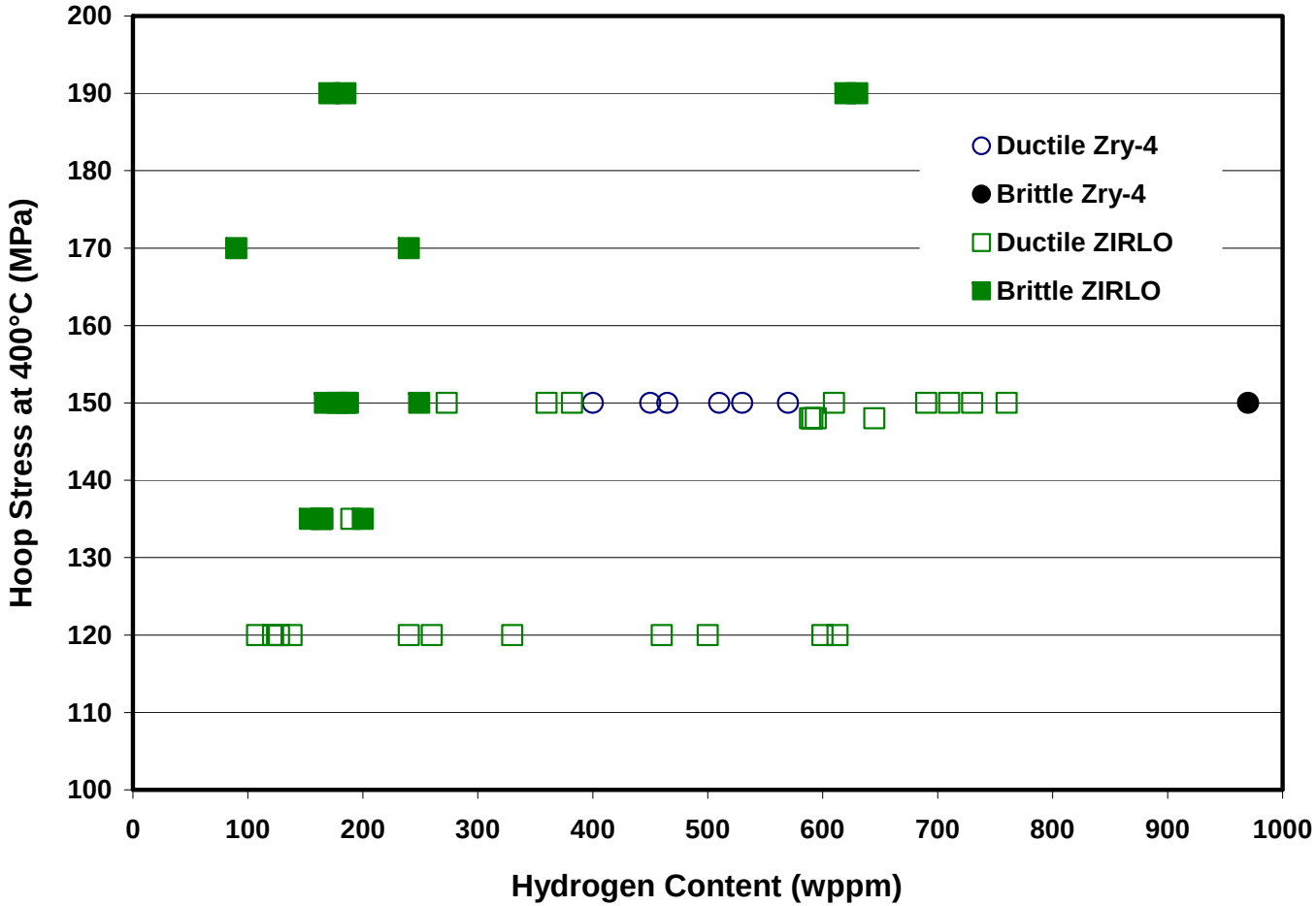

Fig. 5. Data summary for pre-hydrided and radial-hydride-treated Zry-4 and ZIRLO. Open symbols represent samples that survived the ring-compression tests at 150°C with no cracking (most open symbols) or with ≤50% through-wall cracking. The displacement rate was 5 mm/s and the pre-set maximum displacement for the Instron 5566 was 2 mm, which resulted in a sample displacement of 1.6-1.8 mm depending on the outer diameter (9.50-10.9 mm) of the ring.

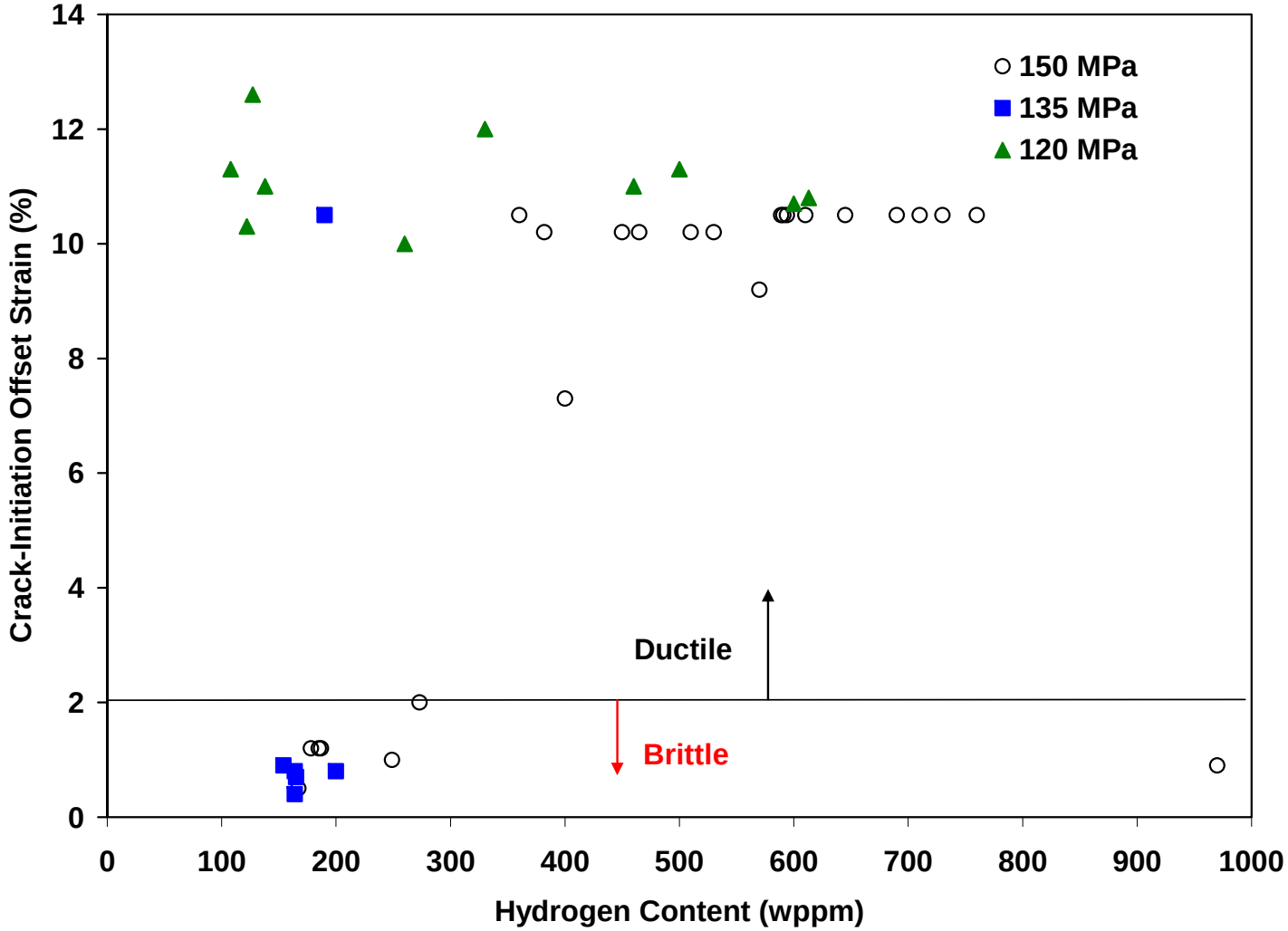

Fig. 6. Offset displacement prior to crack initiation for Zry-4 and ZIRLO rodlets pre-hydrided and subjected to cooling from 400°C at 5°C/h at the indicated hoop stresses (120 MPa, 135 MPa, and 150 MPa) at 400°C just before cooling. Ring compression tests were conducted at 150°C and at a displacement rate of 5 mm/s to a maximum Instron 5566 displacement of 2 mm. All but one of the samples with >7% offset strain exhibited no signs of crack formation. Thus, these values are lower bounds.

For one of the ZIRLO rings sectioned from a 135-MPa RHT rodlet, the load-displacement curve showed no dips indicative of cracking (see Fig. 7). Yet, visual inspection under low magnification indicated possible partial wall cracks at one end, for which the hydrogen content was about 170 wppm. The 8-mm-long ring was sectioned into two 4-mm-long rings: one for metallographic imaging of the suspect end and one for hydrogen analysis. The sub-ring away from the suspect end had 205-wppm hydrogen. Because of the stresses induced in the cladding during met mount preparation (i.e., epoxy drying), the cracks imaged are wider and longer than the cracks formed during ring compression testing. Thus, the results give an upper bound on crack extension into the wall of the cladding. Figure 8 shows the crack extension into the cladding wall at the end (Fig. 8a), at 1 mm into the sample (Fig. 8b) and at 2 mm into the sample (Fig. 8c). Thus, the corresponding crack lengths were <55%, <40%, and <20% of the wall, respectively, prior to met mount preparation. Based on these results, the ring with 190±20 wppm was assessed as ductile in the sense that no local end crack extended >50% into the cladding wall.

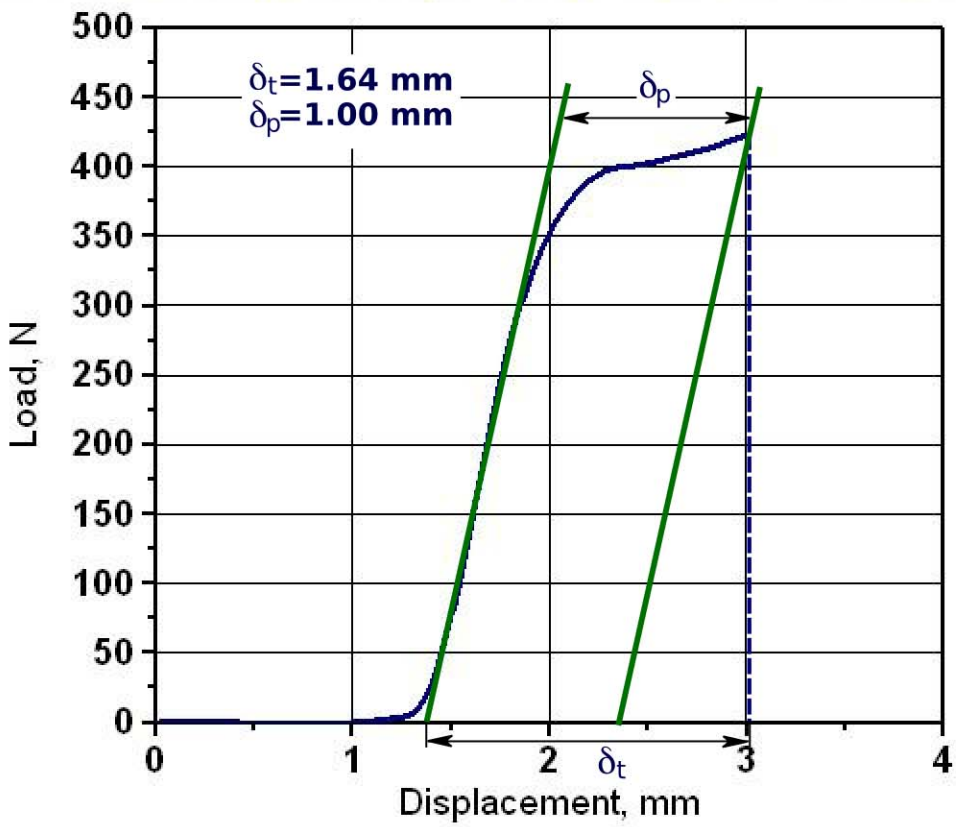

Fig. 7. Load-displacement curve for a ring sectioned from a pre-hydrided ZIRLO rodlet with 190±20 wppm hydrogen and subjected to cooling from 400°C and 135-MPa cladding hoop stress at 5°C/h under conditions of decreasing hoop stress. The ring-compression test was conducted at 150°C and at a displacement rate of 5 mm/s.

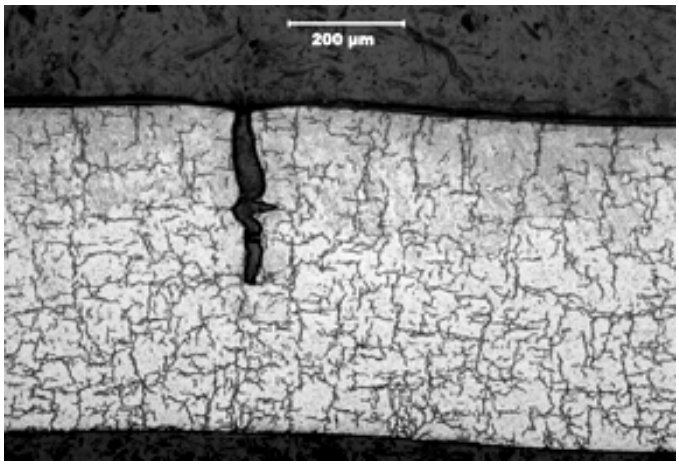

(a) end of ring 8; RHCF = 70%

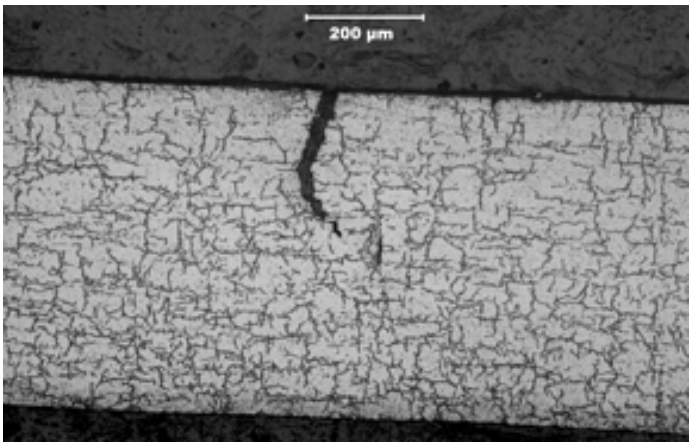

(b) about 1 mm from end of ring 8; RHCF = 57%

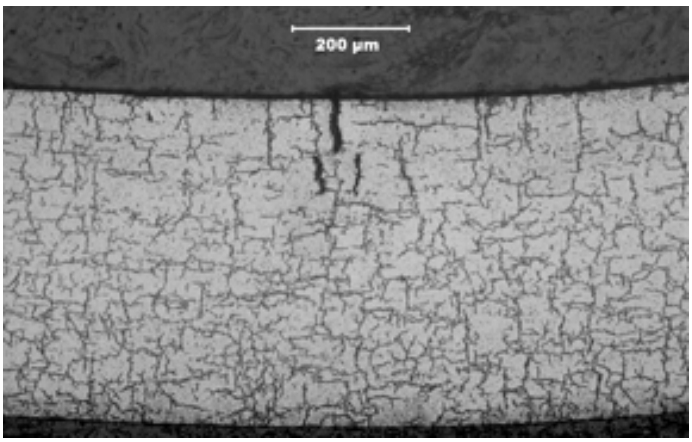

(c) about 2 mm from end of ring 8; RHCF = 30%

Fig. 8. Cross sections of ZIRLO ring 109D5C8B, which was radial-hydride treated during 5°C/h cooling from 400°C at 135-MPa hoop stress and then ring-compressed at 5 mm/s and 150°C: (a) end of ring with ID crack ≈55% deep; (b) about 1 mm from end with ID crack ≈40% deep; and (c) about 2 mm from end with ID crack <20% deep.

For most post-RHT ring-compression samples, interpretation of results was easy: samples with low RHCF exhibited no cracking; and samples with high RHCF cracked through most of the cladding wall with crack-initiation offset strains <2%. In the ductile-to-brittle transition region, interpretation of results was more intricate. The 150-MPa RHT ring with 273±40 wppm hydrogen had 2% offset strain prior to crack initiation. The ring was assessed as ductile because the crack grew through only 50% of the wall. Thus, the success criterion for ZIRLO RHT samples is ≥10% offset strain prior to crack initiation *or* ≤50% through-wall crack after the test.

2.2 Expected differences between high-burnup and pre-hydrided cladding samples

The major difference between high-burnup cladding and pre-hydrided cladding is the gradient in hydride density and hydrogen content across the cladding wall. Relative to pre-hydrided cladding, high-burnup cladding is characterized by very high hydride density at the outer metal surface and very low hydride density from the mid-wall to the inner cladding surface. Secondary differences are: (a) about 50 to 100 wppm of the hydrogen in the cladding is trapped in irradiation-induced defects and is not available for precipitation; and (b) the matrix metal has lower ductility than as-fabricated cladding due to irradiation-induced hardening.

Figure 9 shows the axial locations of North Anna ZIRLO Rod AM2-L17 from which Studsvik sectioned and defueled 80-mm-long cladding segments for ANL. The rod averaged burnup for AM2-L17 was 70 GWd/MTU. This rod was irradiated for four reactor cycles. Segments 1 (648A), 2 (648B), 5 (648E), 6 (648F), and 8 (648H) were used for LOCA embrittlement testing. Segments 3 (648C), 4 (648D), and 7 (648G) were selected for rodlet fabrication and RHT. Characterization results are summarized in Table 1 for corrosion layer thickness determined from eddy current and metallography and for hydrogen content.

The hydrogen content results given in Table 1 are not corrected for the masses of the corrosion and fuel cladding bond layers or for the hydrogen that may be in the corrosion layer. As shown in Ref. 1, the two effects essentially cancel each other out such that the reported values in Table 1 are approximately the average weight fraction of hydrogen in the cladding metal. This was the case for segments 648A and 648B for which the corrosion layer was ≤30 µm. For cladding samples with ≥40-µm corrosion layers, hydrogen content in the metal was determined to be 10-80 wppm less than the hydrogen content measured for the corroded cladding.

Figure 10 is a composite of 8 metallographic images for a cladding cross section from 648F for which the hydrogen content in an adjacent ring was measured to be 657±148 wppm. The radial variation in hydride density and hydrogen content is of no interest in LOCA testing and interpretation of results. Hydrogen redistributes rapidly across the radius during the LOCA heating ramp to >900°C. However, it is of great interest in determining the drying conditions that may lead to radial-hydride-induced embrittlement. Based on equilibrium conditions, the hydrogen content in the cladding metal away from the hydride rim should be about 200 wppm after sufficient time at 400°C. Some of this 200 wppm would come from hydrogen present in the metal between the hydride rim and the cladding inner surface. However, based on annealing studies using cladding from H. B. Robinson high-burnup fuel rods (see Figs. 2 and 3), the hydrogen content within the inner half of the cladding is expected to be <100 wppm after one-cycle heating-cooling with a one-hour hold time at 400°C.

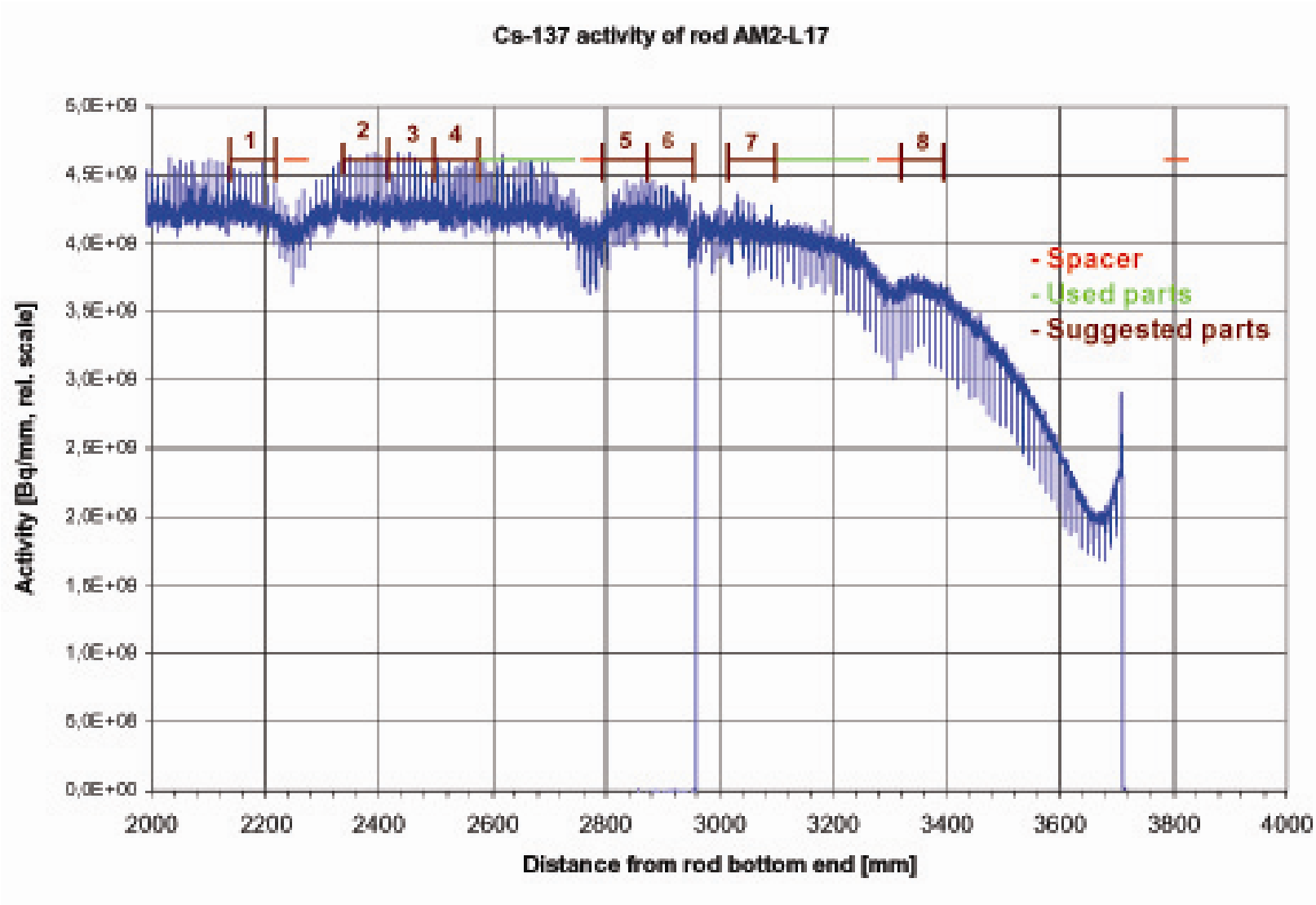

Fig. 9. Sectioning diagram for North Anna ZIRLO defueled cladding segments sent to ANL from Studsvik in second shipment. Corresponding ANL ID numbers are 648A through 648H for segments 1 through 8.

Table 1 Summary of North Anna ZIRLO characterization results for Rod AM2-L17

Sample ID # W (ANL)	Location from Bottom mm	Corrosion Layer from Eddy Cur. (EC), µm	Corrosion Layer from Metallography, µm	LECO Hydrogen Content, wppm	Total Mass of H Samples, g	Local Variation in H, wppm
1 (648A)	2125-2205	25-28	26±1	310±32	0.53	275-348
2 (648B)	2325-2405	25-30	---	366±30	0.53	324-413
3 (648C)[a]	2405-2485	30-35	TBD	TBD	TBD	TBD
4 (648D)[a]	2485-2565	35-40	TBD	TBD	TBD	TBD
5 (648E)	2800-2880	38-42	---	560±140	0.55	414-761
6 (648F)	2880-2960	43-48	41±3 43±2	620±140	0.55	385-840
7 (648G)[a]	3020-3100	48-52	TBD	TBD	TBD	TBD
8 (648H)	3320-3400	40-45	---	670±40	0.1	607-694

[a]Characterization will be performed after radial-hydride treatment in argon: ramp to 400°C in about 45 minutes, hold at 400°C for an hour at 100-140 MPa hoop stress, and cool at 5°C/h under decreasing stress.

Figure 11 shows the hydride morphology at two circumferential locations for a cladding cross section from 648A for which the hydrogen content in an adjacent ring was measured to be 318±30 wppm. The hydride morphology in Fig. 11a is typical of seven of the eight locations imaged. The morphology in Fig. 11b is interesting because radial hydrides are observed at the inner cladding surface in the as-irradiated condition. For both high (Fig. 10) and low (Fig. 11) hydrogen contents, most of the hydrogen resides in the rim at the outer cladding surface

Reference

1. Y. Yan, T. A. Burtseva, and M. C. Billone, "Post-quench Ductility Results for North Anna High-burnup 17×17 ZIRLO Cladding with Intermediate Hydrogen Content," ANL letter report to NRC, April. 17, 2009; available online in NRC ADAMS as ML091200702 at http://www.nrc.gov/NRC/reading-rm/adams.html

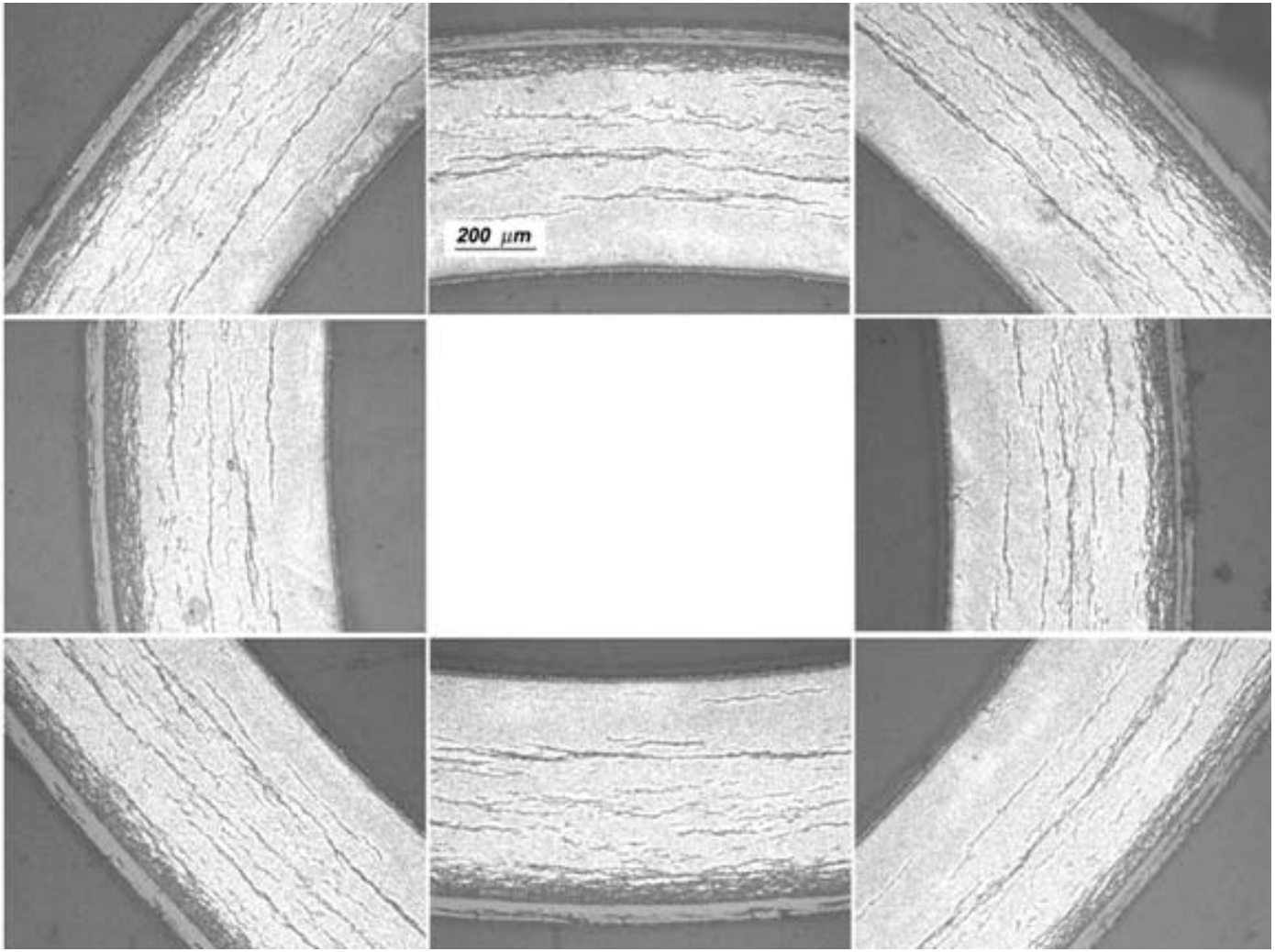

Fig. 10. Images at eight locations around the circumference of the cladding cross section at ≈2910 mm from the rod bottom showing radial and circumferential variation in hydride density. The cladding metal-wall thickness (544±2 μm), as well as the corrosion-layer (43±2 μm) and fuel-cladding-bond (7±2 μm) thickness, is relatively uniform. The hydrogen content measured in an adjacent ring was 657±148 wppm.

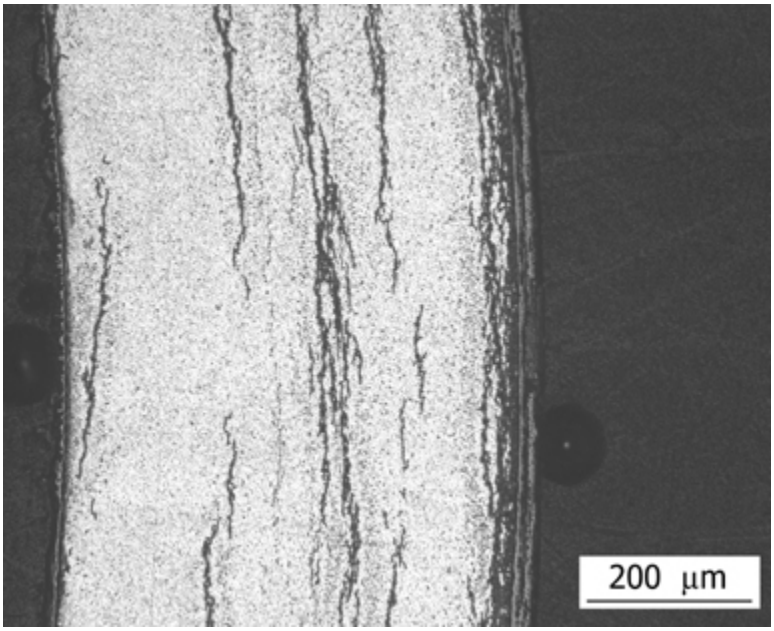

(a) Circumferential hydrides

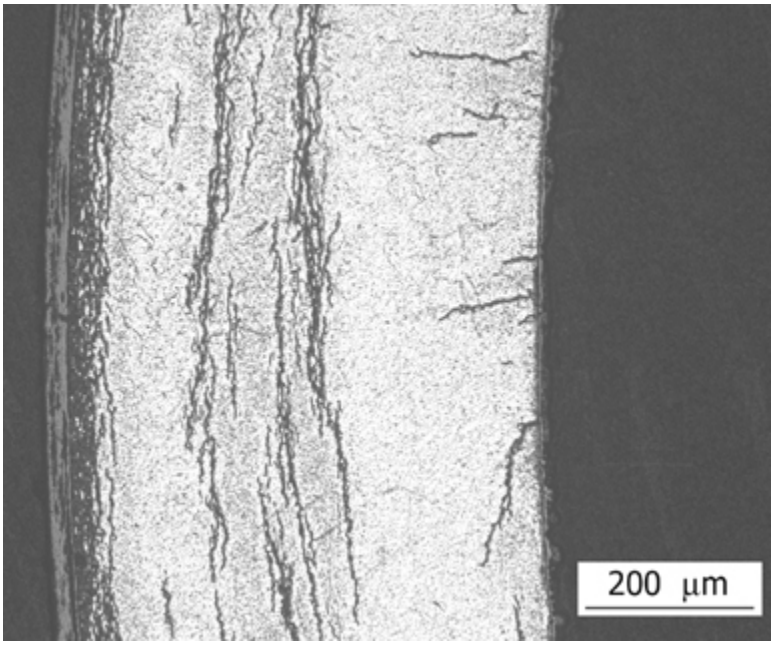

(b) Circumferential and radial hydrides

Fig. 11. Hydride morphology for 648A sample with 318±30 wppm hydrogen based on measurements for an adjacent ring: (a) circumferential hydrides (typical); and (b) circumferential and radial hydrides (one of eight locations).

3 Test Matrix and Post-RHT Characterization Results

3.1 Test matrix

The test matrix for high-burnup ZIRLO rodlets is given in Table 2. The first two tests have been completed. Conditions for the third test will be determined based on close interpretation of the results for the first two tests. The target hoop stress for the 648G rodlet was 130 MPa. The RT pressure of 8.0 MPa was chosen to give a wall-averaged hoop stress of 130 MPa at 400°C based on the dimensions of as-fabricated cladding (9.50-mm OD and 0.57-mm wall thickness). Following RHT, the metal outer diameter and wall thickness were determined from micrometer readings and quantitative metallographic results. For 648G, the actual hoop stress was 140 MPa. The 648D rodlet was pressurized to 6.4 MPa based on anticipated metal-wall outer diameter and wall thickness for corroded cladding. Both the target and actual hoop stress at 400°C were 110 MPa. The stress analysis for these rodlets is documented in Appendix B.

Table 2. Test matrix for radial-hydride treatment of high-burnup ZIRLO rodlets cooled at 5°C/h from 400°C. One-cycle heating-cooling refers to one-hour heat-up to 400°C, one-hour hold at 400°C, and cooling at 5°C/h (see Fig. 4).

Test # (Rodlet ID)	Estimated (Actual) H-content, wppm	RT Pressure, MPa	400°C Pressure, MPa	Target Hoop Stress at 400°C	Actual Hoop Stress at 400°C	Cooling Cycles
1 (648G)	650 (650±190)	8.0	17.9	130	140	1
2 (648D)	500 (425±23)	6.4	14.3	110	110	1
3 (648C)	400 (TBD)	TBD	TBD	TBD	TBD	TBD

3.2 Post-RHT characterization of rodlet 648G

Figure 12 shows the sectioning diagram for rodlet 648G. Following 1-cycle RHT, rings were sectioned for hydrogen analysis (5), for ring-compression testing (4) and for metallographic imaging (2). The hydrogen content results are shown in Fig. 12. In addition to these measurements, the hydrogen content of Ring #10 was measured to be 630±90 MPa following ring-compression testing. The weighted-average hydrogen content based on 1.71 g of samples was 650±190 wppm with minimum and maximum values of 474 and 1161 wppm, respectively, based on quarter-arc segments at multiple axial locations.

Metallographic images were obtained for Rings #7 and #8 at the indicated surfaces. These positions corresponded to the rodlet mid-span and 12 mm from the mid-span. Hydride morphology and metal wall thickness were determined from 100X images; corrosion-layer thickness was determined from 200X images. Images were obtained at 8 circumferential locations (see Appendix C for 100X images). Results are given in Table 3.

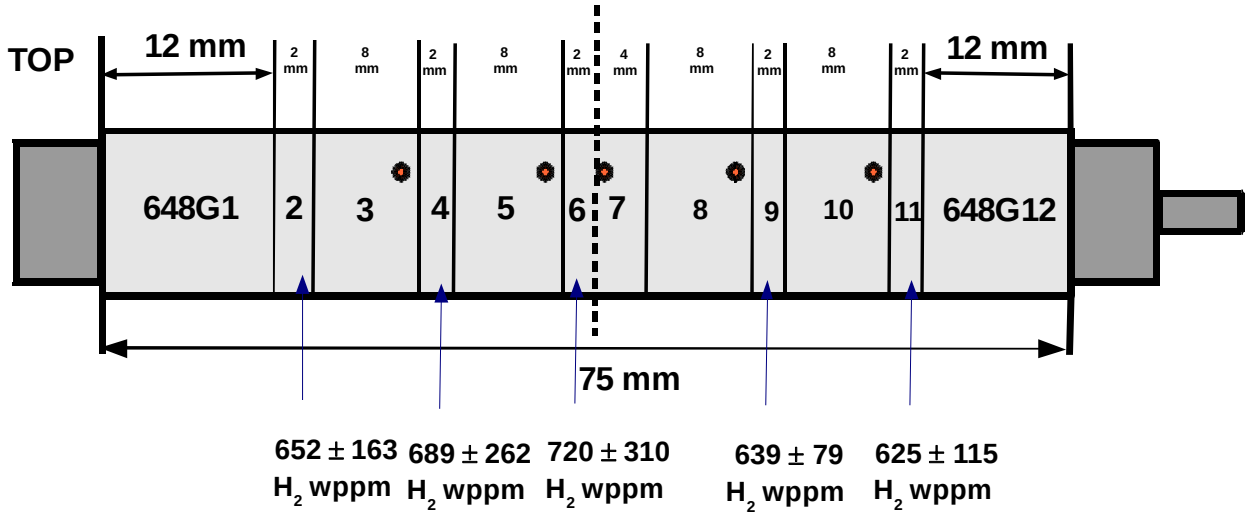

Fig. 12. Sectioning diagram for rodlet 648G, which was subjected to an RHT hoop stress of 140 MPa at 400°C prior to cooling at 5°C/s.

Table 3. Results of quantitative metallography for rodlet 648G following RHT: 140-MPa at 400°C, 5°C/h cooling, and 1-cycle cooling. D_o is the outer diameter of the corroded cladding, δ_c is corrosion layer thickness, D_{mo} is the outer diameter of the cladding metal, h_m is metal wall thickness, and RHCF is radial hydride continuity factor.

Ring #	D_o, mm	δ_c, μm	D_{mo}, mm	h_m, mm	RHCF, %
648G7	9.52	52±7	9.42±0.01	0.539±0.005	70±17
648G8	9.52	52±4	9.42±0.01	0.539±0.004	61±12

Figures 13 and 14, respectively, show regions of maximum and minimum RHCF for metallographic samples 648G7 and 648G8. It is evident from the hydride density and morphology that relatively little hydrogen redistributed across the cladding wall, while there is considerable reorientation of hydrides from circumferential to radial within the inner two-thirds of the cladding wall. With radial hydrides forming a continuous pathway within this region, along with the expected brittle behavior of the hydride rim and the corrosion layer, brittle behavior of the cladding is expected during ring-compression testing.

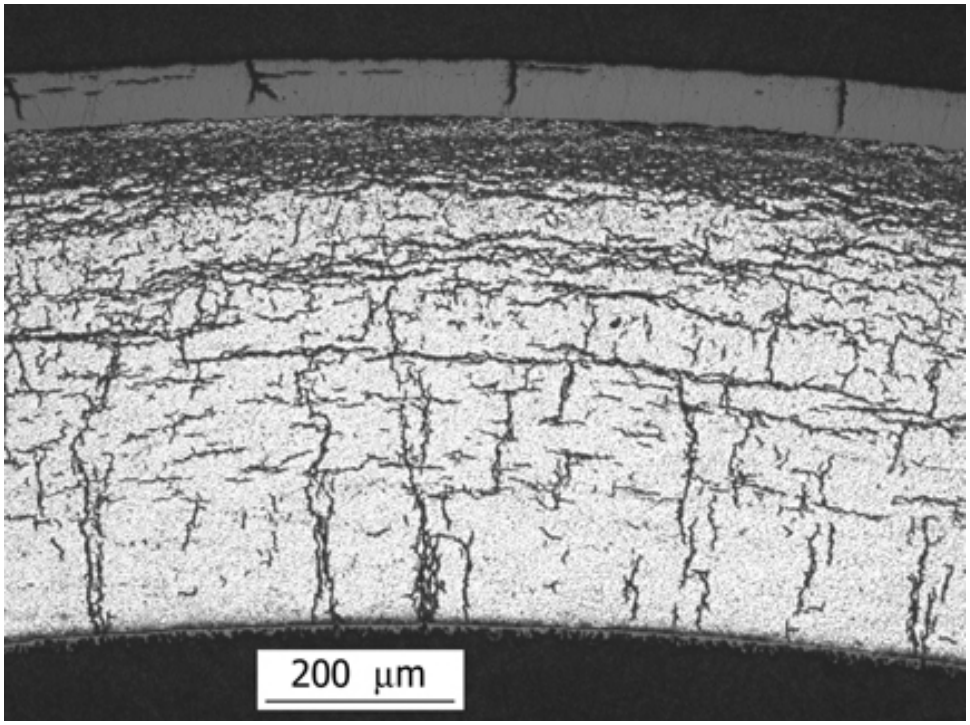

(a) RHCF = 80%

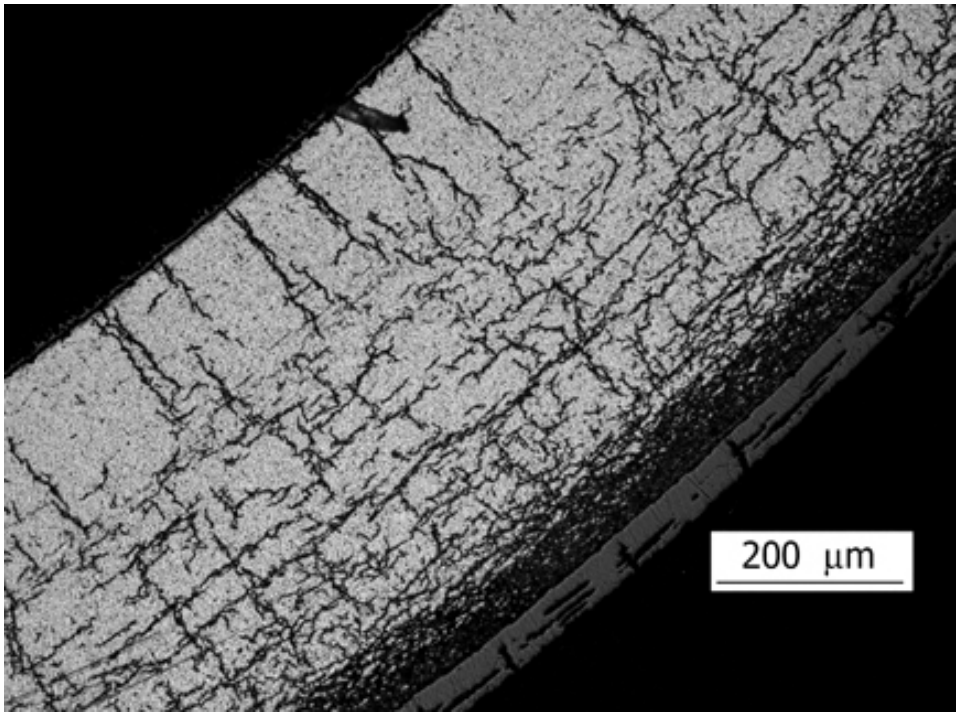

(b) RHCF = 38%

Fig. 13. Hydride morphology for 648G7 showing regions of: (a) high radial hydride continuity factor (RHCF); and (b) low RHCF. Images were taken following 1-cycle-cooling RHT at 5°C/h with 140-MPa hoop stress at 400°C. The hydrogen content for the ring adjacent to this interface was 720±310 wppm.

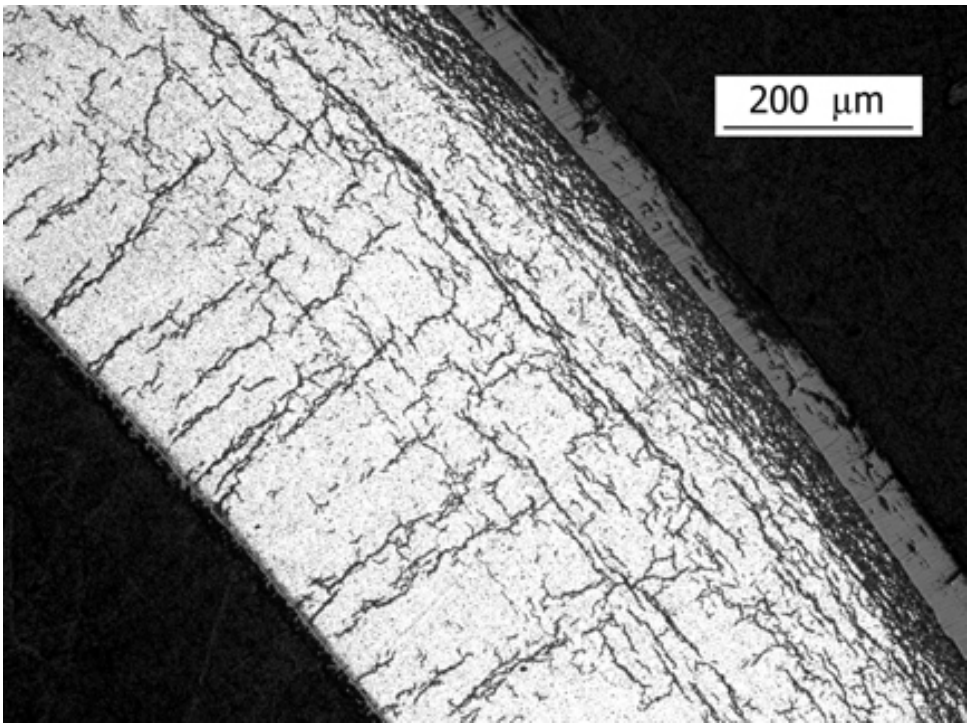

(a) RHCF = 70%

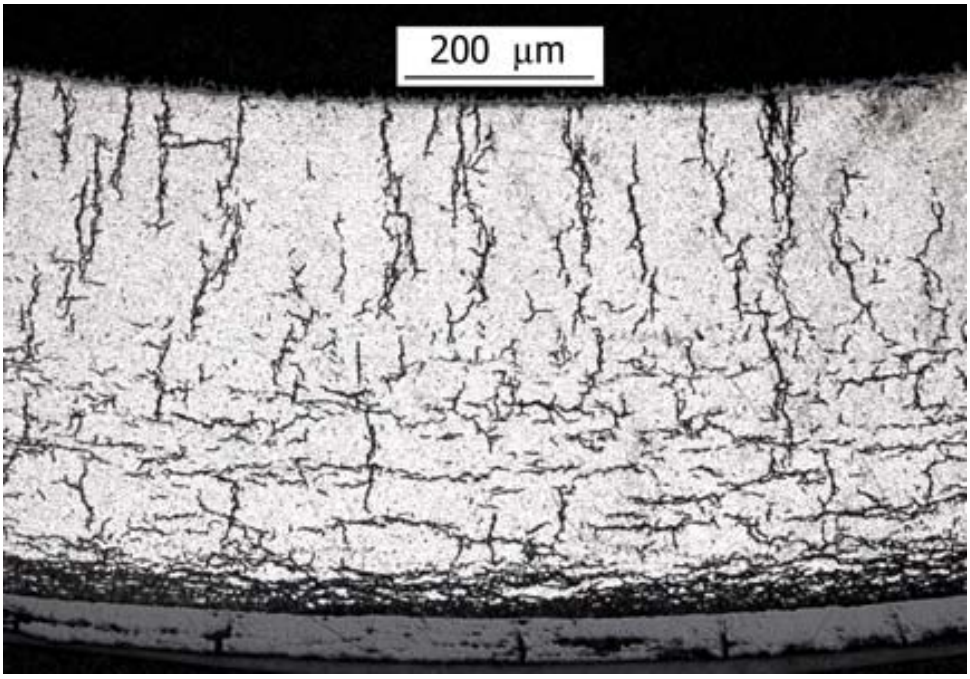

(b) RHCF = 46%

Fig. 14. Hydride morphology for 648G7 showing regions of: (a) high radial hydride continuity factor (RHCF); and (b) low RHCF. Images were taken following 1-cycle-cooling RHT at 5°C/h with 140-MPa hoop stress at 400°C. The hydrogen content for the ring adjacent to this interface was 630±90 wppm.

3.3 Post-RHT characterization of rodlet 648D

Figure 15 shows the sectioning diagram for rodlet 648D. Following 1-cycle RHT, rings were sectioned for hydrogen analysis (5), for ring-compression testing (4) and for metallographic imaging (1). The hydrogen content results are shown in Fig. 15. The weighted-average hydrogen content based on 0.76 g of samples was 425±63 wppm with minimum and maximum values of 362 and 543 wppm, respectively, based on quarter-arc-length segments.

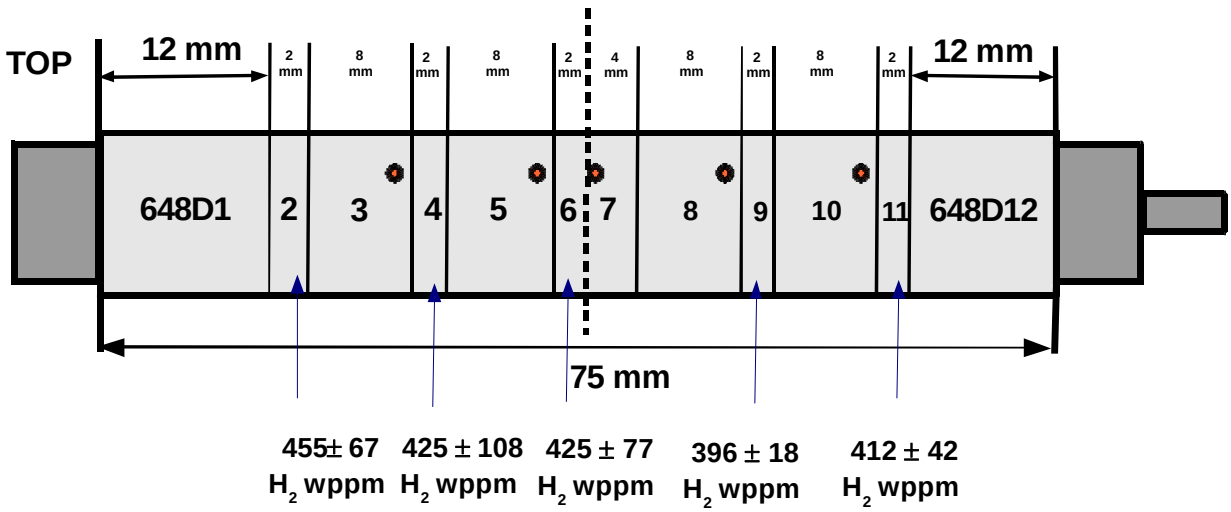

Fig. 15. Sectioning diagram for rodlet 648D, which was subjected to an RHT hoop stress of 110 MPa at 400°C prior to cooling at 5°C/s.

Metallographic images were obtained for Ring #7 at the rodlet mid-span. Hydride morphology and metal wall thickness were determined from 100X images; corrosion-layer thickness was determined from 200X images. Images were obtained at 8 circumferential locations (see Appendix C for 100X images). Results are given in Table 4.

Table 4. Results of quantitative metallography for rodlet 648D following RHT: 110-MPa at 400°C, 5°C/h cooling, and 1-cycle cooling. D_o is the outer diameter of the corroded cladding, δ_c is corrosion layer thickness, D_{mo} is the outer diameter of the cladding metal, h_m is metal wall thickness, and RHCF is radial hydride continuity factor.

Ring #	D_o, mm	δ_c, μm	D_{mo}, mm	h_m, mm	RHCF, %
648D7	9.51	33±3	9.44±0.01	0.555±0.002	27±10

Figure 16 shows regions of maximum and minimum RHCF for 648D7. It is evident from the hydride density and morphology that relatively little hydrogen redistributed across the cladding wall, while there is reorientation of hydrides from circumferential to radial within the inner third of the cladding wall. With radial hydrides forming a continuous pathway that is <50% of the cladding wall, ductile behavior of the cladding is expected during ring-compression testing.

Table 5 is an update of Table 1 showing the characterization results from 648G and 648D.

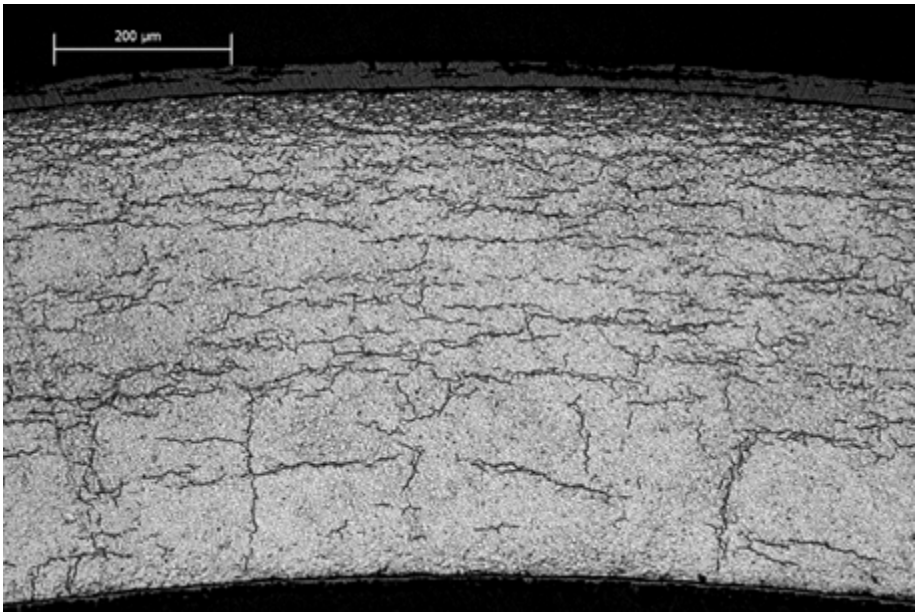

(a) RHCF = 48%

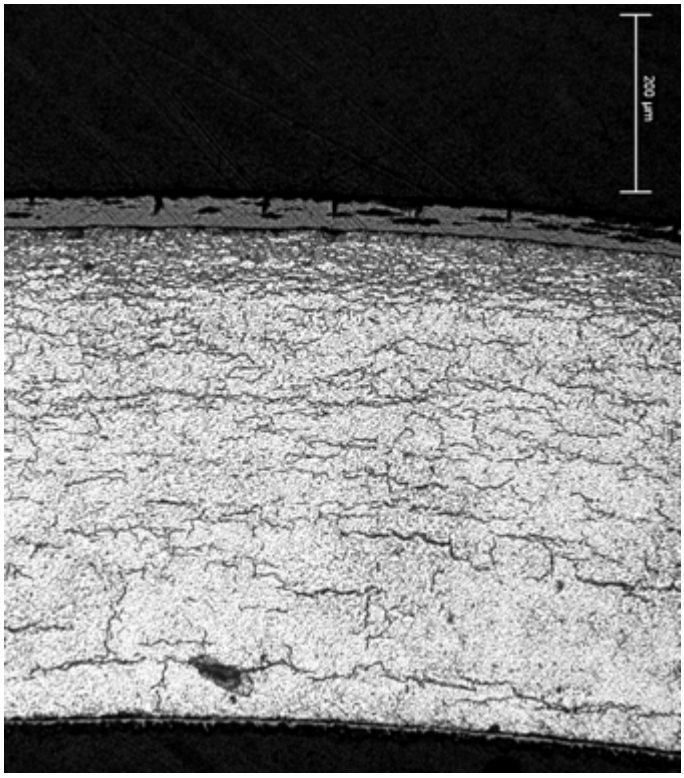

(b) RHCF = 18%

Fig. 16. Hydride morphology for 648D7 showing regions of: (a) high radial hydride continuity factor (RHCF); and (b) low RHCF. Images were taken following 1-cycle-cooling RHT at 5°C/h with 110-MPa hoop stress at 400°C. The hydrogen content for the ring adjacent to this interface was 425±77 wppm.

Table 5. Updated summary of North Anna ZIRLO characterization results for Rod AM2-L17

Sample ID # W (ANL)	Location from Bottom mm	Corrosion Layer from Eddy Cur. (EC), µm	Corrosion Layer from Metallography, µm	LECO Hydrogen Content, wppm	Total Mass of H Samples, g	Local Variation in H, wppm
1 (648A)	2125-2205	25-28	26±1	310±32	0.53	275-348
2 (648B)	2325-2405	25-30	---	366±30	0.53	324-413
3 (648C)[a]	2405-2485	30-35	TBD	TBD	TBD	TBD
4 (648D)[a]	2485-2565	35-40	33±3	425±63	0.76	362-543
5 (648E)	2800-2880	38-42	---	560±140	0.55	414-761
6 (648F)	2880-2960	43-48	41±3 43±2	620±140	0.55	385-840
7 (648G)[a]	3020-3100	48-52	52±7 52±4	650±190	1.71	474-1161
8 (648H)	3320-3400	40-45	---	670±40	0.1	607-694

[a]Characterization was performed after radial-hydride treatment in argon: ramp to 400°C in about 45 minutes, hold at 400°C for an hour at 110-140 MPa hoop stress, and cool at 5°C/h under decreasing stress.

4 Ring Compression Results

Ring compression tests were conducted with 648G Rings #5 and #10 (see Fig. 12) and with 648D Rings #3, #5, #8 and #10. The Instron 8511, which is enclosed in a glove box, was used to perform these tests. The tests were conducted with the same pre-set conditions as the Instron 5566 that was used to test pre-hydrided cladding: 5 mm/s displacement rate, 2-mm maximum displacement, and a test temperature of either 150°C or RT. Results are summarized in Table 6.

Table 6. Summary of ring compression results for rodlet 648G (140-MPa hoop stress at 400°C) and rodlet 648D (110-MPa hoop stress at 400°C). δ_p is the offset displacement prior to crack initiation. It is normalized to the metal outer diameter (D_{mo}) to give ductility in percent. σ_θ is the wall-averaged hoop stress at 400°C for RHT.

Rodlet (RHT σ_θ)	Ring #	H-Content, wppm	RHCF, %	Test T, °C	δ_p/D_{mo}, %	Assessment
648G (140 MPa)	5	700±270	70±11	150	0	2 cracks ≤90% **Brittle**
	10	640±80	61±12	150	1.4	3 cracks ≤100% **Brittle**
648D (110 MPa)	5	426±83	27±10	150	15	Cracks[a] **Ductile**
	8	414±56	27±10	150	13	1 Crack, >50% **Ductile**
	10	404±33	27±10	150	10	1 Crack, >50% **Ductile**
	3	443±83	27±10	20	0.6	4 Cracks, ≤95% **Brittle**

[a]Smooth load-displacement curve suggests that cracks occurred after the test. Data acquisition stops automatically at the end of the test at about 2-mm sample displacement. Loading platen remained fixed for about 20 s after this test, which maintained the ring at the final test load.

Load-displacement curves for the six ring-compression tests are shown in Figs. 17-22. Rings from rodlet 648G were clearly brittle. Figure 23 is a post-test photograph of Ring 648G5 showing cracks at the 12 o'clock (under load) and 6 o'clock (above support) positions. At these positions cracking initiates at the inner surfaces where the tensile stresses are highest and the radial hydrides are long. Ring 648G10 was not imaged because it was broken into two pieces.

For Ring 648D8, cracking occurred at the 3 o'clock position. Such cracks initiate from the outer surface and propagate towards the inner surface. Figure 24 shows a photograph of this sample. Ring 648D5 exhibited post-test cracks, but the load-displacement curve showed no evidence of cracking. It was concluded that the cracking occurred during the period from the end of the test (also, the end of data acquisition) and the time that the loading platen was raised above the ring. During these 20-30 seconds following the test, the ring remained under load while the position of the loading platen was fixed. As a result of this test, the Instron 8511 program was changed to unload the sample at 5 mm/s after test completion. The behavior of Ring #10 was similar to that of Ring #8. Ring #3, tested at RT, was very brittle (see Fig. 25).

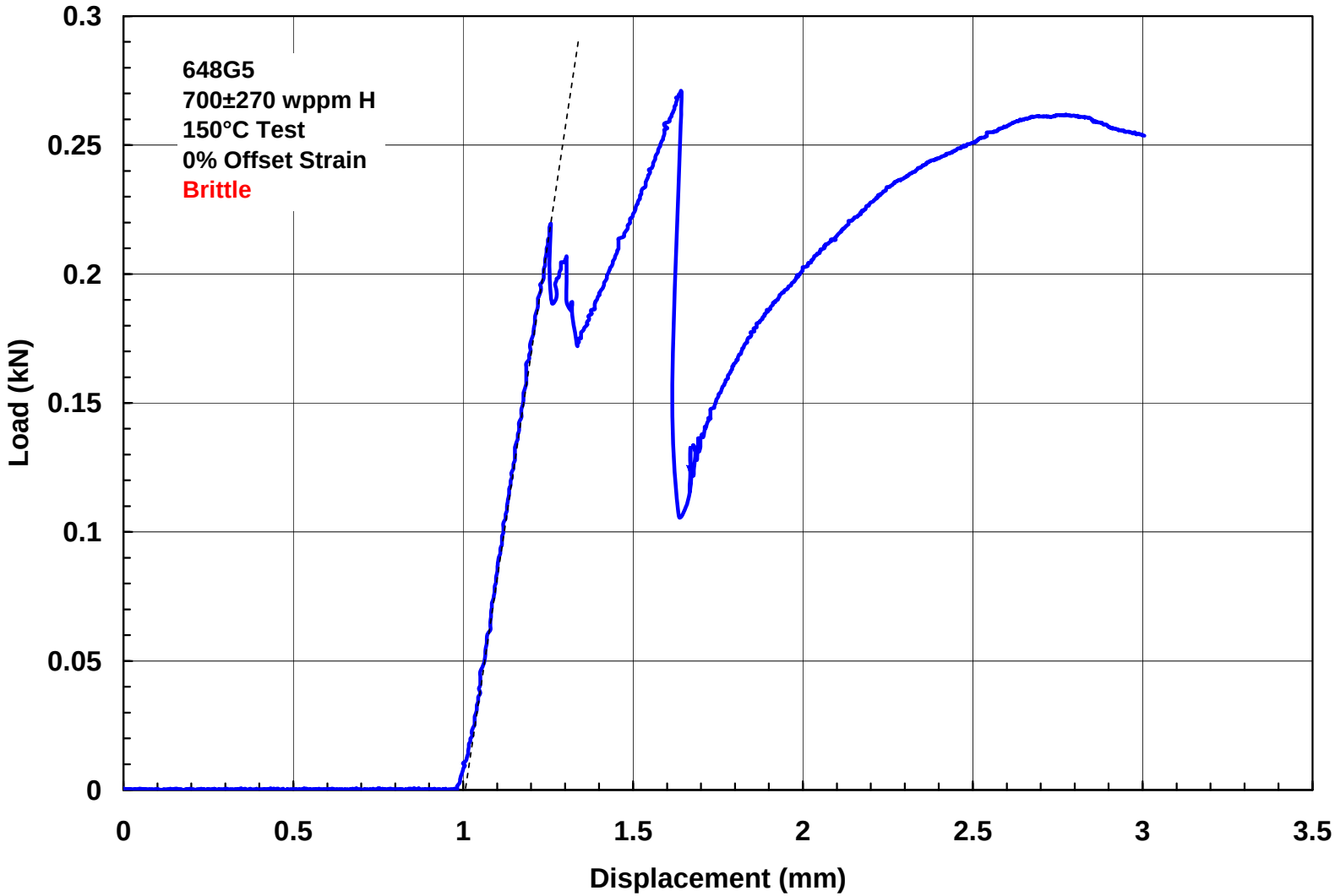

Fig. 17. Load-displacement curve for Ring #5 of RHT rodlet 648G, which was cooled from 400°C and 140 MPa at 5°C/h. The ring was brittle at 150°C and a displacement rate of 5 mm/s. Cracks developed at the 6 and 12 o'clock positions due to radial-hydride-induced embrittlement.

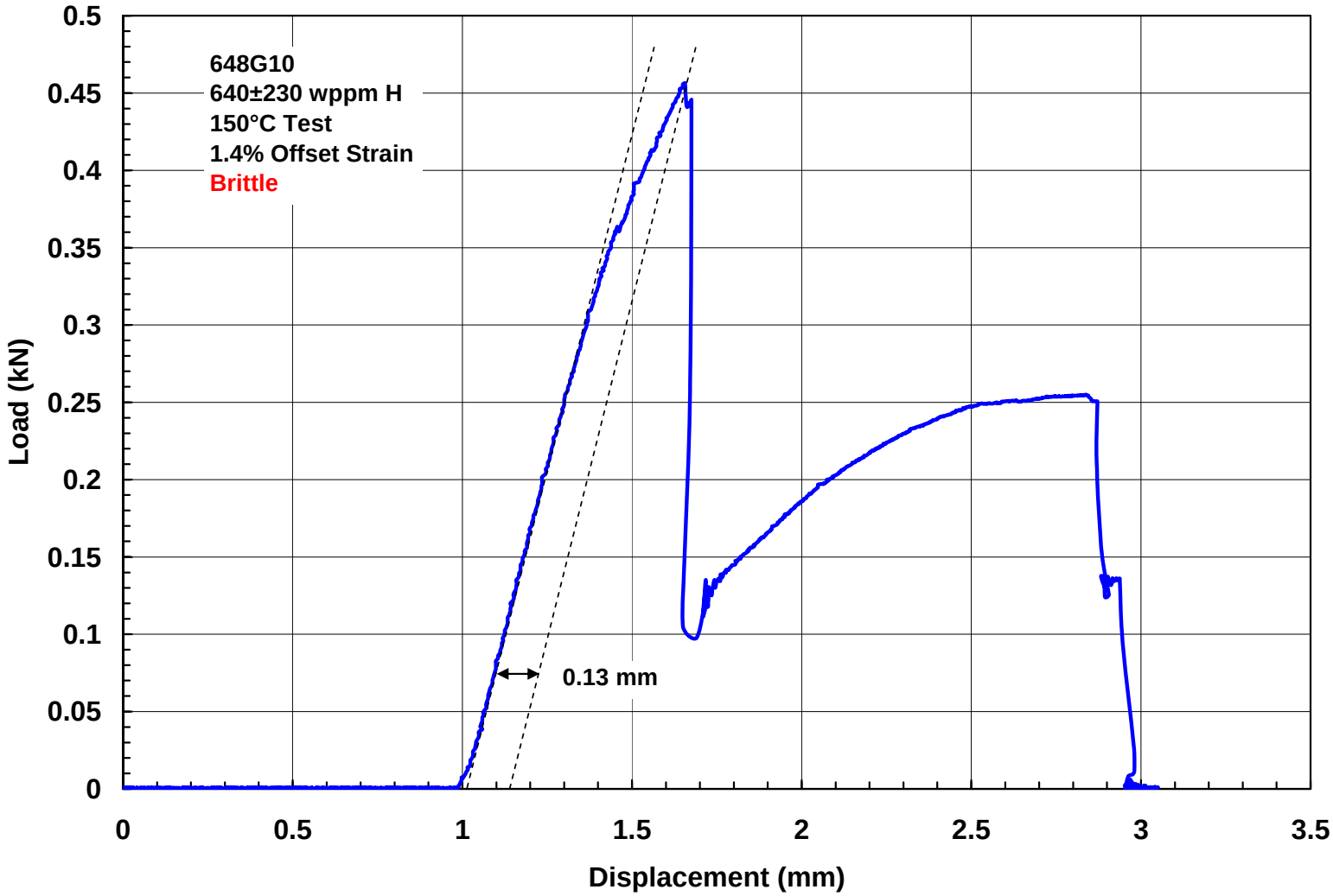

Fig. 18. Load-displacement curve for Ring #10 of RHT rodlet 648G, which was cooled from 400°C and 140 MPa at 5°C/h. The ring was brittle at 150°C and a displacement rate of 5 mm/s. Cracks developed at the 3, 6 and 12 o'clock positions due to radial-hydride-induced embrittlement. The ring was in two pieces at the end of the test.

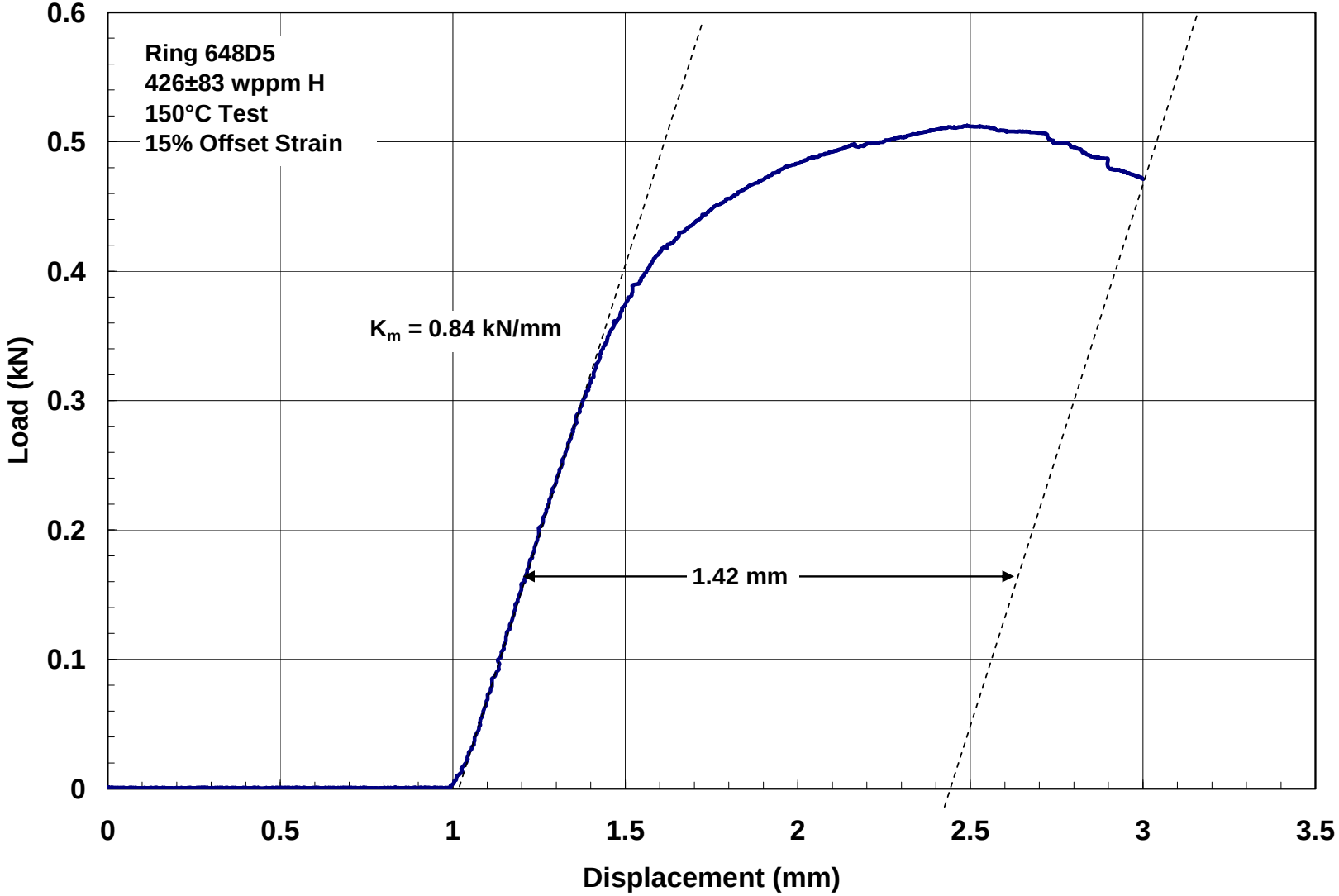

Fig. 19. Load-displacement curve for Ring #5 of RHT rodlet 648D, which was cooled from 400°C and 110 MPa at 5°C/h. The ring was highly ductile at 150°C and a displacement rate of 5 mm/s. Partial-wall cracks developed at the 3, 6, and 9 o'clock positions after completion of the test and before the unloading of the ring.

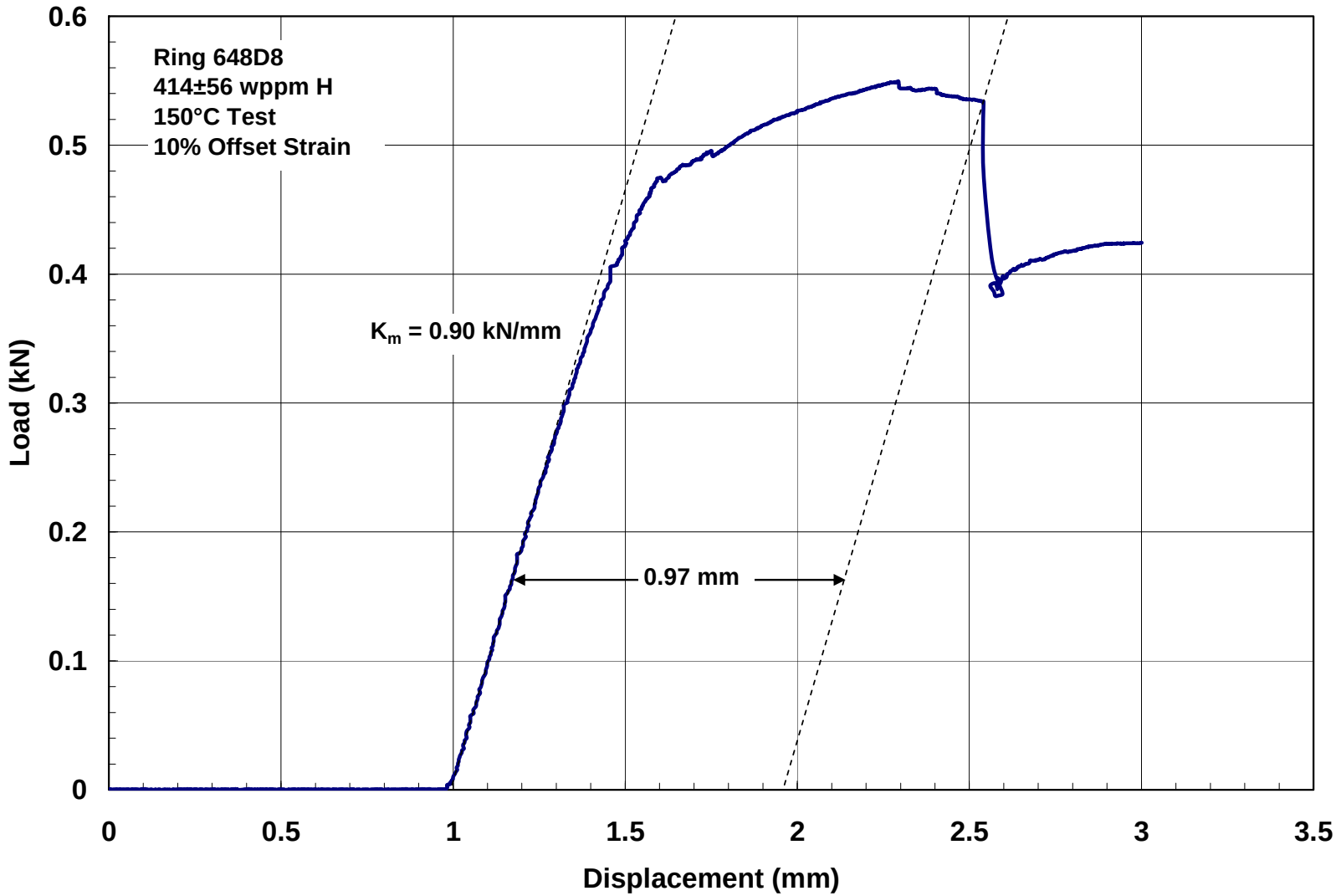

Fig. 20. Load-displacement curve for Ring #8 of RHT rodlet 648D, which was cooled from 400°C and 110 MPa at 5°C/h. The ring was highly ductile at 150°C and a displacement rate of 5 mm/s. A partial-wall crack developed at the 3 o'clock position after 10% offset strain.

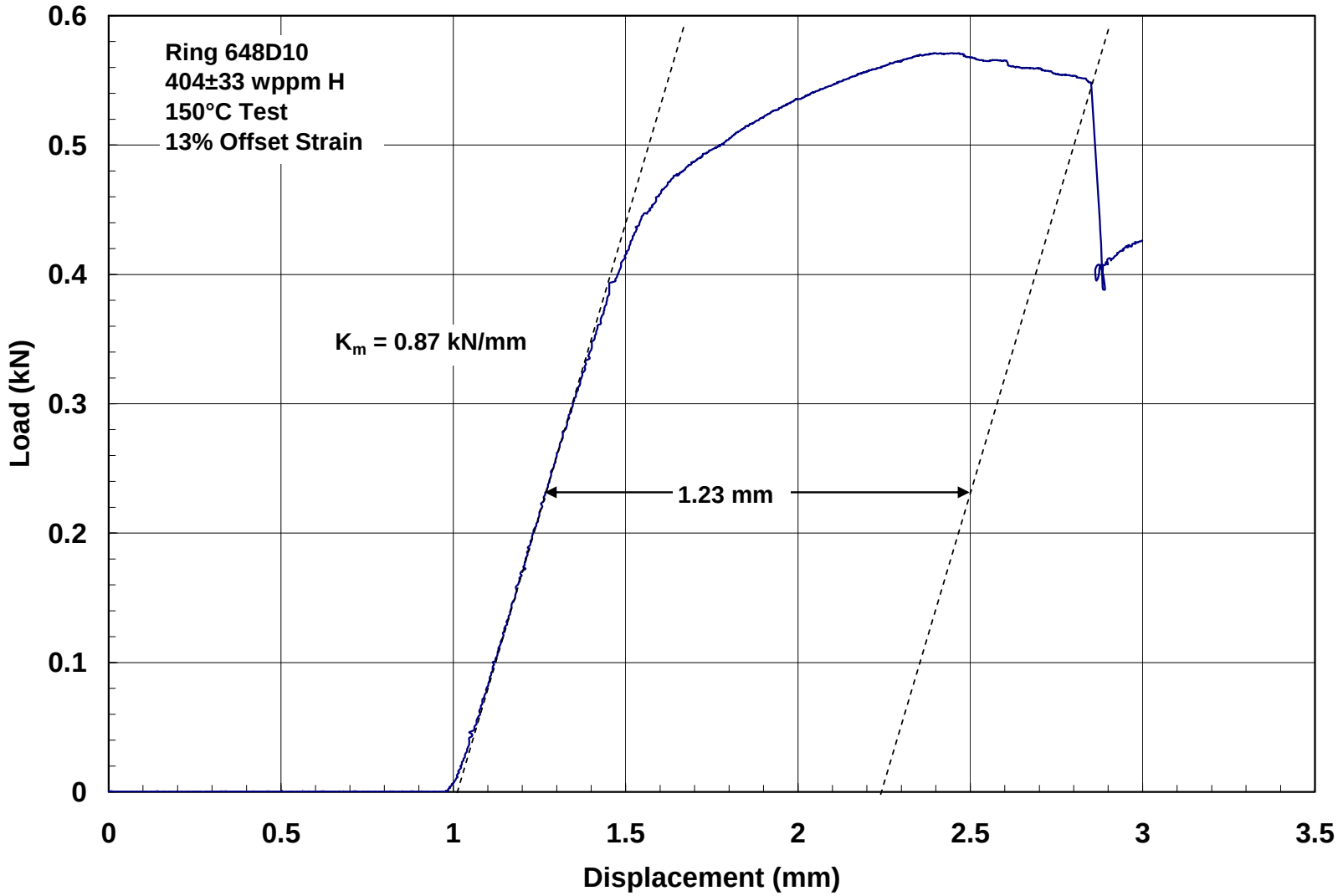

Fig. 21. Load-displacement curve for Ring #10 of RHT rodlet 648D, which was cooled from 400°C and 110 MPa at 5°C/h. The ring was highly ductile at 150°C and a displacement rate of 5 mm/s. A partial-wall crack developed at the 3 o'clock position after 13% offset strain.

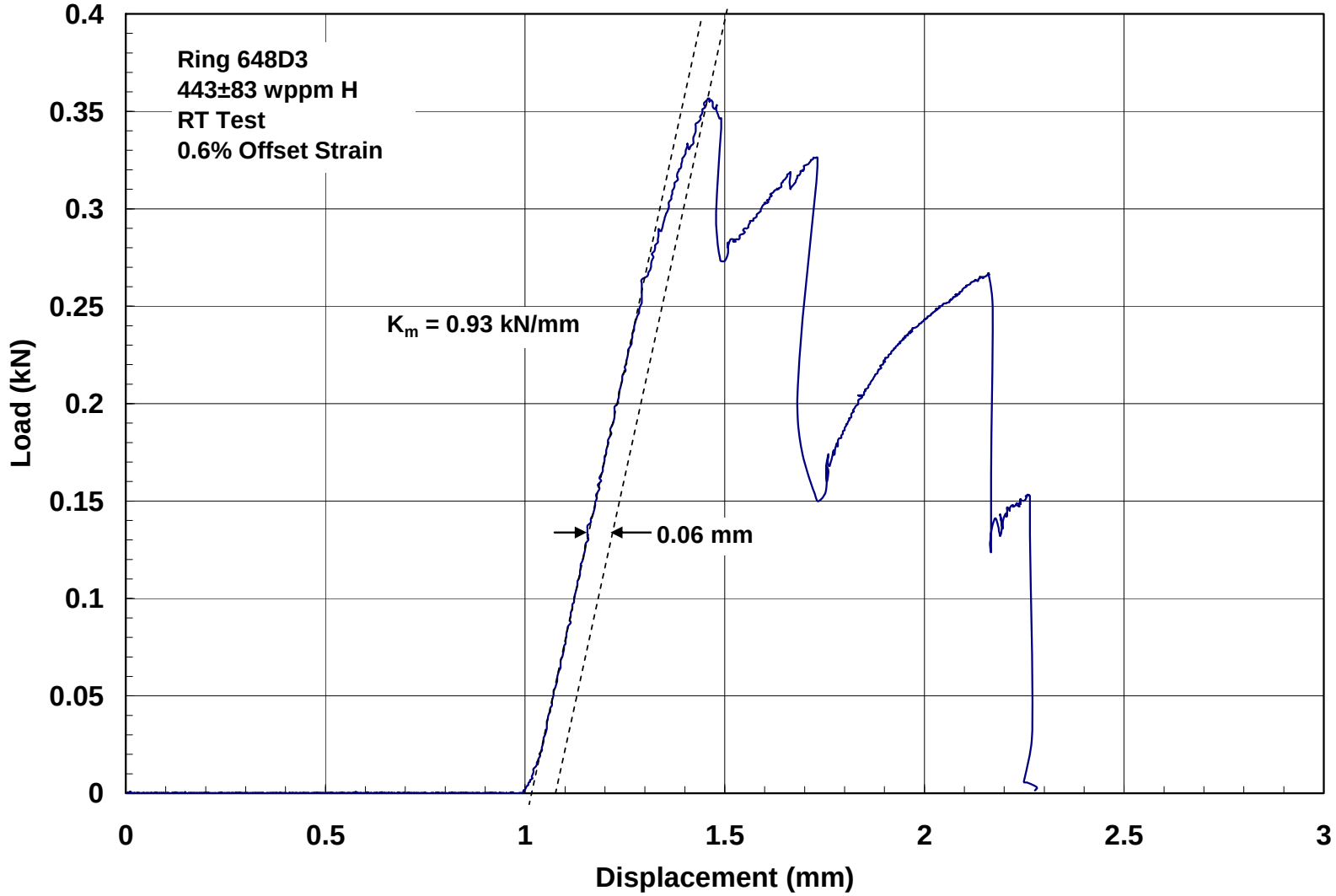

Fig. 22. Load-displacement curve for Ring #3 of RHT rodlet 648D, which was cooled from 400°C and 110 MPa at 5°C/h. The ring was very brittle at RT and a displacement rate of 5 mm/s. Cracks developed at the 3, 6, 9, and 12 o'clock positions.

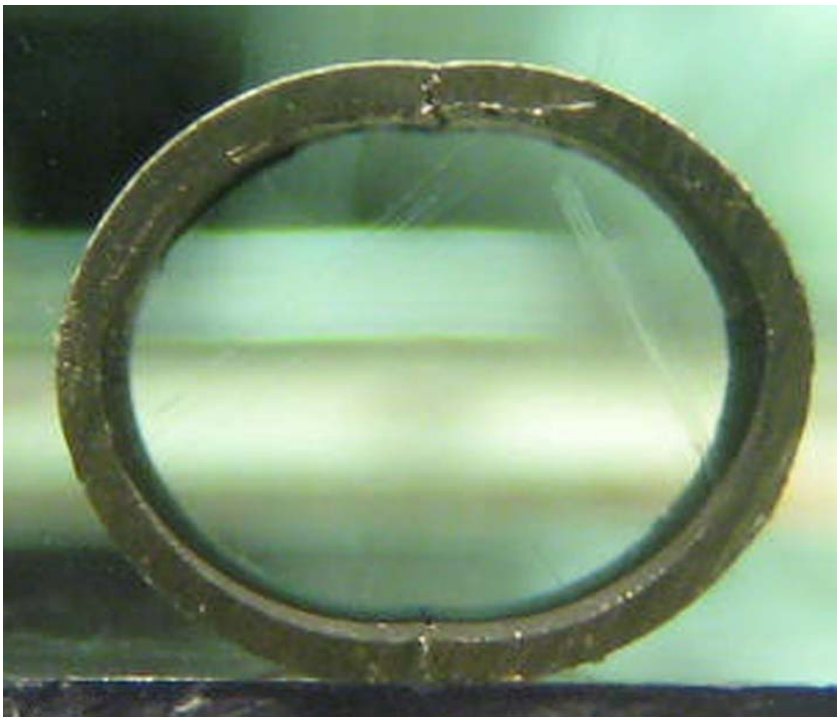

(a) Side view

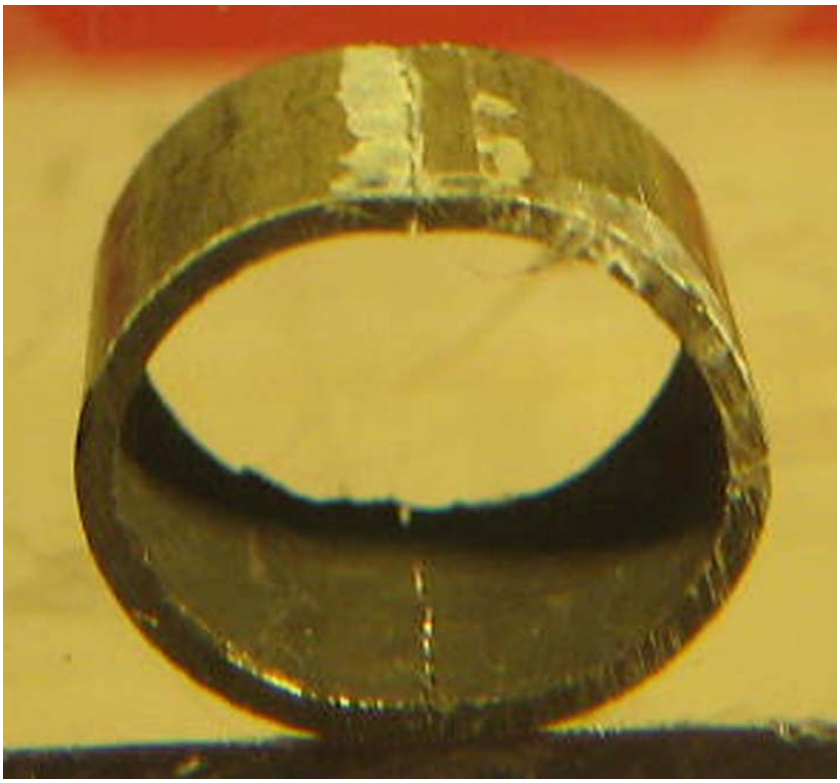

(b) Tilted view

Fig. 23. Photographs of ring 648G5 following 140-MPa RHT and ring compression at 150°C and 5 mm/s to 2-mm pre-set Instron 8511 displacement.

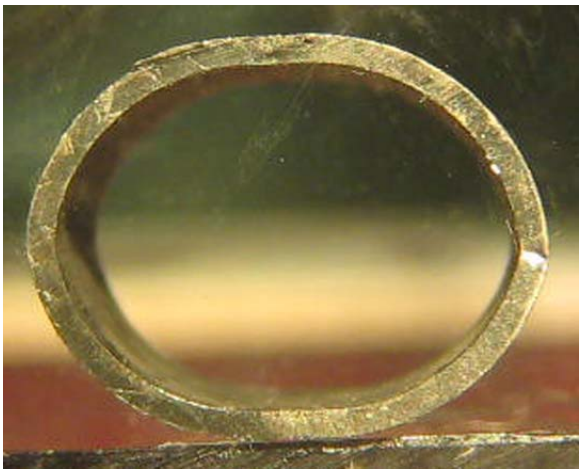

(a) Indication of crack at 3 o'clock position

(b) Outer-surface crack at 3 o'clock position

(c) Bottom is inner-surface 3 o'clock position

Fig. 24. Post ring-compression (150°C) test photos of Ring 648D8 (110-MPa RHT) showing images of crack at 3 o'clock position: (a) edge view; (b) side view showing outer-surface crack; and (c) titled view showing no indication of inner-surface crack.

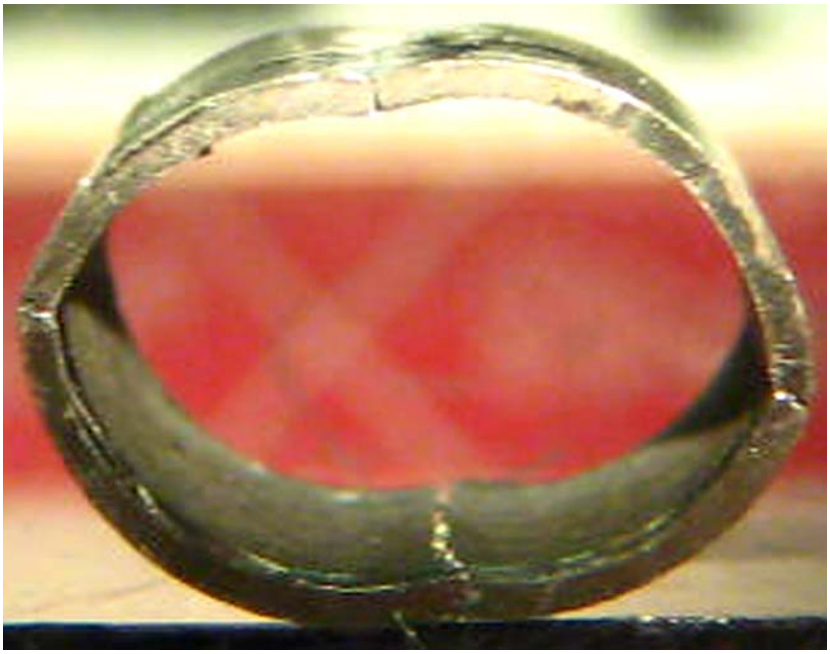

(a) edge view showing 4 cracks

(b) tilted view showing that 12 o'clock crack is through-wall

Fig. 25. Post ring-compression test (RT) photos of Ring 648D3 (110-MPa RHT) showing: (a) edge view with 4 cracks; and (b) tilted view showing that crack at 12 o'clock position is through-wall along the length of the ring.

5. Discussion

For radial-hydride embrittlement tests conducted with pre-hydrided Zry-4 and ZIRLO, the pass-fail criterion used to assess ductility was for the RHT cladding rings to survive a pre-set 2-mm Instron 5566 cross-head displacement with cracks that extended through ≤50% of the cladding wall. Given the load-train lag for the Instron 5566, the 2-mm pre-set displacement corresponded to 1.6 to 1.8 sample displacement for 9.50-mm-OD ZIRLO cladding. This criterion is too severe in that it does not give credit for samples that develop >50% through-wall cracks after significant plastic displacement. Figure 5 shows the test results based on the pass-fail criterion. Figure 6 shows the offset strain (i.e., plastic displacement normalized to the cladding metal outer diameter) prior to crack initiation vs. hydrogen content for several RHT hoop-stress levels at 400°C. The curves show the same trend of increasing radial-hydride-induced embrittlement with increasing RHT stress and decreasing hydrogen content. For RHT ZIRLO, samples with ≥10% offset strain are also samples that exhibited no cracking. The one exception to this is the sample subjected to 135-MPa RHT, which had a smooth load-displacement curve (Fig. 7) and very local cracking (<50% through-wall) at the end of the ring. For a ductile-to-brittle transition 150-MPa RHT ZIRLO ring, crack initiation occurred at 2% offset strain, but the crack extended through only 50% of the wall following 1.7-mm total ring displacement. Thus, a less severe success criterion for avoiding radial-hydride-induced embrittlement of RHT ZIRLO is ≥10% offset strain prior to crack initiation ***or*** ≤50% through-wall cracking after 1.7-mm total ring displacement.

For radial-hydride embrittlement tests conducted with high-burnup ZIRLO, the servo-hydraulic Instron 8511 was used to perform the ring-compression tests. As there is very little load-train lag for this system, the pre-set 2-mm displacement corresponds to about 2-mm ring displacement. Hence, it is a more severe test in that an additional 3% ductility would be needed to survive the pass-fail test as compared to pre-hydrided samples tested in the Instron 5566. In order to relate the two datasets, the revised success criterion is used: ≥10% offset strain prior to crack initiation ***or*** ≤50% through-wall cracking after 1.7-mm total ring displacement. Based on this revised criterion, which is still conservative, high-burnup ZIRLO rings subjected to 140-MPa RHT were assessed as brittle at 150°C, while high-burnup ZIRLO rings subjected to 110-MPa RHT were assessed as ductile at 150°C and brittle at RT. The same assessments would have been reached if the ≥10% offset strain had been reduced to the post-LOCA ductility criterion of ≥2% offset strain.

The RHT treatment for the two high-burnup ZIRLO rodlets (648G and 648D) tested consisted of one heating-cooling cycle. During the 3.3 hours that the rodlets were in the temperature range of 390-400°C, very little hydrogen redistribution across the wall was observed. Following RHT, visible hydrides within the inner half of the cladding appeared to have <100-wppm hydrogen. As this is below the estimated solubility limit (180-210 wppm) at 400°C, very few circumferential hydrides were observed in this region. This resulted in the formation of longer radial hydrides and enhanced the probability of radial-hydride-induced embrittlement. The one heating-cooling cycle may represent a pessimistic case relative to anticipated thermal histories during drying. For high-burnup fuel limited to ≤400°C cladding temperature during vacuum drying, it is highly likely that multiple heating-cooling cycles will be needed. With each heating-cooling cycle, more hydrogen is "pumped" from the dense hydride rim to the low-

hydrogen region of the cladding. Also, longer time at elevated temperature promotes concentration-driven redistribution of hydrogen across the cladding wall. However, it was demonstrated that even under this worse-case thermal history, radial-hydride-induced embrittlement does not occur at 150°C for RHT hoop stresses ≤110 MPa.

Temperature cycling is routinely used in pre-hydriding as-fabricated cladding in order to produce relatively uniform hydrogen concentration in the radial, circumferential, and axial directions. It would be interesting to observe the effects of temperature cycling, as well as increased hold time at 400°C, on the radial distribution of hydrogen in high-burnup cladding.

6. Recommendations for the Next Test with High-Burnup ZIRLO

Referring to Table 5, NA ZIRLO segment 648C has been selected for the next RHT test. Based on interpolation of results for 648B and 648D, the expected hydrogen content is ≈400 wppm, which is typical of the maximum hydrogen content in high-burnup ZIRLO rods discharged from commercial reactors after ≈60 GWd/MTU rod-average burnup. The rodlet should be pressurized to 6.4 MPa at RT to generate a 400°C hoop stress of 110 MPa.

It is also recommended that the RHT consist of 3 cooling cycles. The hold time for each cycle would be one hour. For the first two cooling cycles, the temperature would decrease at 5°C/h from 400°C to 335°C. For the third cooling cycle, the temperature would decrease at 5°C/h from 400°C to 200°C, followed by faster cooling from 200°C to room temperature.

The combination of increased hold time and temperature cycling within regulatory limits may result in higher hydrogen contents within the inner half of the cladding. If both circumferential and radial hydrides precipitate within this cladding region, then the ductility at RT may be enhanced due to the expected decrease in radial hydride continuity factor. It is also possible that the proposed RHT treatment will have little effect on the hydride distribution across the cladding wall and the radial hydride continuity factor.

Due to the higher decay heat in high-burnup fuel, it may not be possible to dry a fuel assembly in one vacuum-drying cycle before the 400°C temperature limit is exceeded. If that is the case, the transfer canister is back-filled with helium and either returned to the pool or externally cooled by flowing gas (air or nitrogen) for a minimum of 24 hours. After 24 hours, there is another cycle of vacuum drying. The process is repeated until the moisture content is below the specified limit. If it is assumed that the temperature decrease is restricted to ≤65°C, then the "average" cooling rate between cycles would be ≤3°C/h. Thus, the proposed cooling rate, temperature drop during cooling between cycles, and number of cycles proposed for the third RHT test with high-burnup ZIRLO appear to be reasonable.

Appendix A

Radial Hydride Continuity Factor (RHCF)

The radial hydride continuity factor (RHCF) is generally defined as the faction of the cladding wall within a certain arc length that has radial hydrides. With this definition, parallel radial hydrides with no interconnecting circumferential hydrides can result in an RHCF of 1 (100%). However, with this definition, it is not clear how a crack would propagate through the cladding wall. The RHCF definition used in this work is based on empirical data from crack propagation through the cladding wall during ring compression testing. Figure A. 1 shows through-wall cracking in ZIRLO with high and low hydrogen concentrations. These rodlets were radial-hydride-treated at high cladding hoop stress (170-190 MPa) at 400°C. In Fig. 1a, the radial and circumferential hydrides form a "brick-like" structure. Cracking is predominantly along radial hydrides, but there are two critical locations at which the crack path is along the circumferential direction. The total horizontal distance that the crack travels is ≈150 μm. In Fig. A.1b, long radial hydrides precipitate. The crack extends from the inner-surface along a radial hydride though ≈40% of the wall, branches for a short distance along a circumferential hydride, and proceeds along another radial hydride through the remaining 60% of the wall. The short circumferential hydride is <150 μm.

Based on the two failures shown in Fig. A.1, the RHCF is defined as the fraction of wall thickness within a 150-μm arc length for which radial hydrides form a continuous path. With this definition, RHCF = 100% for the cross sections shown in Fig. A.1a and Fig. A.1b. Rodlets with high values (>50%) of RHCF are vulnerable to cracking under ring-compression loading through >50% of the cladding wall. However, because of the circumferential and radial variation in ring-compression-induced hoop stress, radial hydrides that initiate at the inner-surface of the cladding and extend 50% into the cladding have a higher probability of embrittling cladding than radial hydrides that initiate at the outer-surface of the cladding and extend 50% into the cladding.

In order to test RHCF as a metric for determining the embrittlement effects of radial hydrides, the metallographic images are examined for a modern Zry-4 rodlet that was ductile at both 150°C (with 400±110 wppm H) and RT (with 465±120 wppm H). The hoop stress for this rodlet was 150 MPa at 400°C. Figure A.2 shows the hydride morphology at the rodlet mid-span for which the local hydrogen content of an adjacent ring was 450±90 wppm. Figure A.2a shows one of eight 100X images. The figure is useful for determining the cladding wall thickness (0.65 mm), but the hydrides are too dense to allow a determination of RHCF. Figures A.2b and A.2c show 200X images at the same location for the inner-surface and outer-surface cross sections, respectively. The RHCF at the inner surface is only 14%, and the RHCF at the outer surface is 16%. As these do not form a continuous path across the cladding wall, they are not combined. The low RHCF is consistent with the ductile behavior of the material at 150°C and RT. Thus, RHCF appears to be a reasonable metric for assess the vulnerability of RHT cladding to radial-hydride-induced embrittlement. It is also much easier to determine than the radial hydride fraction, which is commonly used to assess the degree of radial hydride formation. The main uncertainty in measuring RHCF is in the determination of the connectivity of radial hydrides with circumferential hydrides.

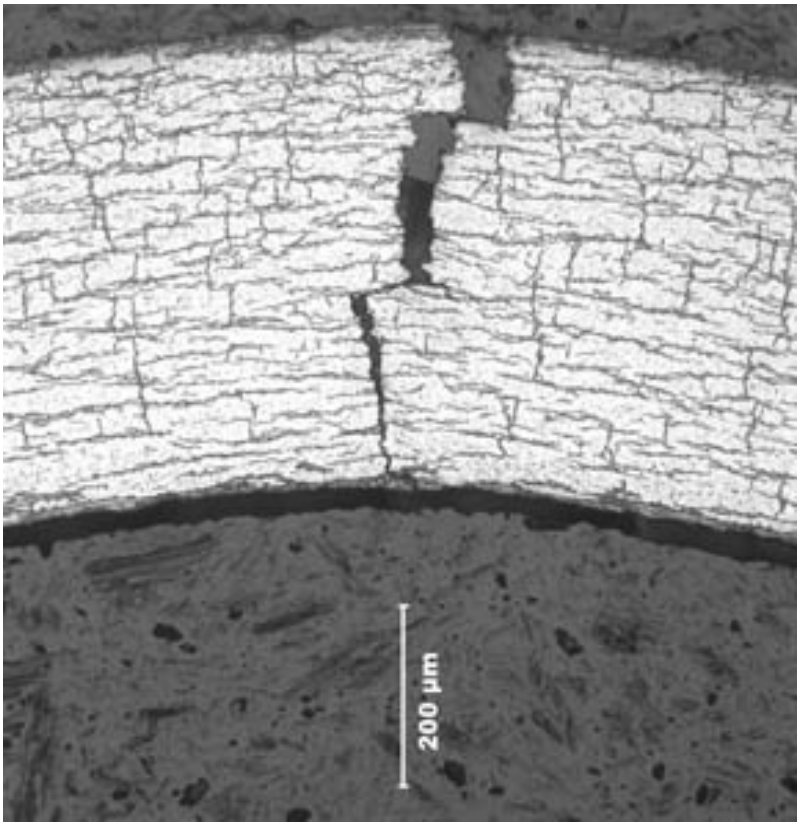

(a) Pre-hydrided RHT ZIRLO with 610±110 wppm H

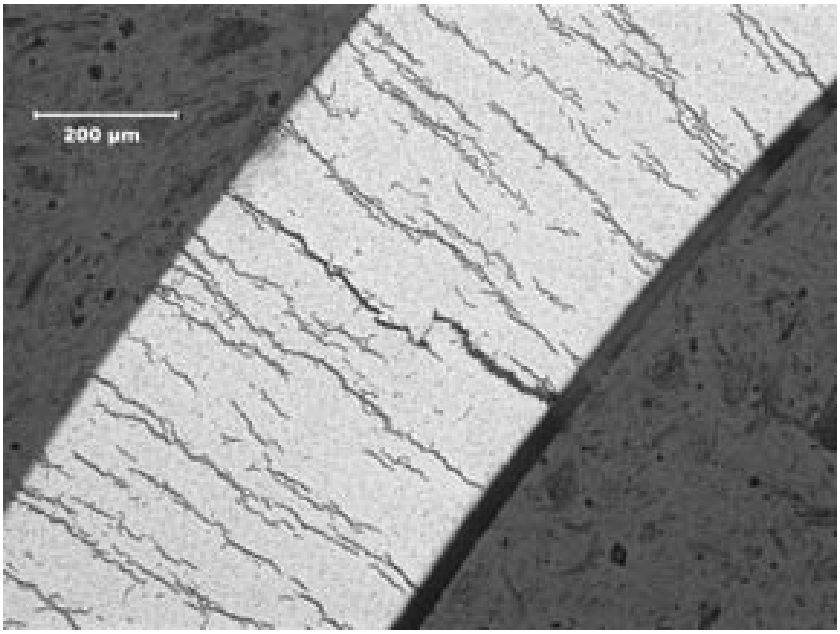

(b) Pre-hydrided RHT ZIRLO with 180±10 wppm H

Fig. A.1 Through-wall crack paths for RHT pre-hydrided ZIRLO with (a) high-hydrogen content of 610±110 wppm; and (b) low-hydrogen content of 180±10 wppm.

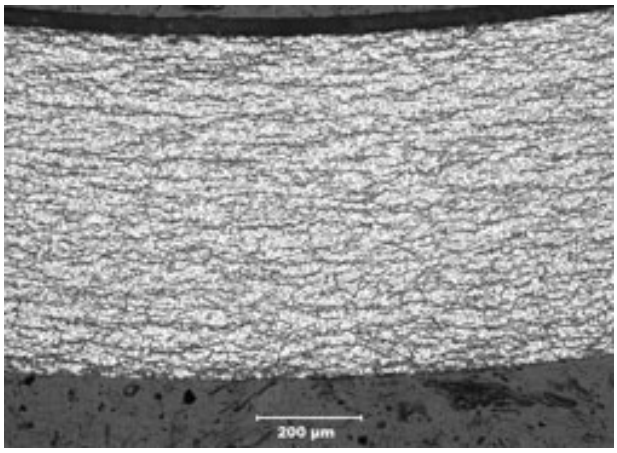

(a) Cross section at 100X

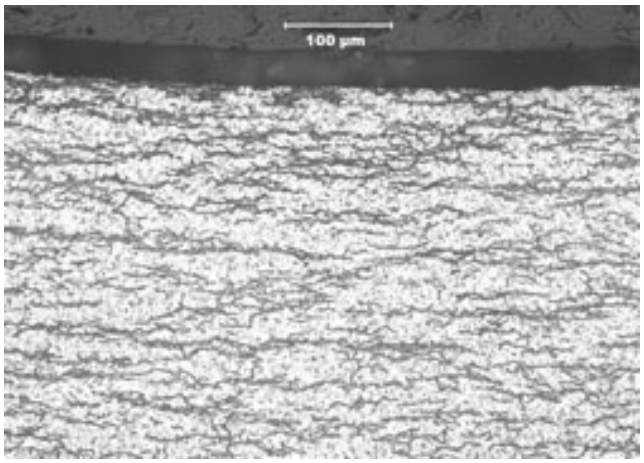

(b) Inner surface at 200X

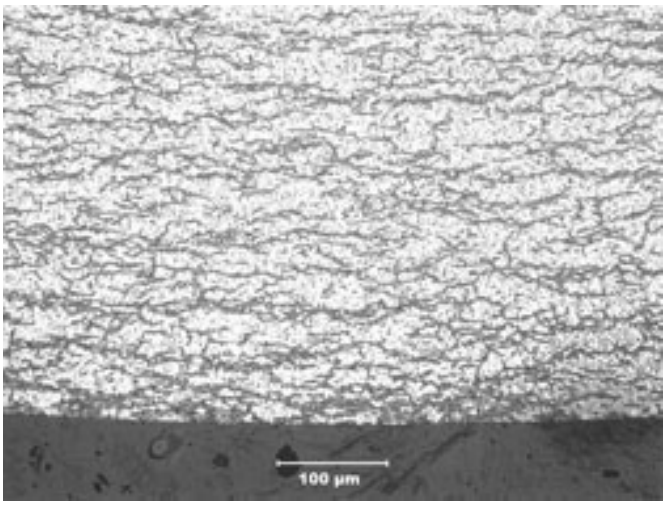

(c) Outer surface at 200X

Fig. A.2 Metallographic images of hydride morphology in modern Zry-4 rodlet with 450±90 wppm H following RHT at 150-MPa: (a) cross section; (b) inner surface with 14% maximum RHCF; and (c) outer surface with 16% maximum RHCF.

Appendix B

Stress Analysis

B.1 Internal Pressure

Finite element analysis has been used to predict the internal volume and pressure as a function of temperature and time at temperature for pre-hydrided, as-fabricated ZIRLO with room-temperature (RT) gauge pressures of 11.58 Pa, 10.45 Mpa, 9.10 Mpa, and 8.30 Mpa. The 8.30 Mpa corresponds to a wall-averaged hoop stress of 135 Mpa after a one-hour hold time at 400°C. The calculations include thermal creep of the cladding. This case is particularly relevant to the RT pressures (6.40 Mpa and 8.00 Mpa) used to fabricate rodlets from high-burnup ZIRLO cladding. Table B.1 lists the volumes and internal pressures as a function of temperature and time at temperature for pre-hydrided ZIRLO pressurized to 8.30 Mpa at RT. Figure B.1 shows pressure and temperature vs. time for this case.

Table B.1 FEA results for pre-hydrided ZIRLO rodlet pressurized to 8.30 Mpa at RT

Hold Time, h	Temperature °C	Pressure, Mpa	Gas Volume, mm^3
---	27	0	1732
---	27	8.300	1738.5
0	400	18.565	1753
1	400	18.494	1760

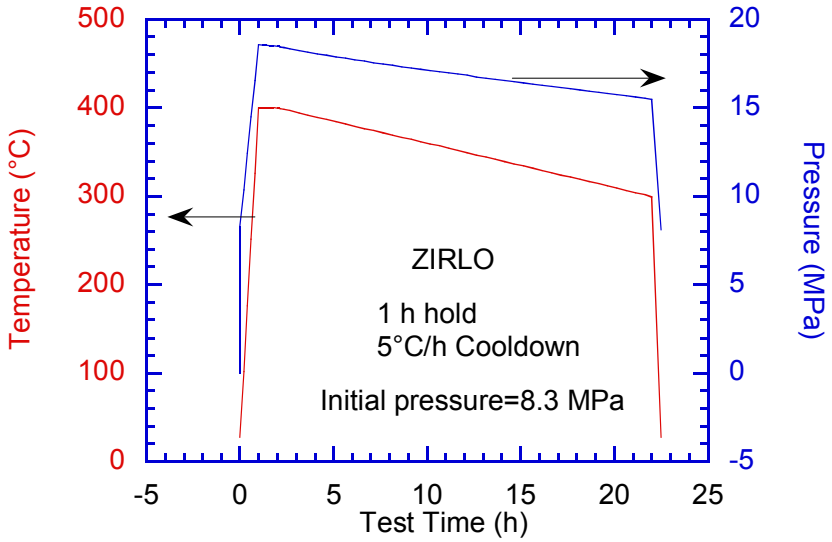

Fig. B.1 Temperature and pressure vs. time for pre-hydrided ZIRLO rodlet.

The small (0.4%) increase in gas volume is due to thermal creep of the cladding during the one-hour hold time. It has an insignificant effect on the internal pressure. Also, for irradiated cladding, the thermal creep is expected to be negligible during such a short hold time at relatively low stress. Basically, lower pressures at 400°C can be obtained by linear scaling of the RT pressures. Based on such scaling, RT pressures of 8.00 Mpa and 6.40 Mpa would result in 400°C pressures of 17.894 Mpa and 14.315 Mpa.

B.2 Hoop Stress Calculation

Two assumptions are made in the calculation of hoop stress: (a) following radial hydride treatment, the corrosion layer has no tensile strength in the hoop direction; and (b) during radial hydride treatment, thermal creep of the irradiated cladding has a negligible effect on internal pressure and relaxation of outer- and inner-surface hoop stresses. The first assumption is justified by the radial cracks observed in the corrosion layer following RHT. The second assumption is justified by the increase in creep resistance with irradiation.

Following RHT, the outer-diameter (D_o) is measured at several axial locations by means of a micrometer. The metal wall thickness (h_m) is measured at 8 circumferential locations from 100X metallographic images. The corrosion layer thickness (δ_c) is measured at 8 circumferential locations from 200X metallographic images. The metal outer (D_{mo}) and inner (D_{mi}) are determined from:

$$D_{mo} = D_o - 2\,\delta_c \tag{B.1}$$

$$D_{mi} = D_{mo} - 2\,h_m \tag{B.2}$$

Let $\sigma_{\theta i}$, $\sigma_{\theta a}$, and $\sigma_{\theta o}$ be the inner-surface, wall-averaged, and outer-surface hoop stresses, respectively. The elastic solution for these stresses can be expressed as a function of the internal gauge pressure (P_i) as:

$$\sigma_{\theta i} = [(D_{mo}/D_{mi})^2 + 1]\,[(D_{mo}/D_{mi})^2 - 1]^{-1}\,P_i \tag{B.3}$$

$$\sigma_{\theta a} = [D_{mi}/(2h_m)]\,P_i \tag{B.4}$$

$$\sigma_{\theta o} = 2\,[(D_{mo}/D_{mi})^2 - 1]^{-1}\,P_i \tag{B.5}$$

Table B.2 lists the stress values at the 8 circumferential locations for which D_{mo}, h_m, and D_{mi} were determined. For rodlet 648G pressurized to 8.0 Mpa at RT, the ID, average, and OD stresses at 400°C were 148±2 Mpa, 138±1 Mpa, and 130±2 Mpa, respectively. The average hoop stress is independent of possible creep relaxation of stresses. It is rounded off to 140 Mpa based on uncertainties. For rodlet 648D pressurized to 6.4 Mpa at RT, the ID, average, and OD stresses at 400°C were 115±1 Mpa, 108±0 Mpa, and 101±1 Mpa, respectively. The average hoop stress is rounded off to 110 Mpa based on uncertainties.

Table B.2 Calculated stresses at the cladding metal ID ($\sigma_{\theta i}$), at about the mid-wall ($\sigma_{\theta a}$), and at the metal OD ($\sigma_{\theta o}$) for rodlets 648G and 648D with internal pressures at 400°C of 17.894 Mpa and 14.315 Mpa, respectively.

Rodlet	Met Area	D_{mo}, mm	h_m, mm	D_{mi}, mm	Hoop Stress, Mpa		
					$\sigma_{\theta i}$	$\sigma_{\theta a}$	$\sigma_{\theta o}$
648G	1	9.397	0.535	8.324	148	139	130
	2	9.398	0.537	8.350	152	139	134
	3	9.434	0.542	8.341	146	138	128
	4	9.423	0.541	8.341	147	138	130
	5	9.403	0.531	8.350	151	141	133
	6	9.428	0.539	8.338	146	138	128
	7	9.428	0.545	8.333	146	137	128
	8	9.421	0.544	8.338	147	137	129
	Average	9.42	0.54	8.34	148±2	138±1	130±2
648D	1	9.445	0.553	8.339	116	108	101
	2	9.447	0.554	8.341	116	108	101
	3	9.447	0.553	8.342	116	108	101
	4	9.452	0.555	8.328	114	107	99
	5	9.442	0.557	8.323	114	107	100
	6	9.437	0.557	8.327	115	107	101
	7	9.437	0.555	8.343	117	108	103
	8	9.447	0.552	8.335	115	108	101
	Average	9.44	0.56	8.33	115±1	108±0	101±1

Appendix C

Metallographic Images of Hydride Morphology in High-Burnup ZIRLO Rodlets 648G and 648C

Two of sixteen and two of eight 100X micrographs are shown in Section 3.3 for RHT rodlets 648G and 648D. This appendix contains all 100X micrographs taken for these high-burnup ZIRLO rodlets. Images at 200X used to determine corrosion-layer thickness are available upon request.

For convenience, sectioning diagrams shown in Figs. 12 and 15, respectively, for rodlets 648G and 648D are repeated below as Figs. C.1 and C.2.

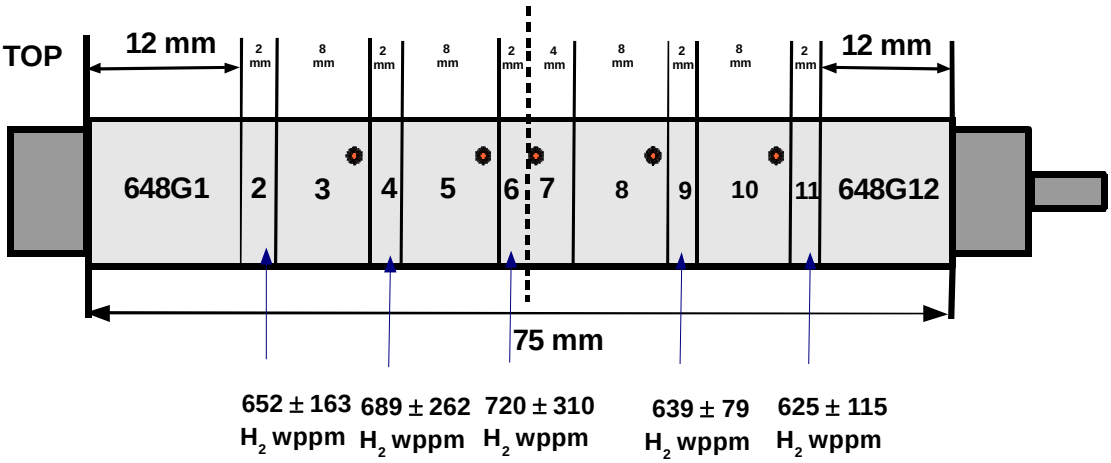

Fig. C.1 Sectioning diagram for rodlet 648G, which was subjected to an RHT hoop stress of 140 MPa at 400°C prior to cooling at 5°C/s.

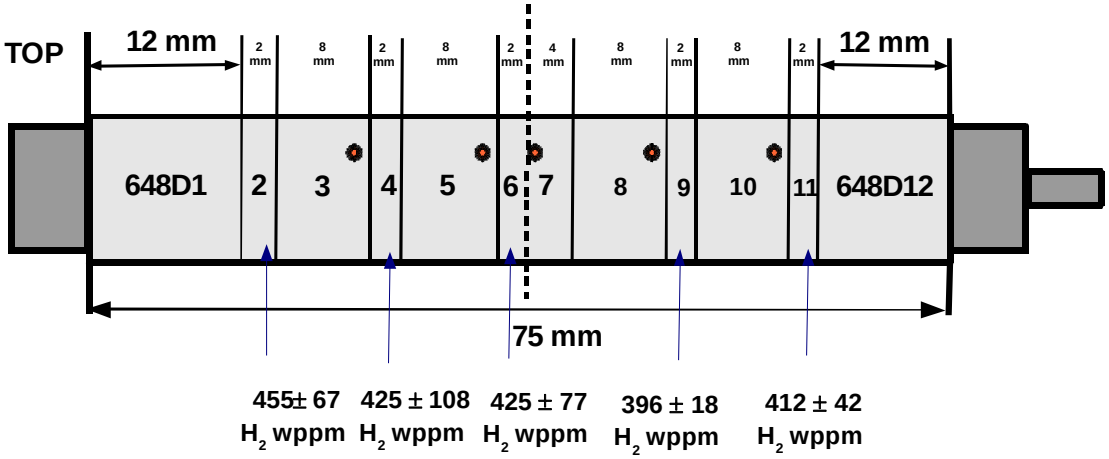

Fig. C.2 Sectioning diagram for rodlet 648D, which was subjected to an RHT hoop stress of 110 MPa at 400°C prior to cooling at 5°C/s.

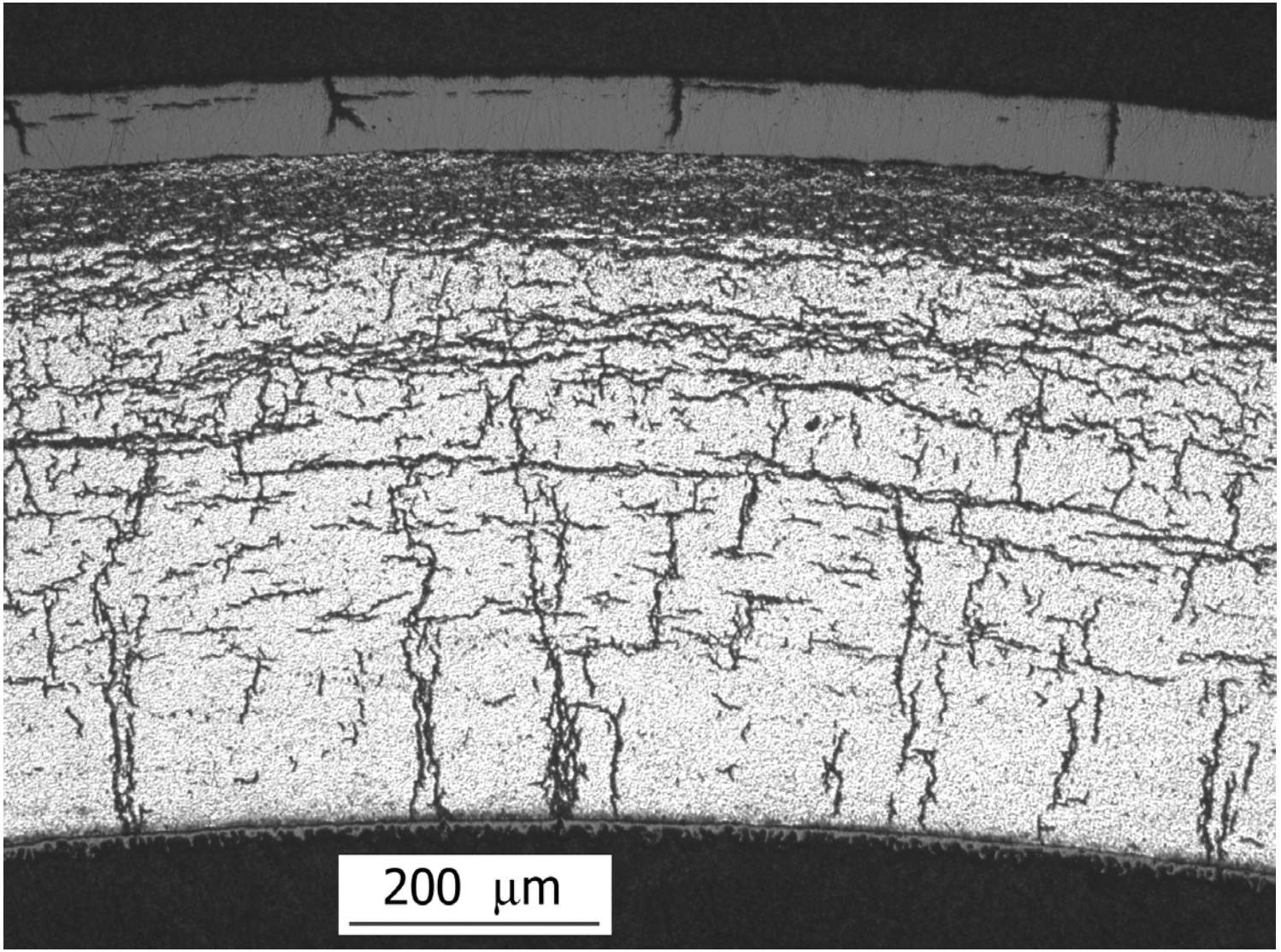

Fig. C.3 Area 1 image for ring 648G7 sectioned from high-burnup ZIRLO rodlet with RHT stress of 140 MPa. Hydrogen content of adjacent ring was 720±310 wppm. Maximum RHCF = 79%. See Fig. C.1 for sample location.

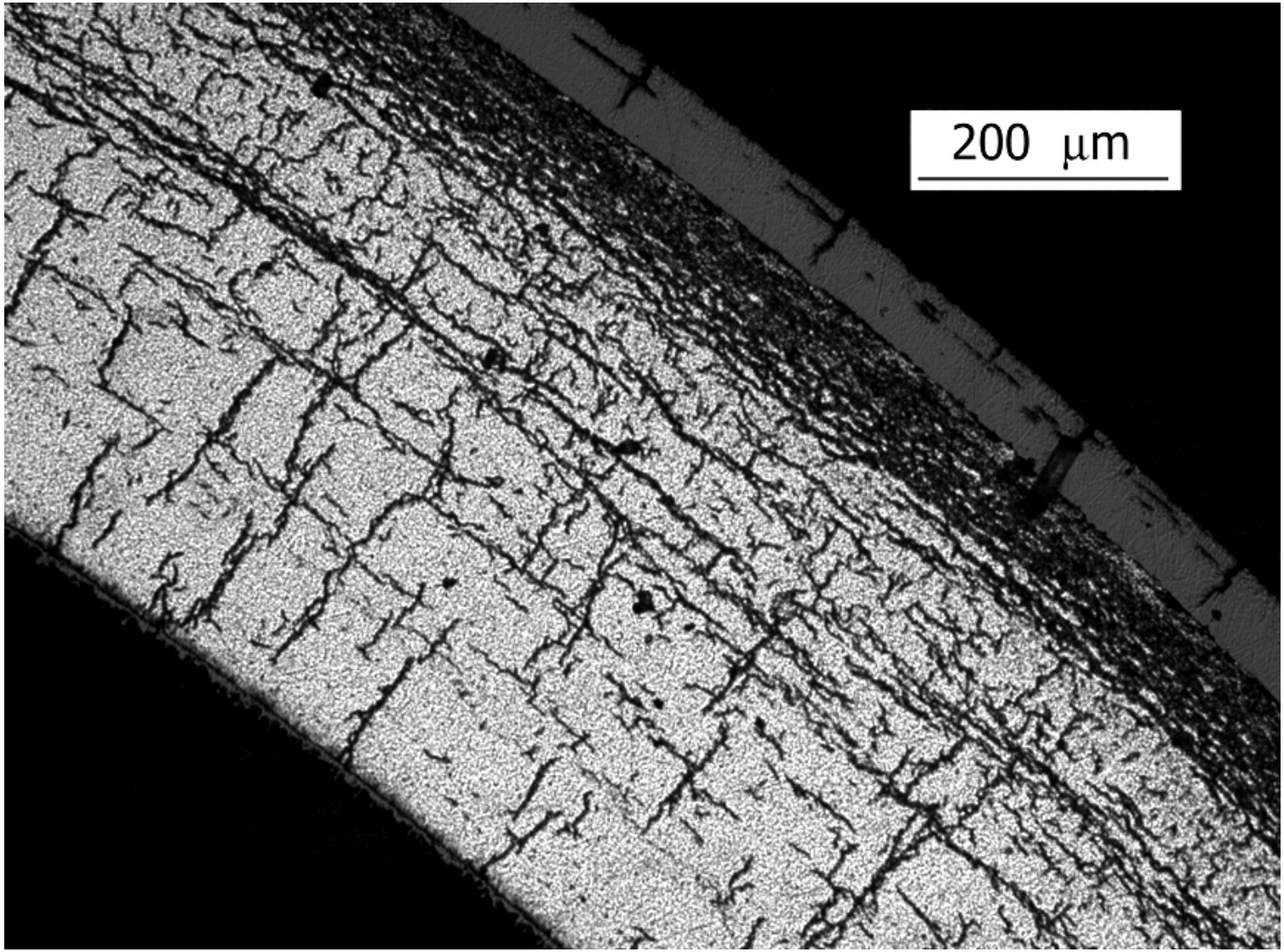

Fig. C.4 Area 2 image for ring 648G7 sectioned from high-burnup ZIRLO rodlet with RHT stress of 140 MPa. Hydrogen content of adjacent ring was 720±310 wppm. Maximum RHCF = 81%. See Fig. C.1 for sample location.

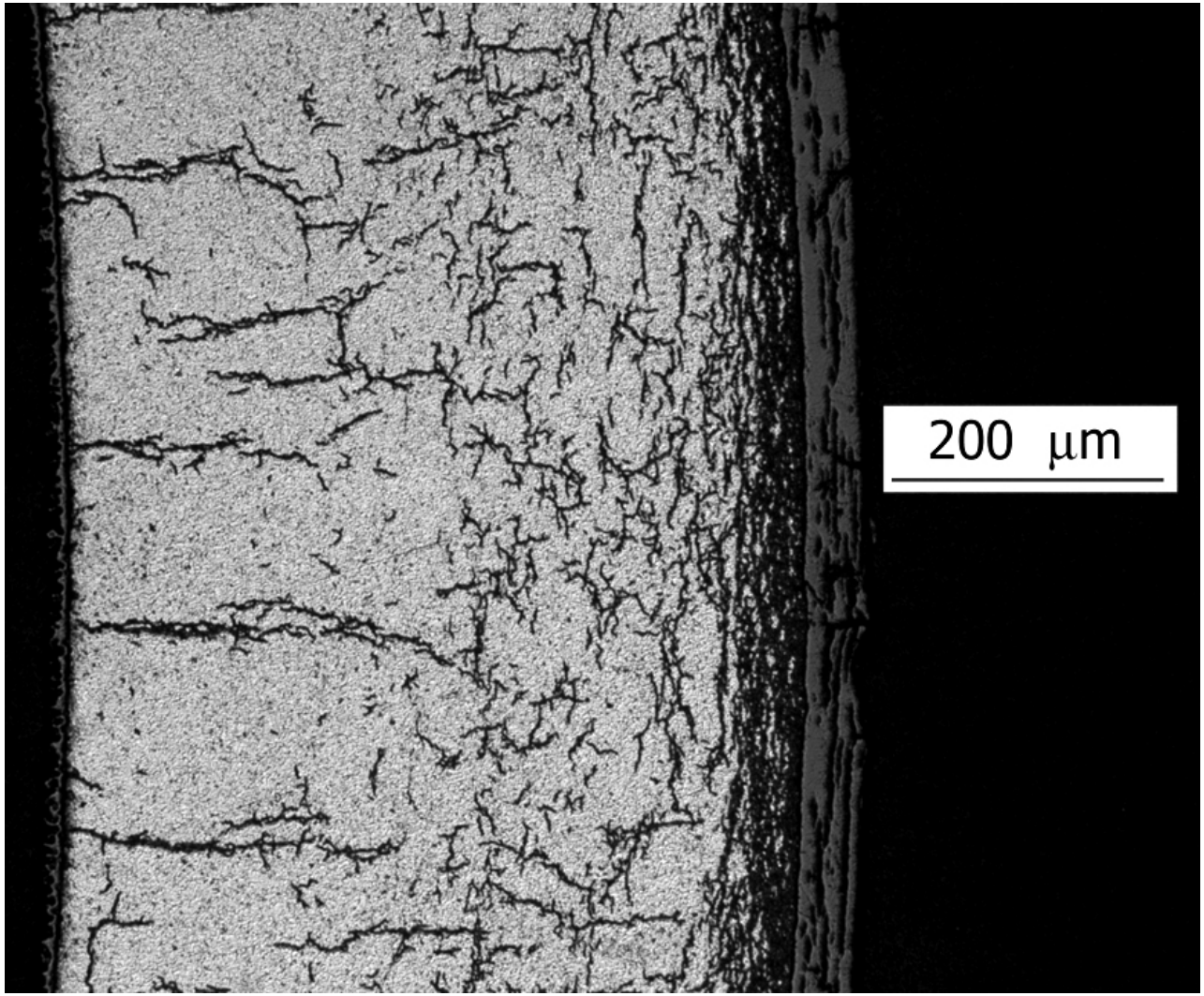

Fig. C.5 Area 3 image for ring 648G7 sectioned from high-burnup ZIRLO rodlet with RHT stress of 140 MPa. Hydrogen content of adjacent ring was 720±310 wppm. Maximum RHCF = 52%. See Fig. C.1 for sample location.

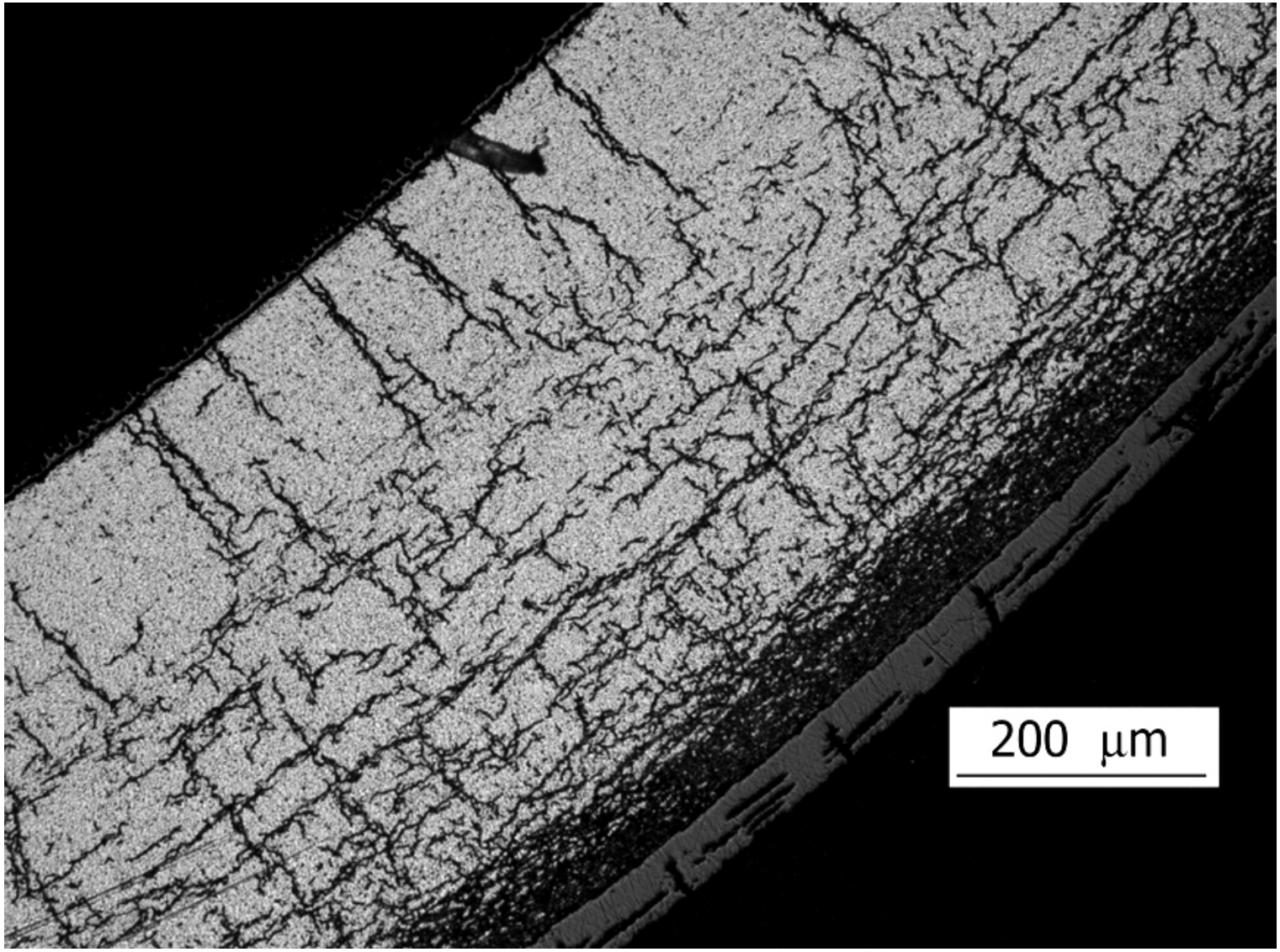

Fig. C.6 Area 4 image for ring 648G7 sectioned from high-burnup ZIRLO rodlet with RHT stress of 140 MPa. Hydrogen content of adjacent ring was 720±310 wppm. Maximum RHCF = 38%. See Fig. C.1 for sample location.

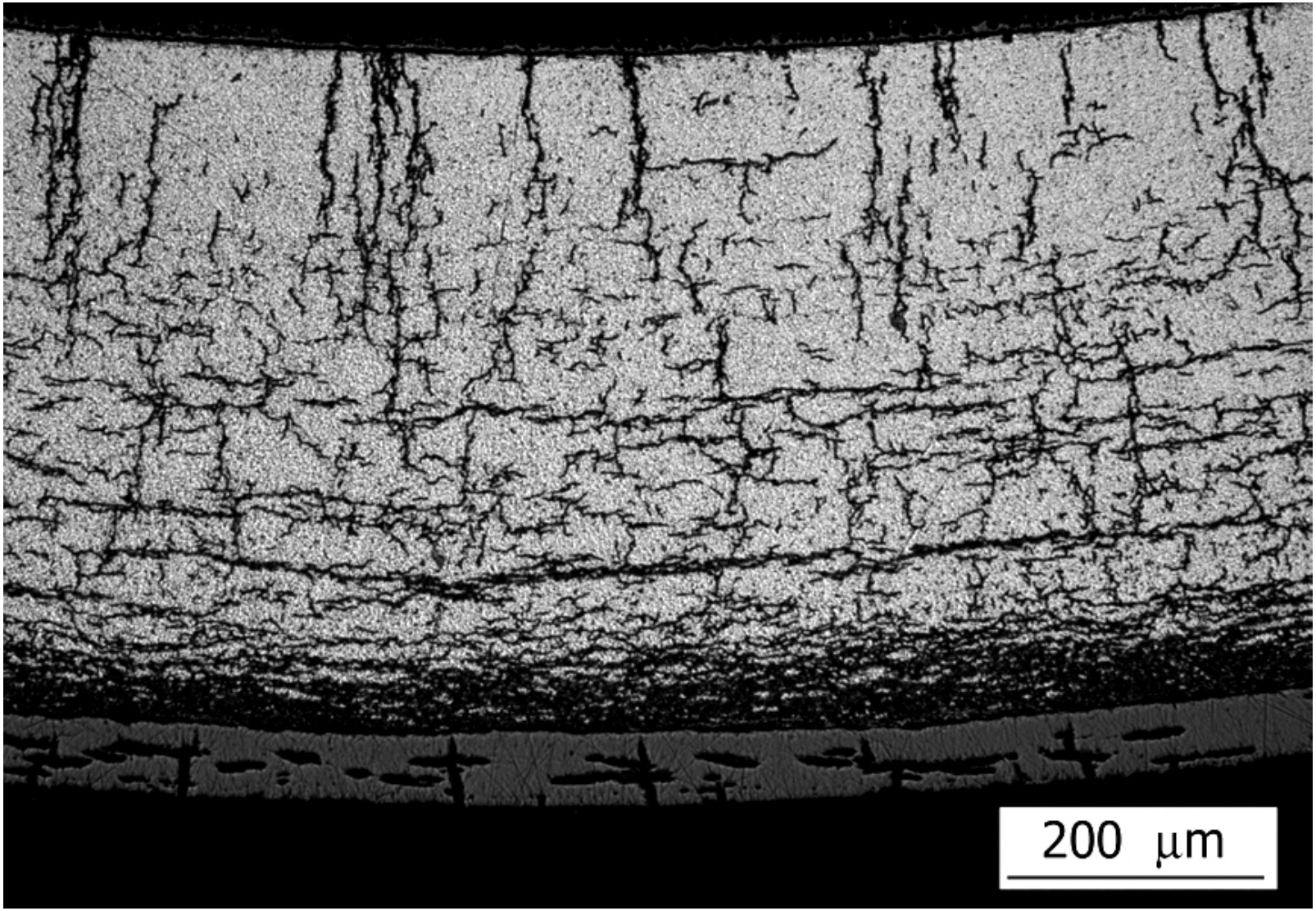

Fig. C.7 Area 5 image for ring 648G7 sectioned from high-burnup ZIRLO rodlet with RHT stress of 140 MPa. Hydrogen content of adjacent ring was 720±310 wppm. Maximum RHCF = 82%. See Fig. C.1 for sample location.

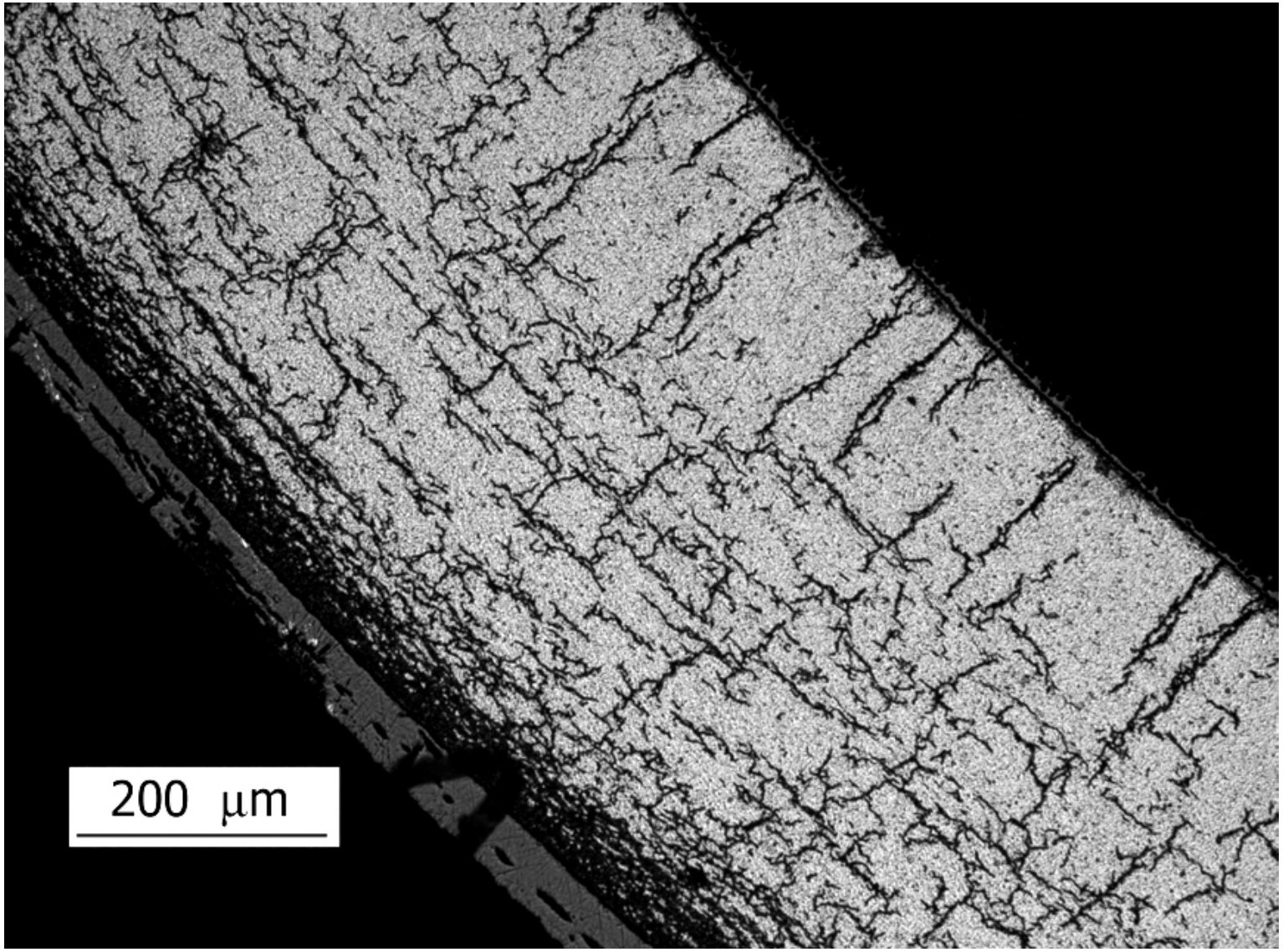

Fig. C.8 Area 6 image for ring 648G7 sectioned from high-burnup ZIRLO rodlet with RHT stress of 140 MPa. Hydrogen content of adjacent ring was 720±310 wppm. Maximum RHCF = 67%. See Fig. C.1 for sample location.

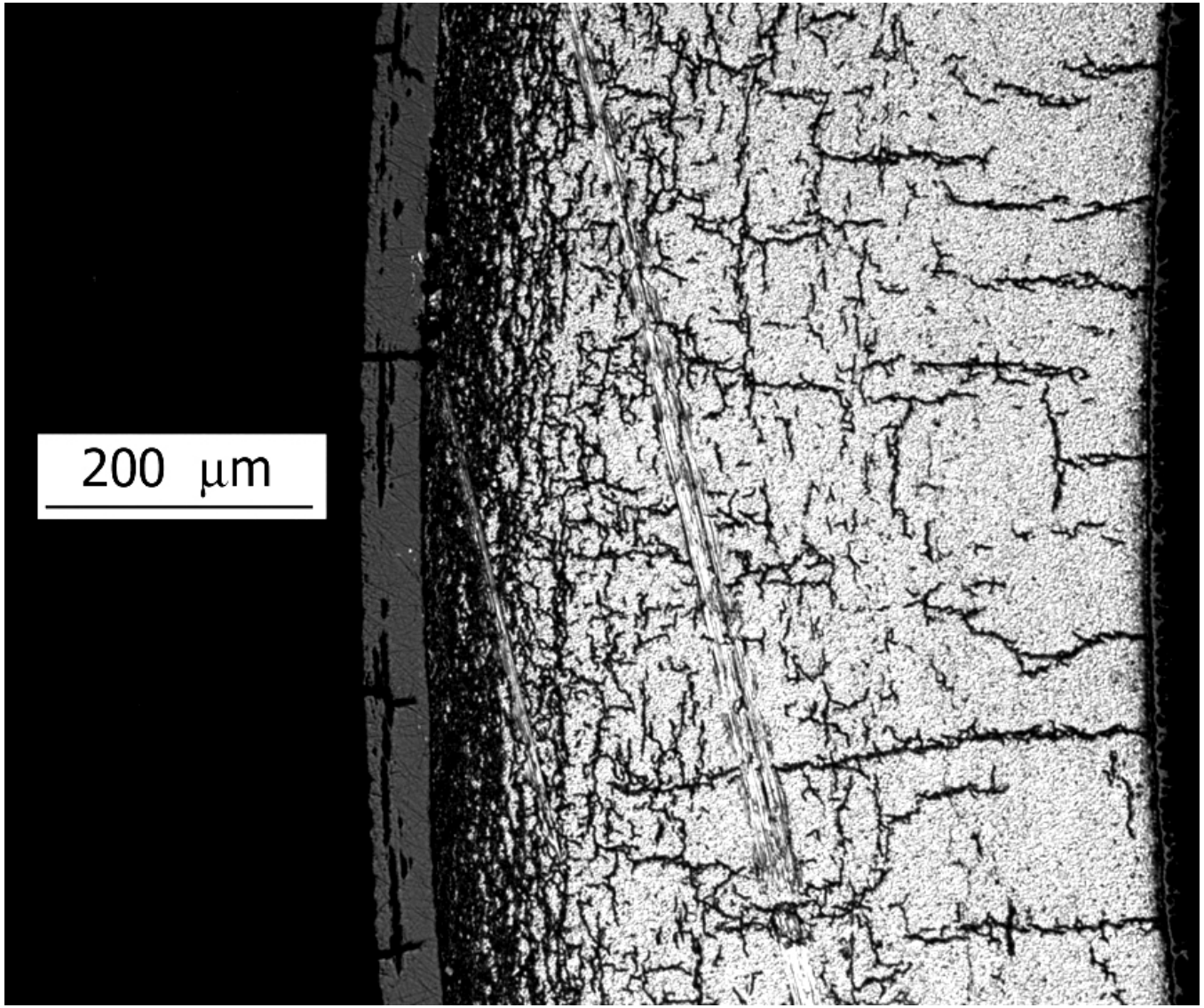

Fig. C.9 Area 7 image for ring 648G7 sectioned from high-burnup ZIRLO rodlet with RHT stress of 140 MPa. Hydrogen content of adjacent ring was 720±310 wppm. Maximum RHCF = 86%. See Fig. C.1 for sample location.

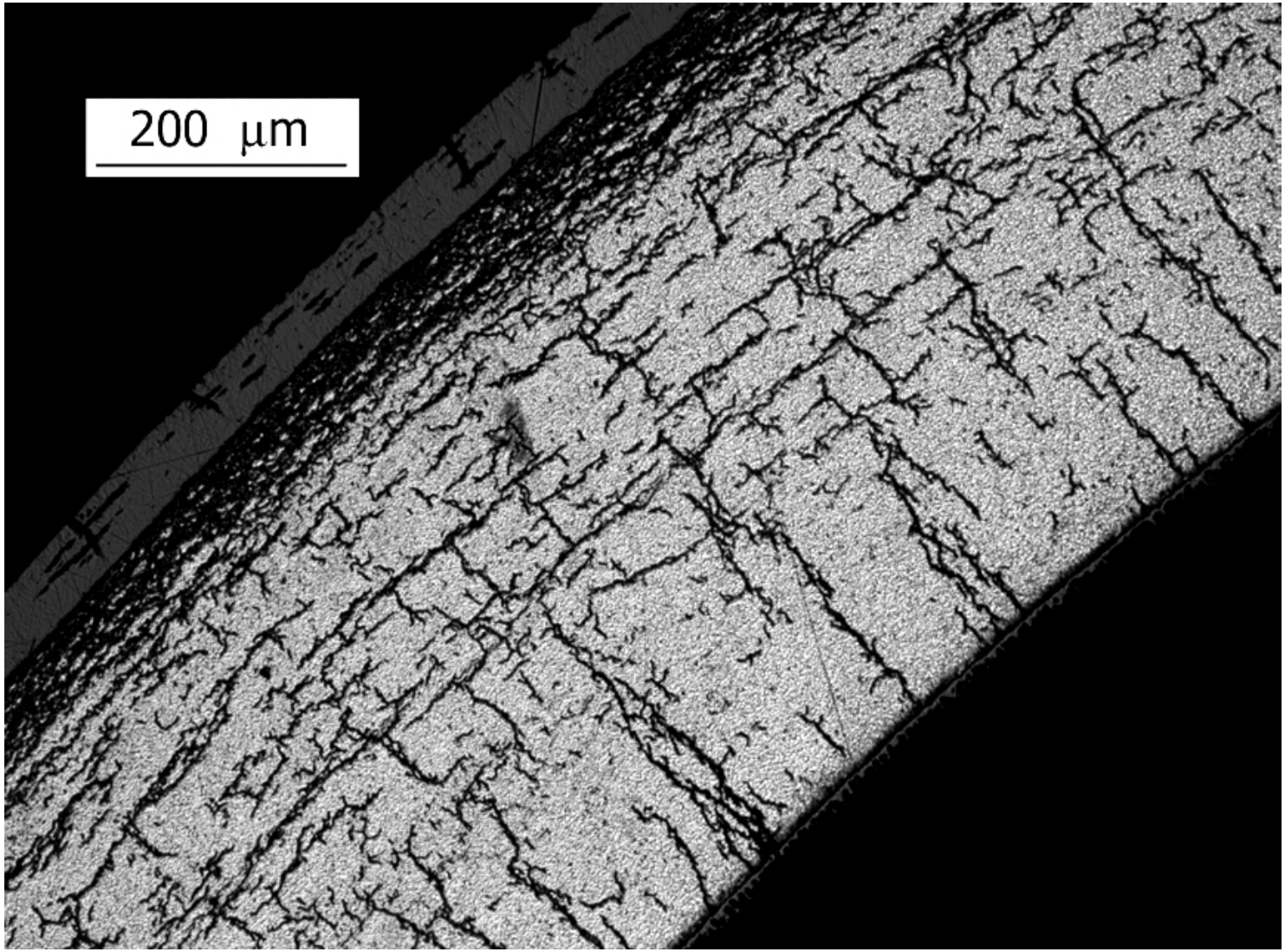

Fig. C.10 Area 8 image for ring 648G7 sectioned from high-burnup ZIRLO rodlet with RHT stress of 140 MPa. Hydrogen content of adjacent ring was 720±310 wppm. Maximum RHCF = 65%. See Fig. C.1 for sample location.

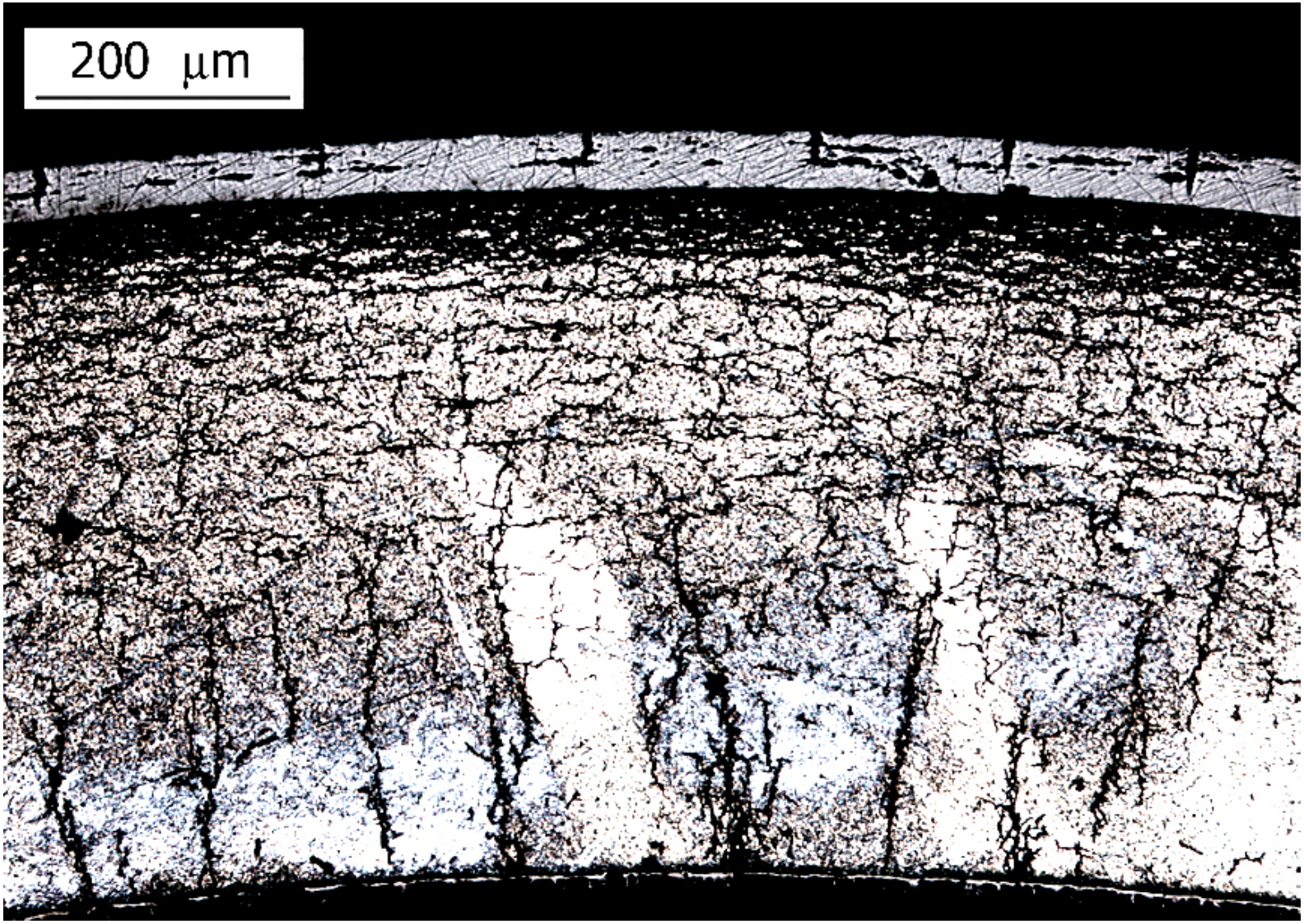

Fig. C.11 Area 1 image for ring 648G8 sectioned from high-burnup ZIRLO rodlet with RHT stress of 140 MPa. Hydrogen content of adjacent ring was 640±80 wppm. Maximum RHCF = 80%. See Fig. C.1 for sample location.

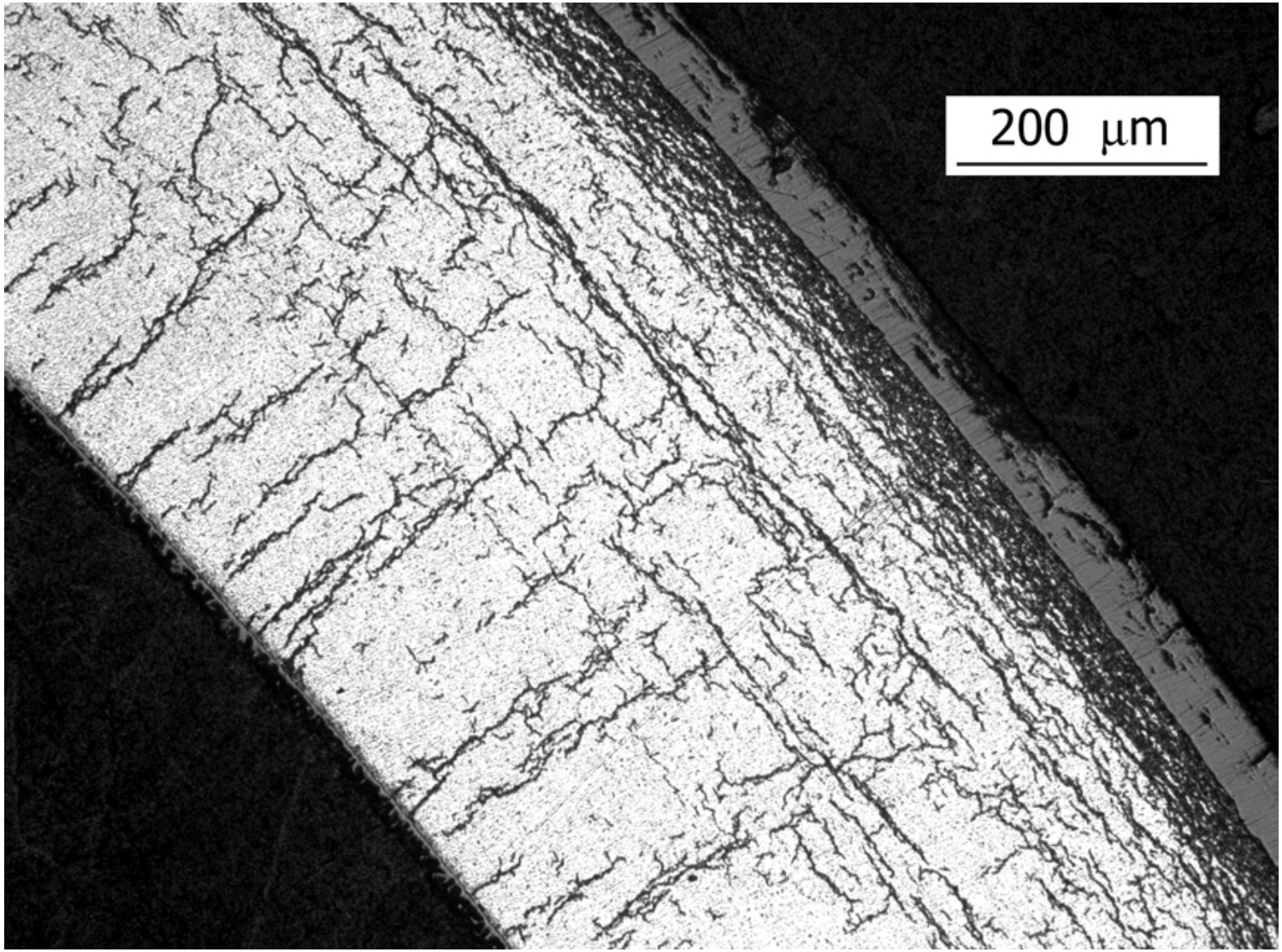

Fig. C.12 Area 2 image for ring 648G8 sectioned from high-burnup ZIRLO rodlet with RHT stress of 140 MPa. Hydrogen content of adjacent ring was 640±80 wppm. Maximum RHCF = 70%. See Fig. C.1 for sample location.

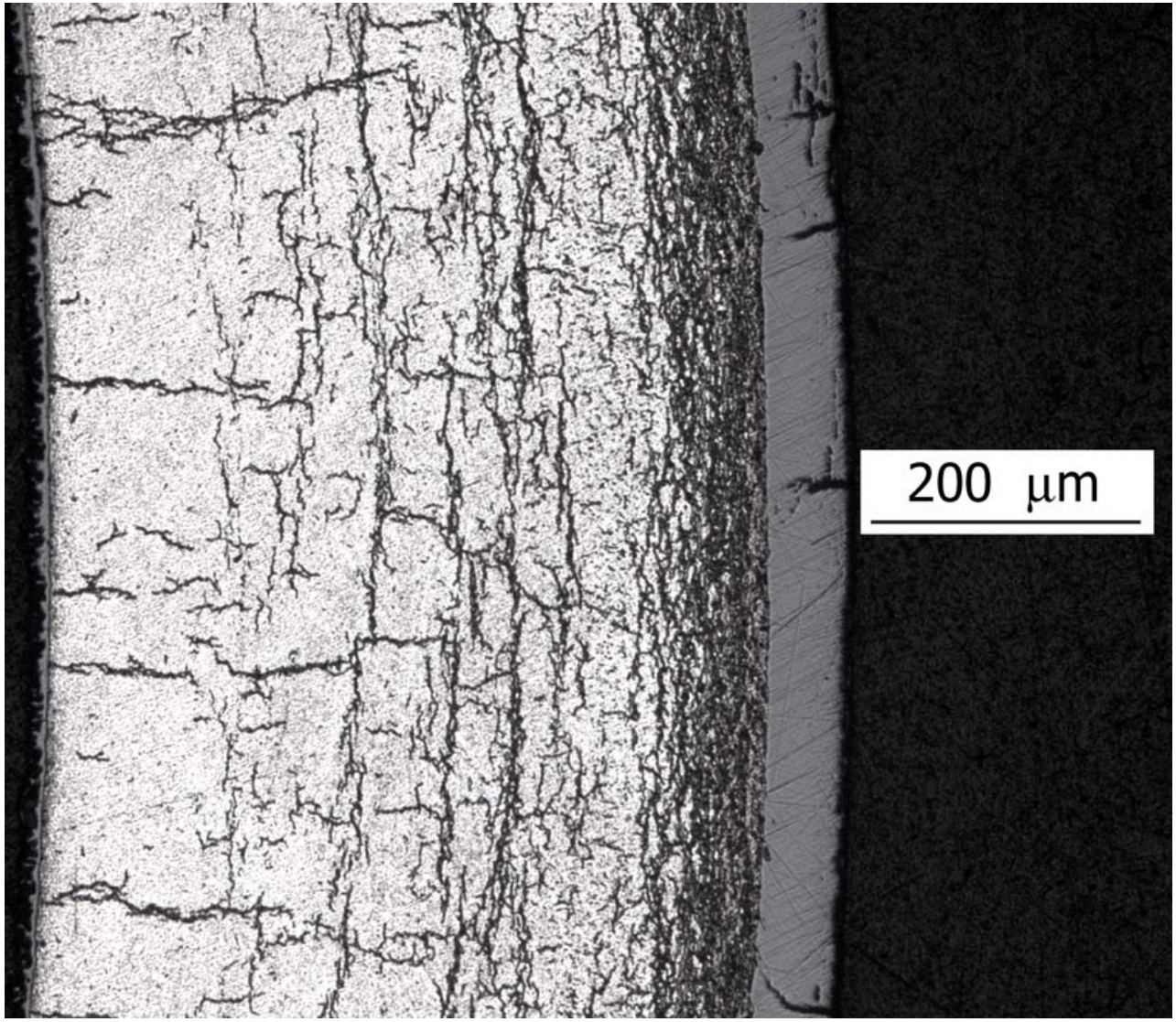

Fig. C.13 Area 3 image for ring 648G8 sectioned from high-burnup ZIRLO rodlet with RHT stress of 140 MPa. Hydrogen content of adjacent ring was 640±80 wppm. Maximum RHCF = 61%. See Fig. C.1 for sample location.

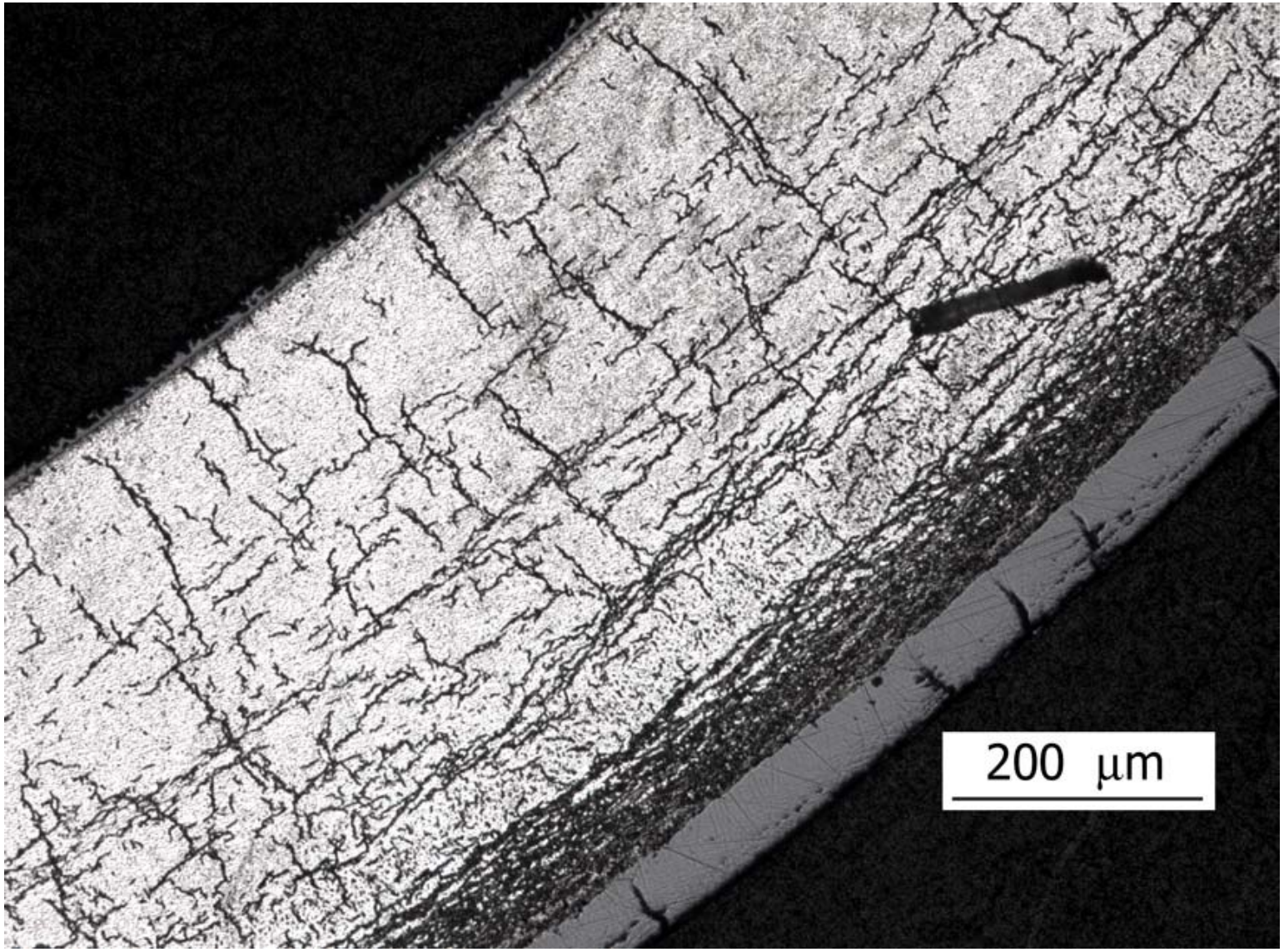

Fig. C.14 Area 4 image for ring 648G8 sectioned from high-burnup ZIRLO rodlet with RHT stress of 140 MPa. Hydrogen content of adjacent ring was 640±80 wppm. Maximum RHCF = 71%. See Fig. C.1 for sample location.

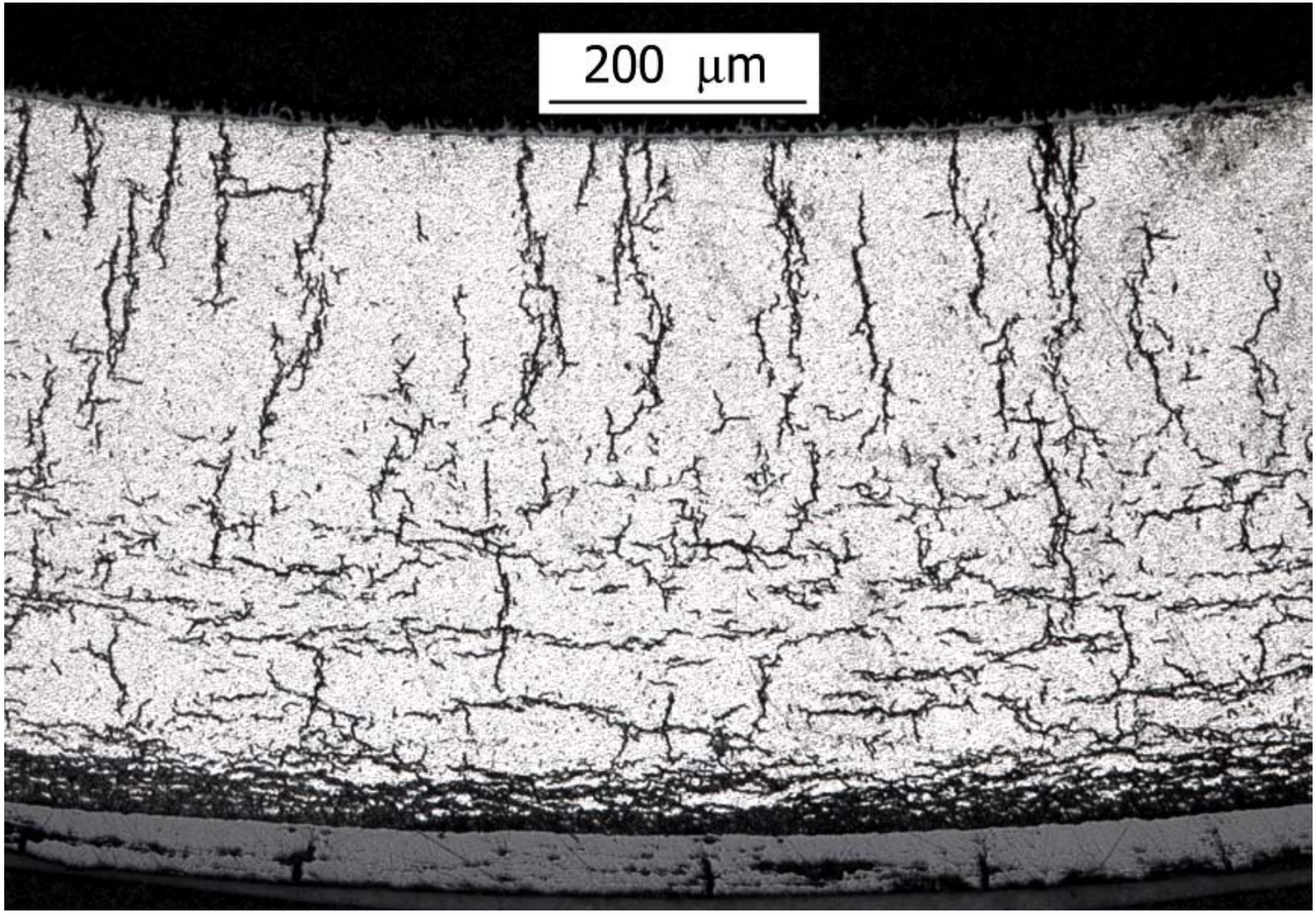

Fig. C.15 Area 5 image for ring 648G8 sectioned from high-burnup ZIRLO rodlet with RHT stress of 140 MPa. Hydrogen content of adjacent ring was 640±80 wppm. Maximum RHCF = 46%. See Fig. C.1 for sample location.

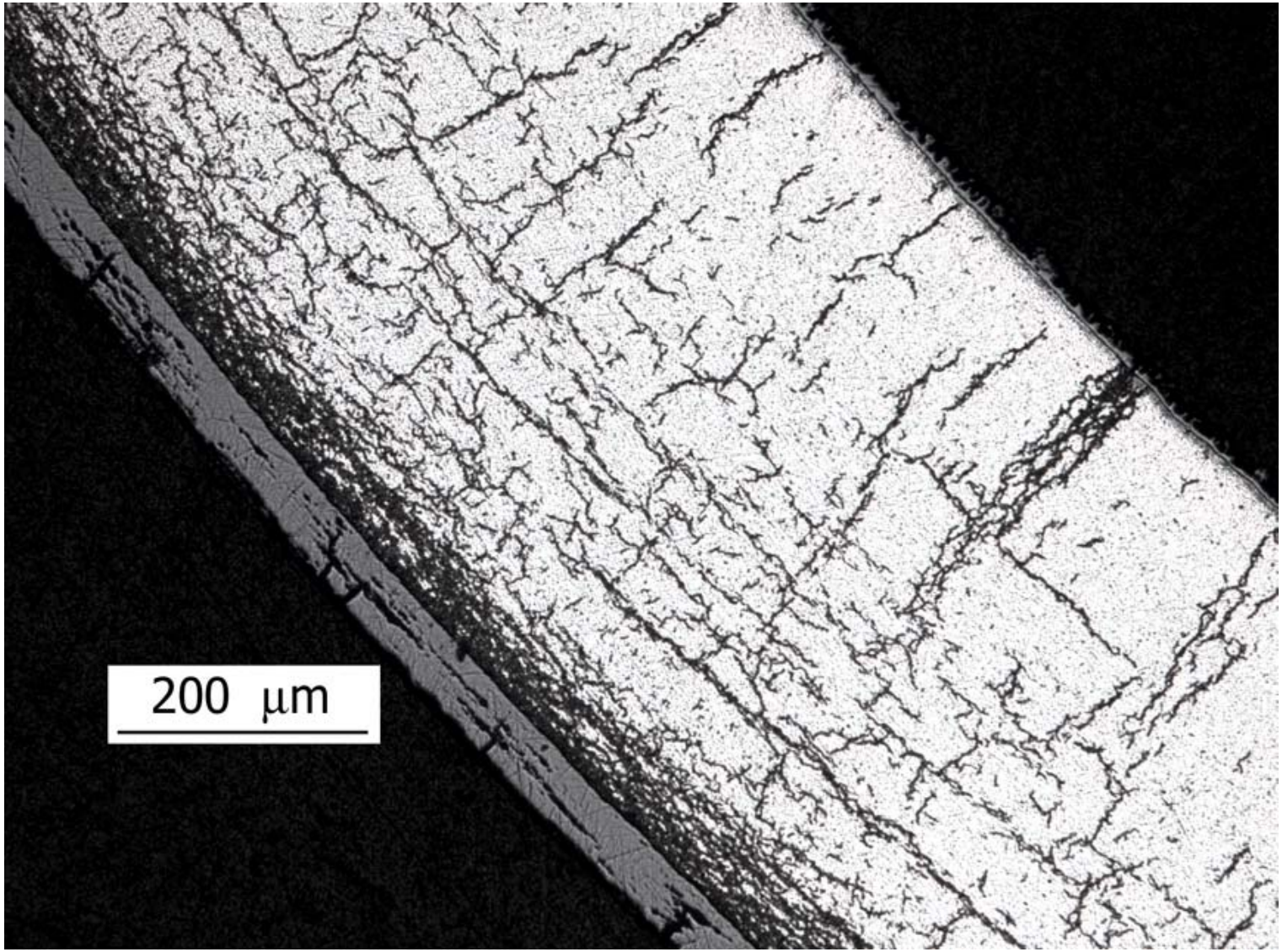

Fig. C.16 Area 6 image for ring 648G8 sectioned from high-burnup ZIRLO rodlet with RHT stress of 140 MPa. Hydrogen content of adjacent ring was 640±80 wppm. Maximum RHCF = 58%. See Fig. C.1 for sample location.

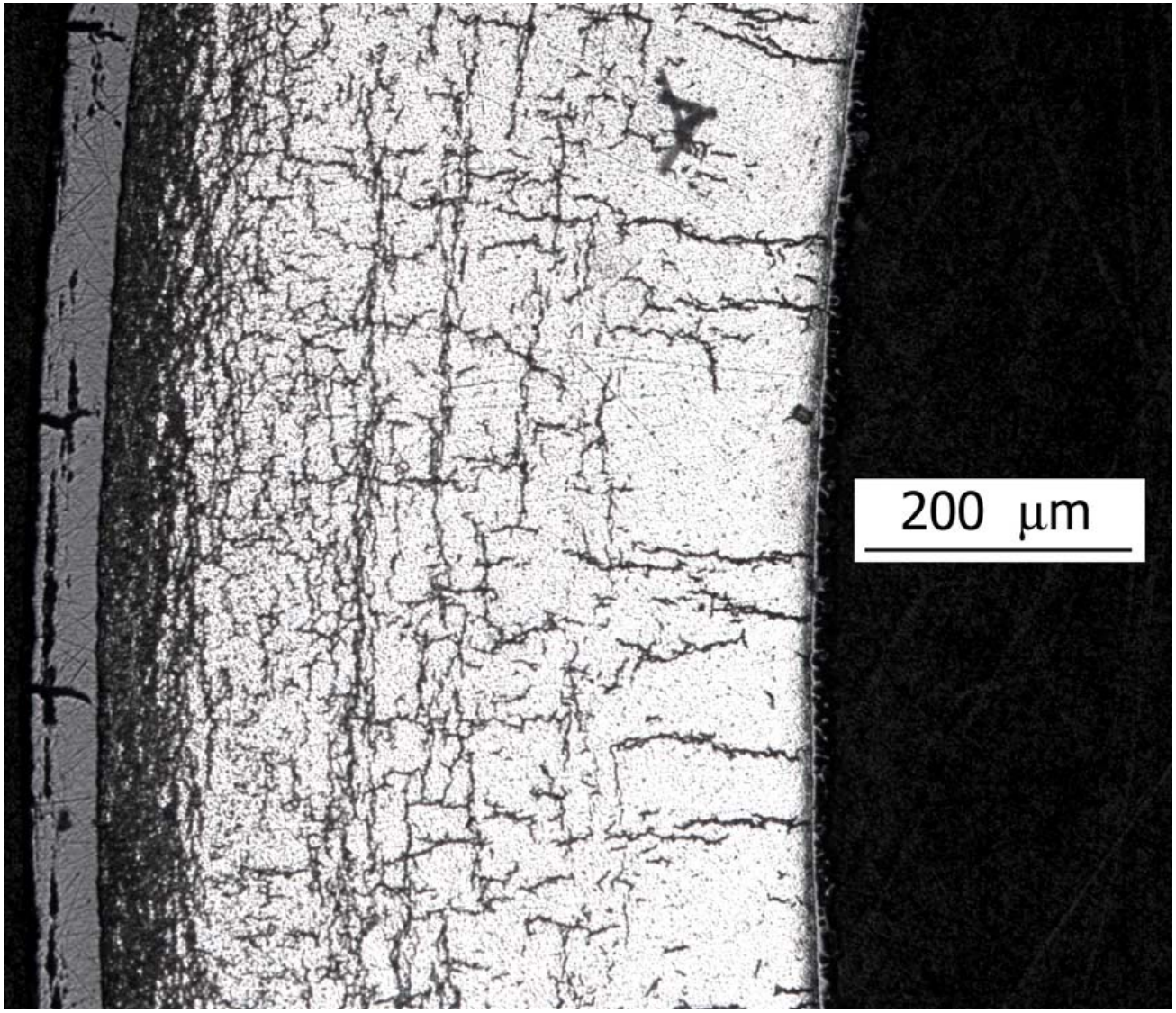

Fig. C.17 Area 7 image for ring 648G8 sectioned from high-burnup ZIRLO rodlet with RHT stress of 140 MPa. Hydrogen content of adjacent ring was 640±80 wppm. Maximum RHCF = 51%. See Fig. C.1 for sample location.

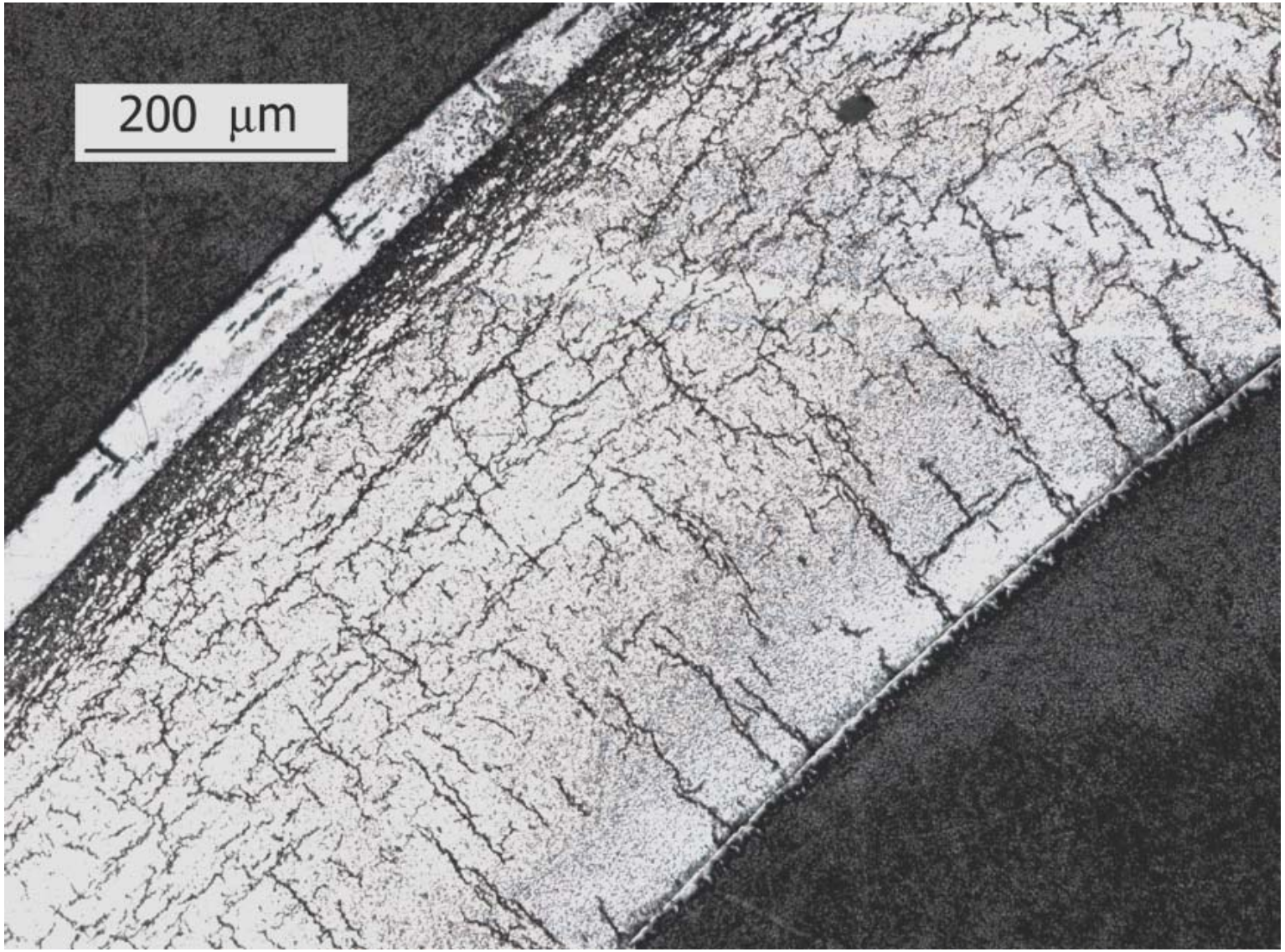

Fig. C.18 Area 8 image for ring 648G8 sectioned from high-burnup ZIRLO rodlet with RHT stress of 140 MPa. Hydrogen content of adjacent ring was 640±80 wppm. Maximum RHCF = 47%. See Fig. C.1 for sample location.

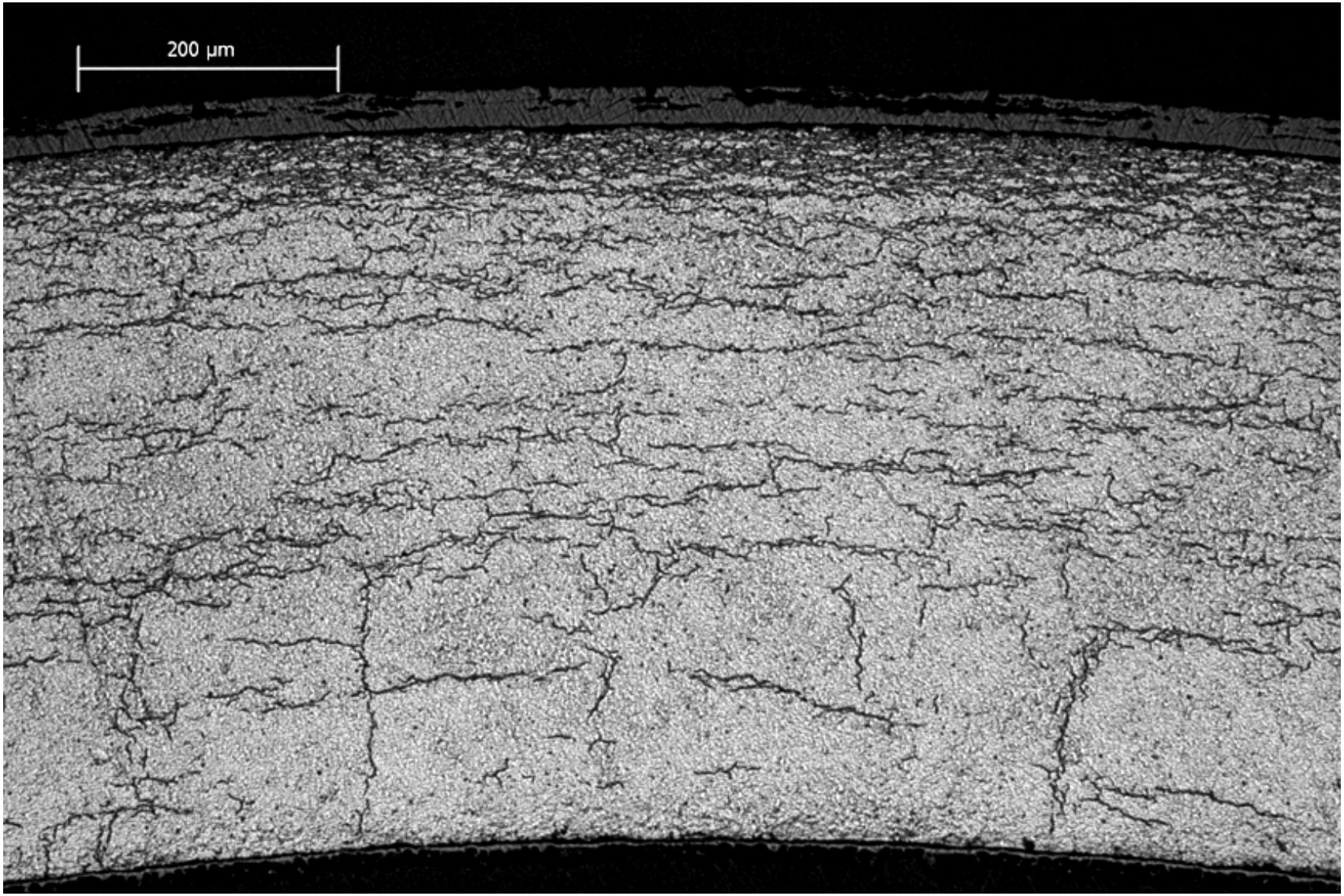

Fig. C.19 Area 1 image for ring 648D7 sectioned from high-burnup ZIRLO rodlet with RHT stress of 110 MPa. Hydrogen content of adjacent ring was 425±75 wppm. Maximum RHCF = 39%. See Fig. C.2 for sample location.

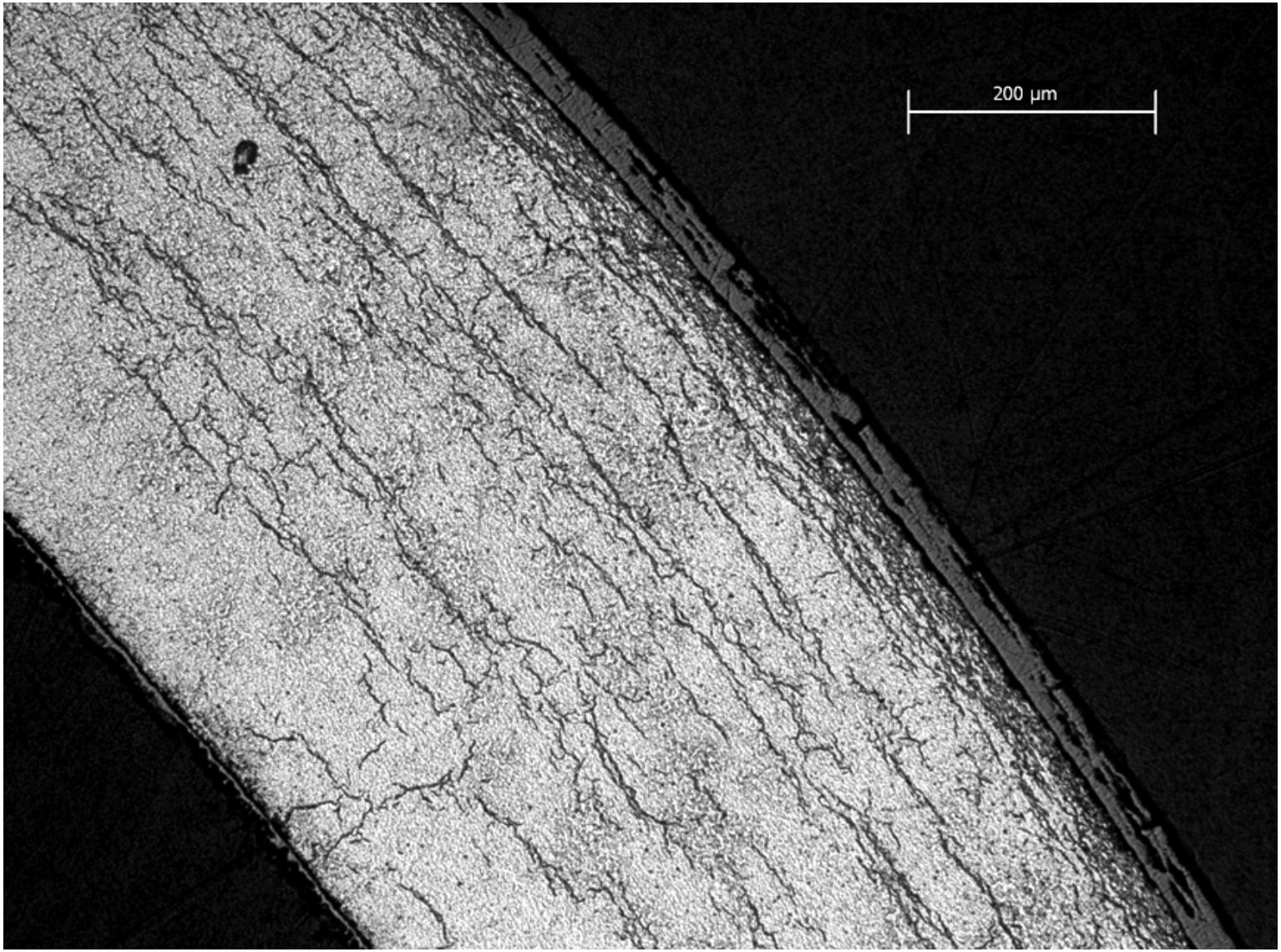

Fig. C.20 Area 2 image for ring 648D7 sectioned from high-burnup ZIRLO rodlet with RHT stress of 110 MPa. Hydrogen content of adjacent ring was 425±75 wppm. Maximum RHCF = 30%. See Fig. C.2 for sample location.

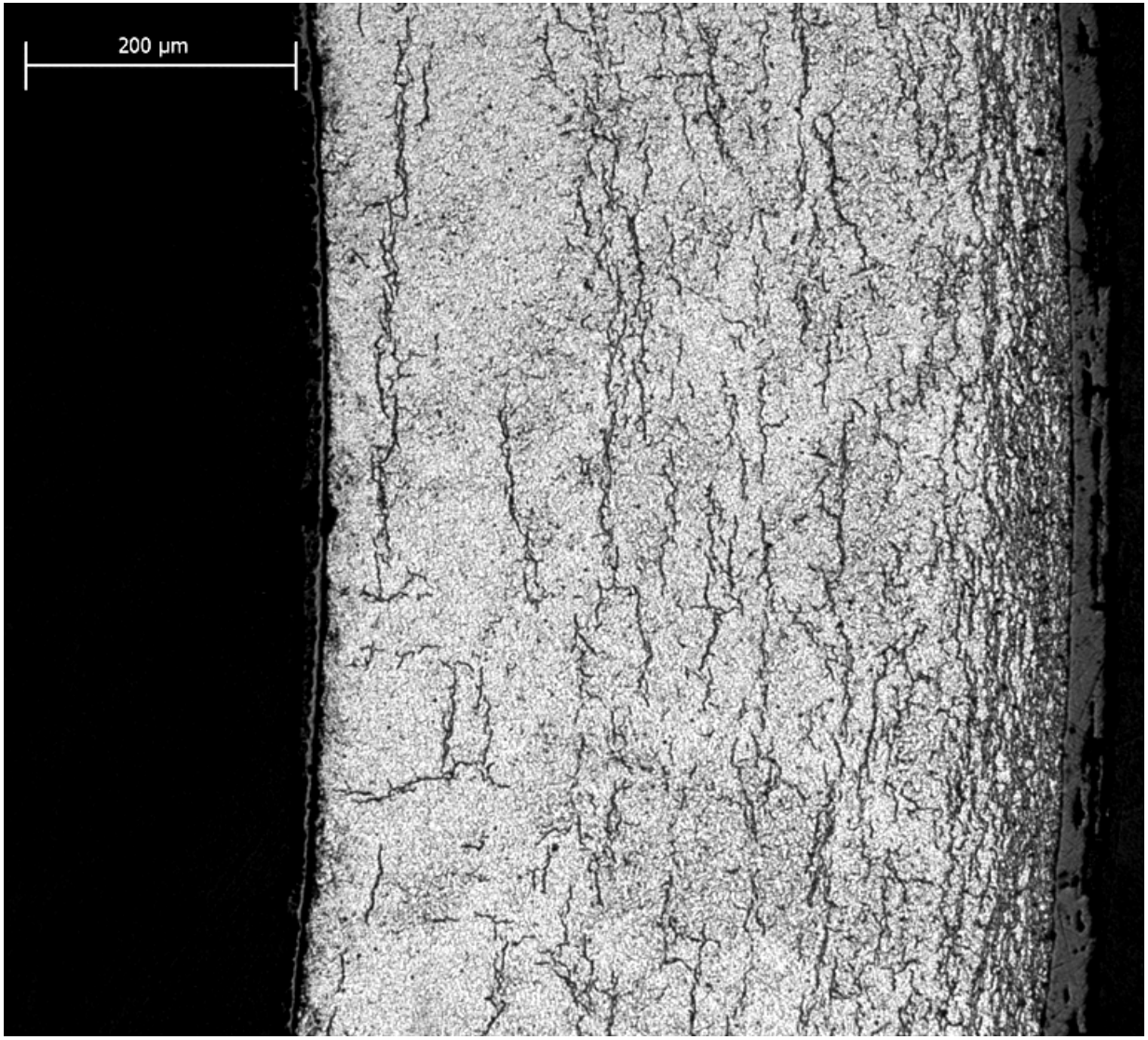

Fig. C.21 Area 3 image for ring 648D7 sectioned from high-burnup ZIRLO rodlet with RHT stress of 110 MPa. Hydrogen content of adjacent ring was 425±75 wppm. Maximum RHCF = 23%. See Fig. C.2 for sample location.

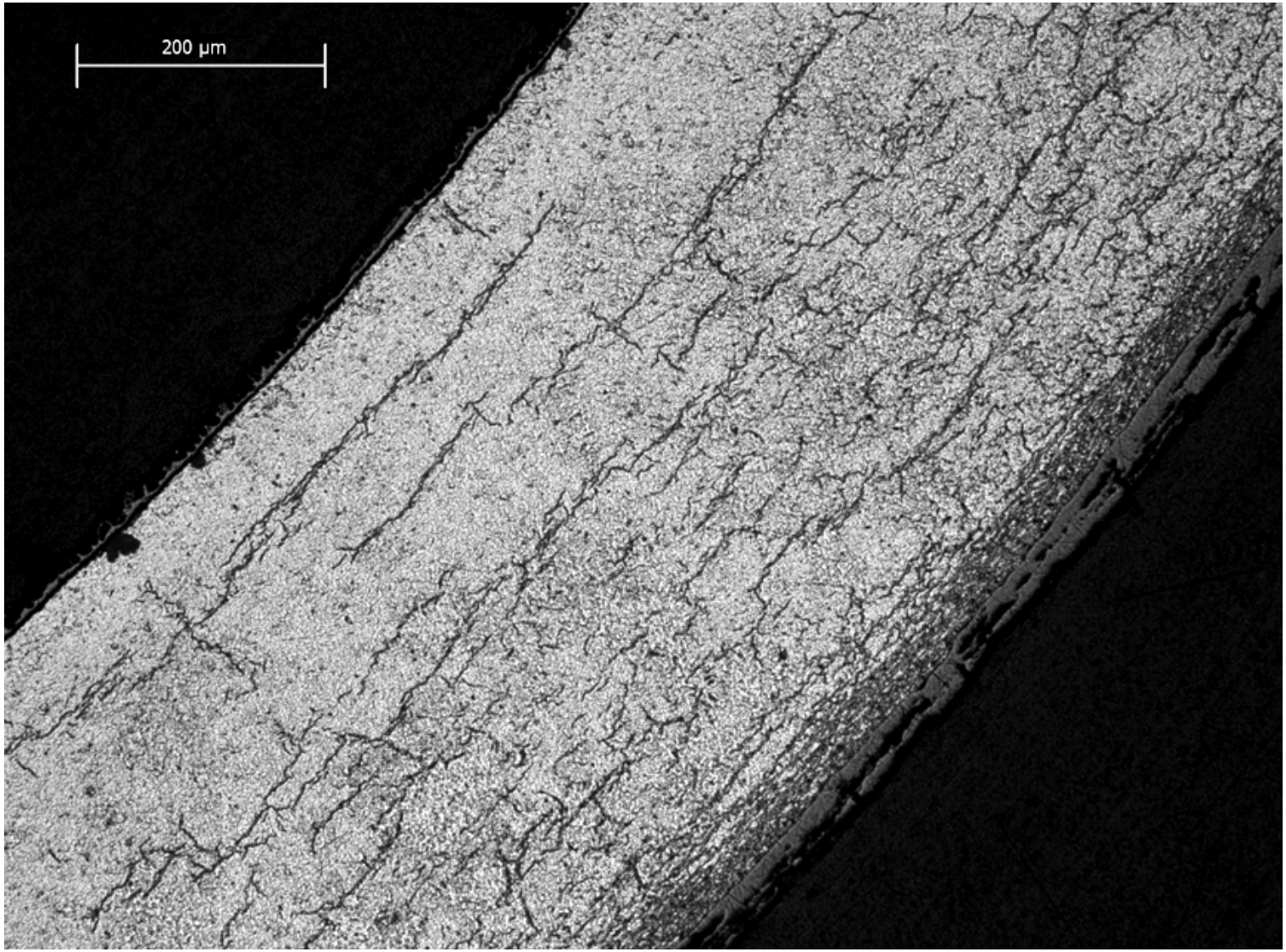

Fig. C.22 Area 4 image for ring 648D7 sectioned from high-burnup ZIRLO rodlet with RHT stress of 110 MPa. Hydrogen content of adjacent ring was 425±75 wppm. Maximum RHCF = 20%. See Fig. C.2 for sample location.

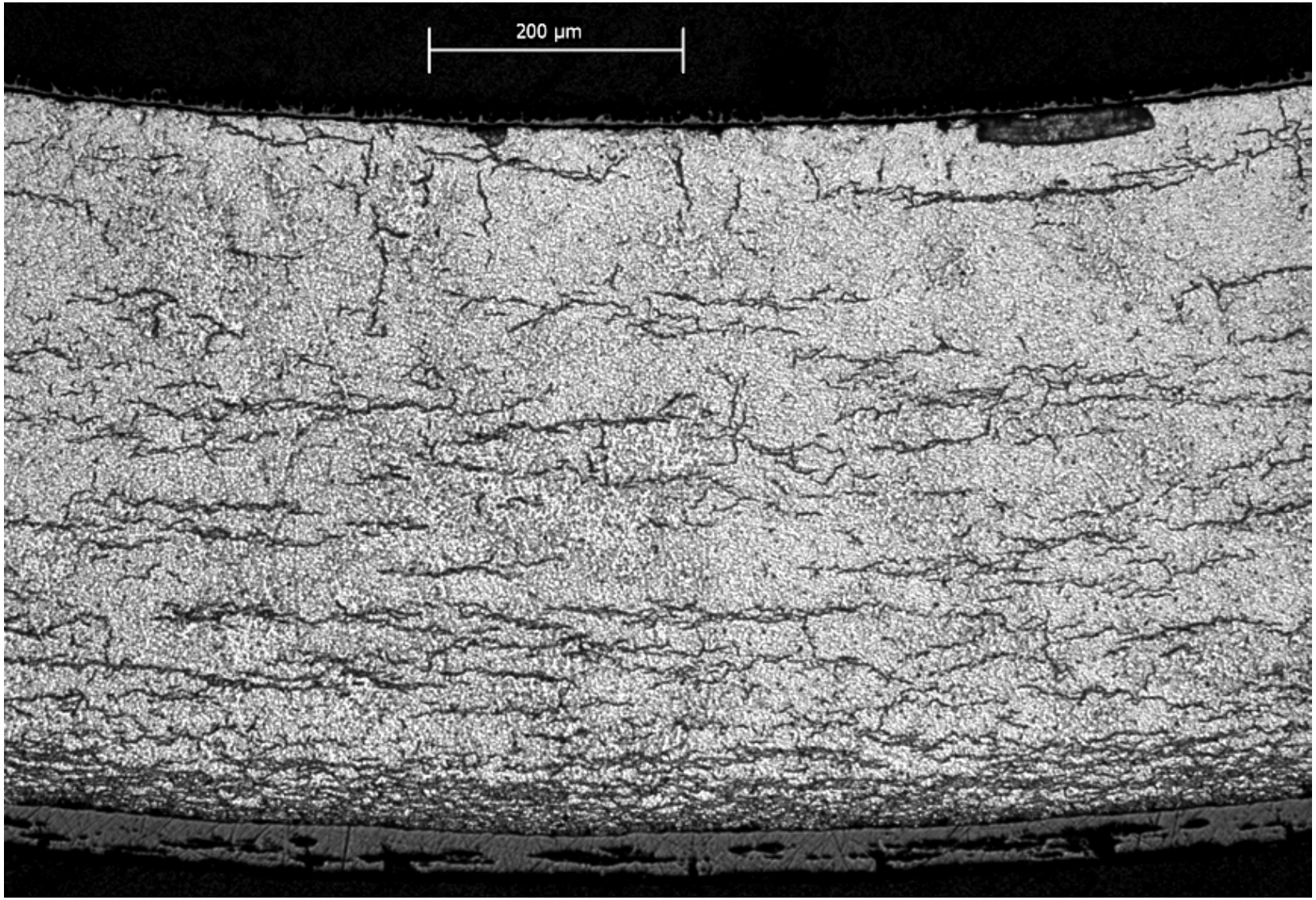

Fig. C.23 Area 5 image for ring 648D7 sectioned from high-burnup ZIRLO rodlet with RHT stress of 110 MPa. Hydrogen content of adjacent ring was 425±75 wppm. Maximum RHCF = 19%. See Fig. C.2 for sample location.

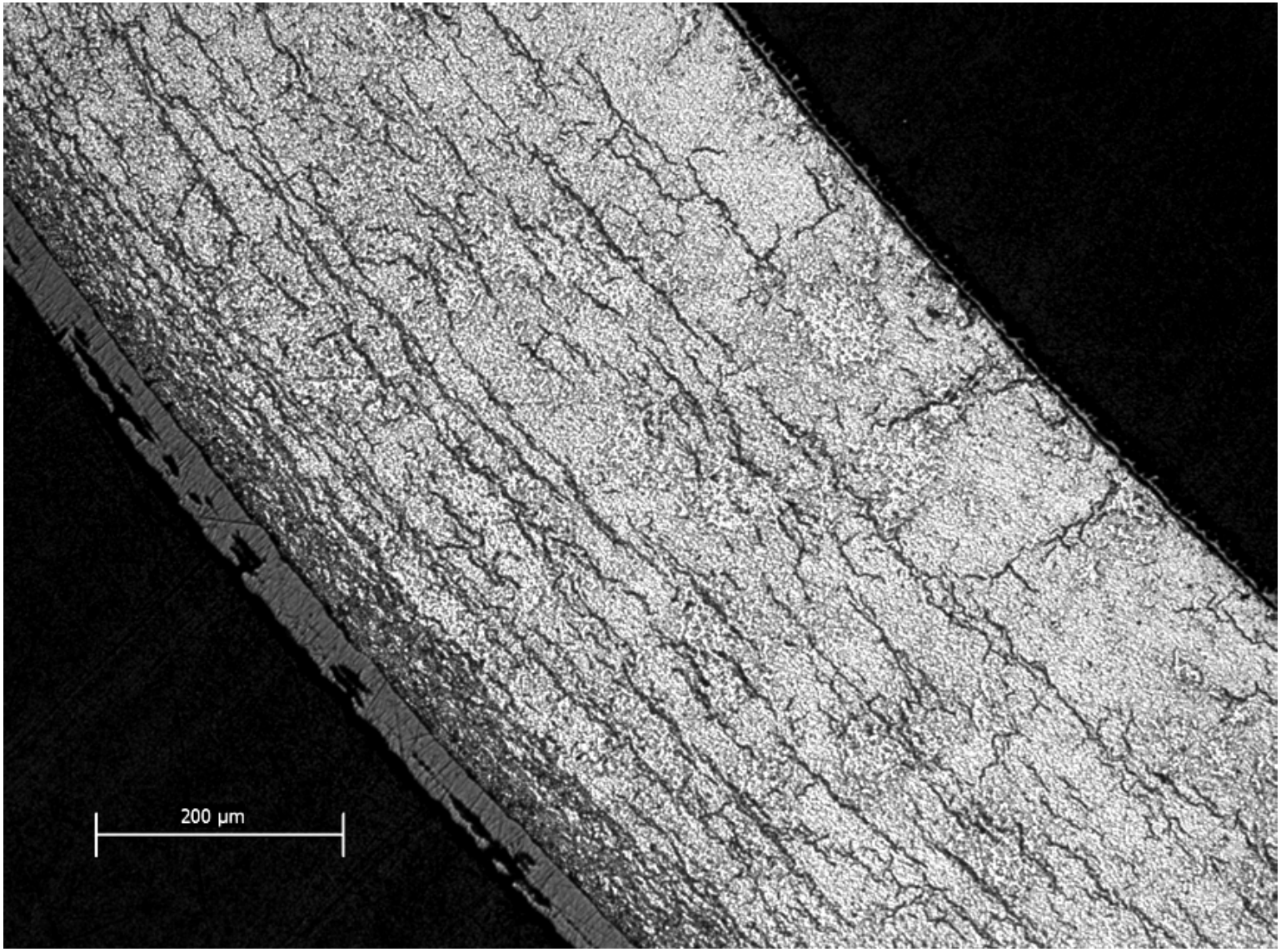

Fig. C.24 Area 6 image for ring 648D7 sectioned from high-burnup ZIRLO rodlet with RHT stress of 110 MPa. Hydrogen content of adjacent ring was 425±75 wppm. Maximum RHCF = 34%. See Fig. C.2 for sample location.

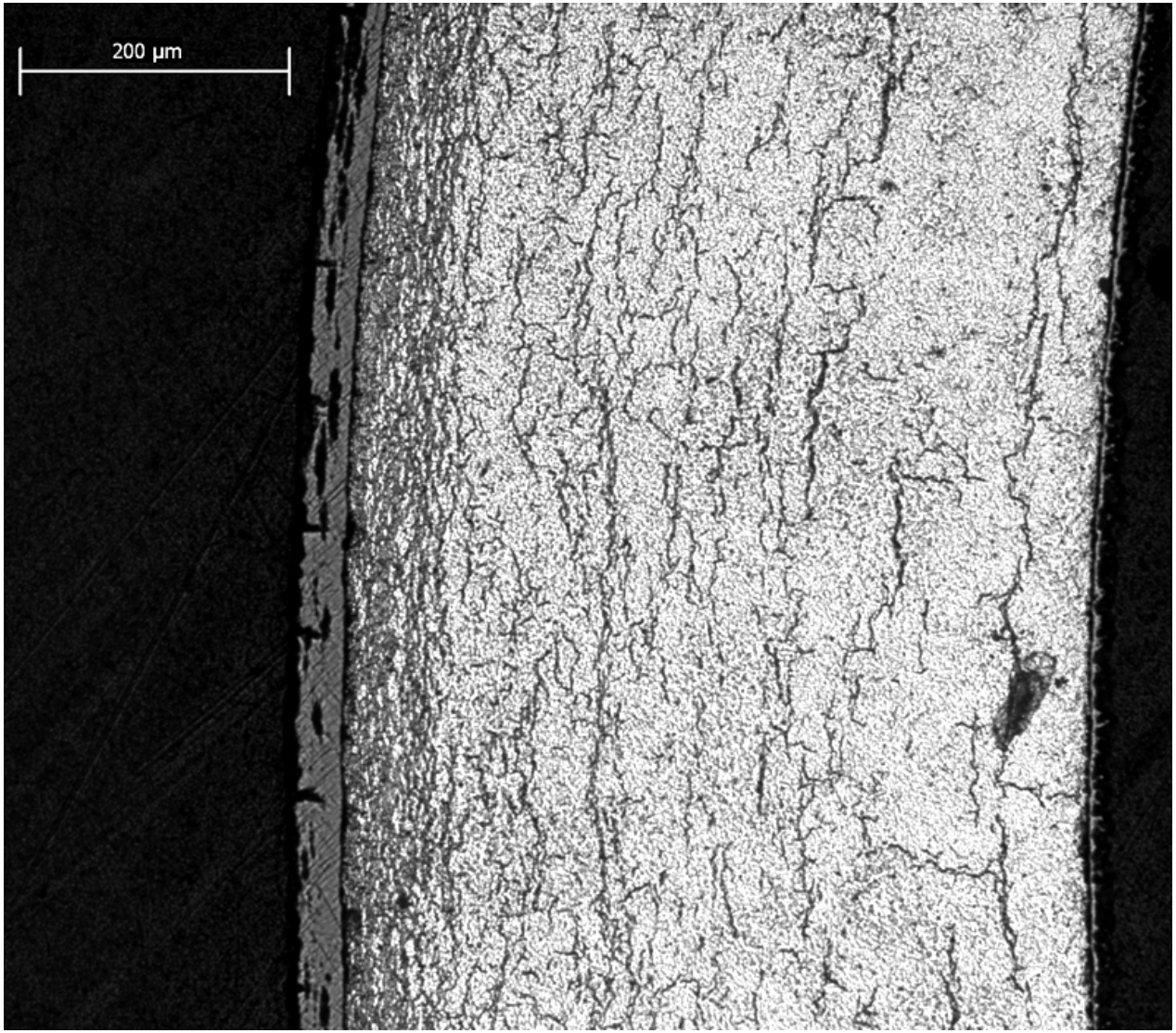

Fig. C.25 Area 7 image for ring 648D7 sectioned from high-burnup ZIRLO rodlet with RHT stress of 110 MPa. Hydrogen content of adjacent ring was 425±75 wppm. Maximum RHCF = 18%. See Fig. C.2 for sample location.

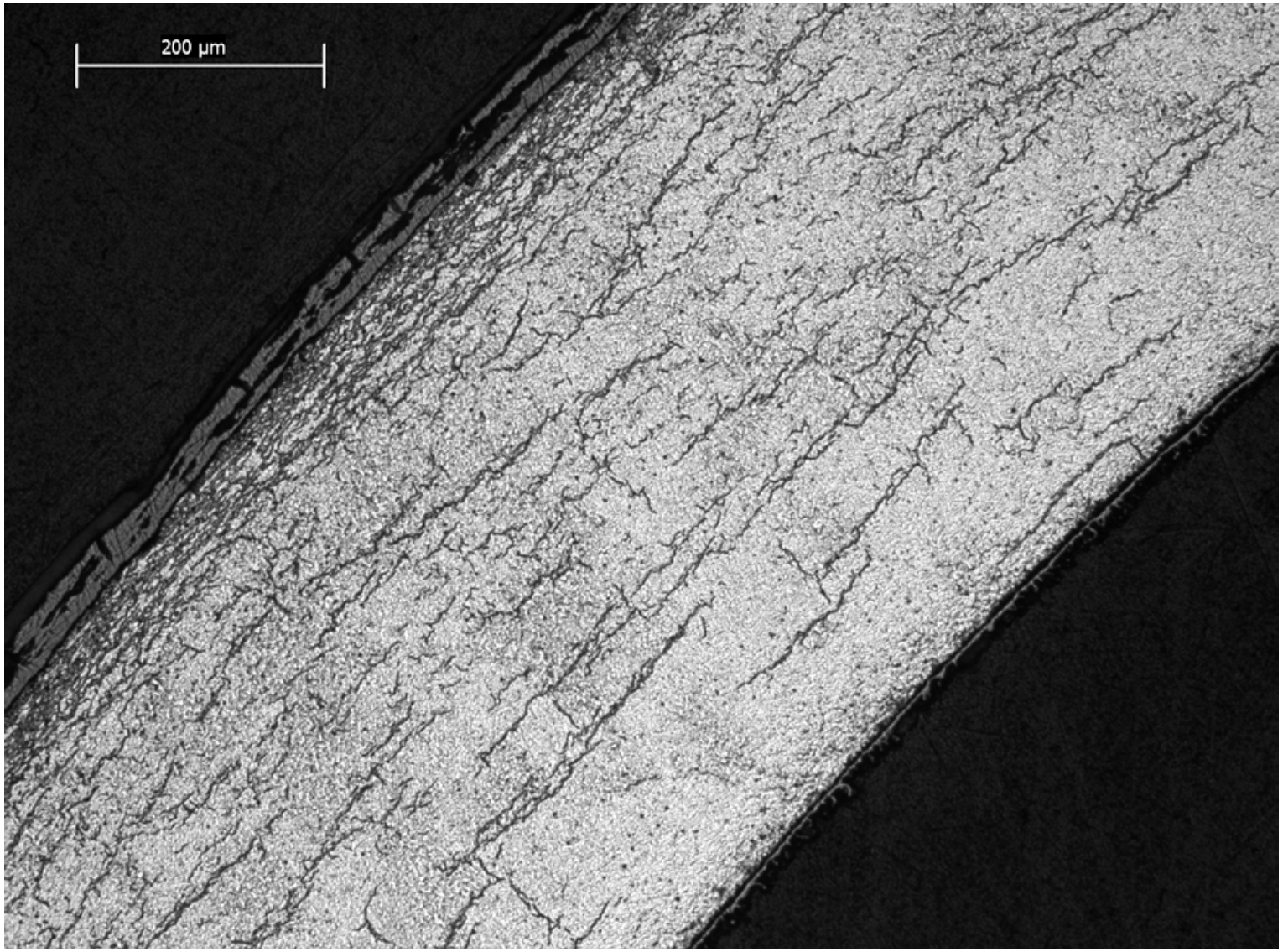

Fig. C.26 Area 8 image for ring 648D7 sectioned from high-burnup ZIRLO rodlet with RHT stress of 110 MPa. Hydrogen content of adjacent ring was 425±75 wppm. Maximum RHCF = 20%. See Fig. C.2 for sample location.